Doctoral Thesis

Development of Nickel-Catalyzed Azide–Alkyne Cycloaddition: Regioselective Control and Mechanistic Investigation

Woo Gyum Kim

Department of Chemical Engineering

Graduate School of UNIST

2019

Development of Nickel-Catalyzed Azide–Alkyne Cycloaddition: Regioselective Control and Mechanistic Investigation

Woo Gyum Kim

Department of Chemical Engineering

Graduate School of UNIST

Development of Nickel-Catalyzed Azide–Alkyne Cycloaddition: Regioselective Control and Mechanistic Investigation

A thesis/dissertation
submitted to the Graduate School of UNIST
in partial fulfillment of the
requirements for the degree of
Doctor of Philosophy

Woo Gyum Kim

12/28/2018 of submission

Approved by

Sung You Hong

Advisor

Sung You Hong

Development of Nickel-Catalyzed Azide–Alkyne Cycloaddition: Regioselective Control and Mechanistic Investigation

Woo Gyum Kim

This certifies that the thesis/dissertation of Woo Gyum Kim is approved.

12/28/2018 of submission

Advisor: Prof. Sung You Hong

Prof. Sebyung Kang: Thesis Committee Member #1

Prof. Jan-Uwe Rohde: Thesis Committee Member #2

Prof. Jung-Min Kee: Thesis Committee Member #3

Prof. Changduk Yang: Thesis Committee Member #4;

Abstract

Exponentially increased numbers of publication covering click chemistry have proved its significance and versatility in interdisciplinary studies. Numerous scientific fields including material science, medicinal chemistry, and bioconjugate chemistry get support of click chemistry to explore profound researches. Certain chemical reactions eliciting high yield in mild conditions are categorized as click reactions such as strained ring opening by nucleophiles, non-aldol type carbonyl chemistry, thiol-ene/yne reaction, and Diels-Alder reaction. Especially, azide and alkyne functional groups are biologically and chemically compatible, orthogonal to each other, and small to introduce in various complexes. These properties prompt exploration to expand cross-coupling pools. Copper catalyzed azide–alkyne cycloaddition is favorably selected in click reaction toolbox, because of the broad substrate scope, high yield, regioselectivity, and mild reaction conditions. Strain-promoted azide–alkyne cycloaddition, utilizing ring strain energy, have also been spotlighted as an alternative method to evade toxic metal and increase the biocompatibility. Transition metals are good candidates in cross-coupling reactions. Ruthenium catalyzes azide–alkyne cycloaddition to access selective 1,5-disubstituted 1,2,3-triazoles, isomers of 1,4-disubstituted triazoles, prepared by copper click reactions. But harsh conditions such as organic solvents and elevated temperatures, disrupt its wide usage in interdisciplinary studies.

In chapter 2, I utilized copper click reactions to formulate iron oxide nanoparticles including small molecules, imidazoquinoline derivatives. Adjuvant conjugated iron oxide nanoparticles have multivalent effects on immune responses compared to individual doses. Covalent conjugation of nanoparticles facilitate quantitative analysis and fluorescence tracking to dendritic cells. Chapter 3 includes establishments of nickel catalyzed cycloadditions. Highly regioselective 1,5-disubstituted triazoles are synthesized by mixing nickelocene and Xantphos ligands under room temperature and aqueous media. Wide substrate scope and certain evidence of active catalysts are described and characterized by various analytical methods such as NMR, MS, XRD, and EPR. In the last chapter, we explored cross-coupling between organic azide and cyanoalkynes to prepare 4-cyano-1,5-disubstituted 1,2,3-triazoles using nickelocene/Xantphos complex. Enhanced reaction conditions and broad substrates tolerance proved its versatility and reactivity comparison between cyanoalkynes and terminal alkynes opened possibilities applied to chemo-selective double/multiple click chemistry.

Table of Contents

Abstract ---------- i

Table of Contents ---------- ii

List of Figures ---------- iv

List of Tables ---------- vi

List of Schemes ---------- vii

Abbreviation ---------- viii

Chapter I. Introduction

1.1. Click Chemistry ---------- 1

1.1.1. Reactions ---------- 2

1.1.2. Applications ---------- 5

1.2. 1,2,3-triazoles ---------- 8

1.2.1. Synthesis of 1,4-disubstituted 1,2,3-triazoles ---------- 10

1.2.2. Synthesis of 1,5-disubstituted 1,2,3-triazoles ---------- 13

1.3. References ---------- 15

Chapter II. Covalent Conjugation of Small Molecule Adjuvants to Nanoparticles Induces Robust Cytotoxic T Cell Responses via DC Activation

2.1. Abstract ---------- 20

2.2. Introduction ---------- 20

2.3. Results and discussion ---------- 22

2.4. Conclusion ---------- 32

2.5. Experimental ---------- 33

2.6. References ---------- 37

Chapter III. Nickel-Catalyzed Azide−Alkyne Cycloaddition To Access 1,5-Disubstituted 1,2,3-Triazoles in Air and Water

3.1. Abstract ---------- 40

3.2. Introduction ---------- 40

3.3. Results and discussion ---------- 42

3.4. Conclusion ---------- 51

3.5. Experimental ---------- 52

3.6. References ---------- 67

Chapter IV. Preparation of 4-Cyano-1,5-Disubstituted 1,2,3-Triazoles and Establishment of Chemoselective Sequential 1,2,3-Triazoles via NiAAC

4.1. Abstract ---------- 71

4.2. Introduction ---------- 71

4.3. Results and discussion ---------- 73

4.4. Experimental ---------- 77

4.5. References ---------- 85

Chapter V. Acknowledgement ---------- 87

List of Figures

Figure 1.1. Graphic representation of click chemistry publications in 2002 – 2017.

Figure 1.2. (A) Well-known Diels-Alder reactions, (B) Schematic representation of polymer synthesis.

Figure 1.3. Schematic representation of SPAAC and well-known cyclooctynes.

Figure 1.4. Schematic synthetic representations of (A) rotaxane, and (B) catenane.

Figure 1.5. Schematic representation of metabolic labeling and SPAAC.

Figure 1.6. (A) Structures of 1,4- and 1,5-disubstituted triazoles, and *trans* and *cis* amide bonds. (B) Examples of surrogating peptide bonds to triazoles.

Figure 1.7. Structures of 1,2,3-triazoles to depict amide bonds.

Figure 1.8. Examples of 1,2,3-triazoles eliciting high bio-activities.

Figure 1.9. Remarkable synthetic approaches in azide−alkyne cycloaddition.

Figure 1.10. Proposed mechanism of CuAAC explained by (A) mononuclear and (B) dinuclear copper intermediate, (C) Representative water soluble chelating ligands.

Figure 1.11. (A) Unsymmetrical biazide preparation. (B) Schematic representation of sequential CuAAC.

Figure 1.12. Proposed mechanism of RuAAC of (A) whole catalytic cycle and (B) possible orientation of azide and alkyne coordination.

Figure 1.13. Examples of polymerization via RuAAC.

Figure 2.1. General attributes of Adjuvant-NPs in inducing DC activation and a robust CTL response.

Figure 2.2. Synthetic scheme of Adjuvant-NPs (i) HBTU, TEA, DCM, (ii) $CuSO_4 \cdot 5H_2O$, sodium ascorbate, DMF, (iii) 0.1 M Tris buffer (pH 6), and (iv) diluted hydrogen chloride solution. (b,c) ^{1}H and ^{13}C NMR spectra (MeOD) of Adjuvant **1**.

Figure 2.3. Characterization of Adjuvant-NPs. (a) TEM image of Adjuvant-NPs, (b) DLS analysis, (c) UV−vis spectra, and (d) fluorescence spectra.

Figure 2.4. Adjuvant effects on in vivo DC activation: (a) flow cytometry analyses, and (b,c) the mean fluorescence intensity (MFI) levels of DC activation markers (CD80, CD86, CCR7, and MHC I). The P values of <0.05(*), <0.01(**), and <0.001(***) were considered significant.

Figure 2.5. DC activation tests at various concentration of Adjuvant **1′**.

Figure 2.6. DC activation tests at various concentration of Adjuvant-NPs.

Figure 2.7. DC activation tests at various concentration of Amine-NPs.

Figure 2.8. (a) IL-12p40 secretion of Adjuvant-NPs in DCs. Samples were analyzed by ELISA after 48 hours culture. The P values < 0.001(***) were considered significant. (b) Flow cytometry analyses of OT-1 peptide specific T cell receptor expressing $CD8^+$ T cells.

Figure 2.9. (a,b) Fluorescence imaging studies to examine the internalization of Fluorescein-Adjuvant-

NPs in DCs. Samples were characterized by confocal fluorescent microscopy.

Figure 2.10. Z-stacking 3D Fluorescence images to examine the internalization of Fluorescein-Adjuvant-NPs in DCs.

Figure 2.11. In vivo CTL assay on splenocytes. (a) Percentages of OT-1 peptide unpulsed $CFSE^{low}$ (left) and that of pulsed $CFSE^{high}$ (right) were analyzed by flow cytometry. Each group was stimulated with indicated adjuvants: Sample A: R848 10 μg, 28.5 nmol, sample B: R 848 50 μg, 142.5 nmol, sample C: amine-NPs 100 μg Fe, sample D: amine NPs 200 μg Fe, sample E: Adjuvant-NPs (100 μg Fe, 13.9 nmol of imidazoquinoline), sample F: Adjuvant-NPs (200 μg Fe, 27.8 nmol of imidazoquinoline) along with OVA protein. (b) Conversion of the percentages of $CFSE^{high}$ based on the negative control of PBS treated group. The P values of <0.01(**) were considered significant.

Figure 2.12. Synthesis of Fluorescein-Adjuvant-NPs.

Figure 2.13. A calibration curve of NHS fluorescein.

Figure 3.1. 2D NMR (^1H–^1H NOESY and HSQC) spectroscopic studies.

Figure 3.2. EPR spectrum of a sample from the reaction between Cp_2Ni and Xantphos in tol uene (X-band microwave frequency, 9.385 GHz, modulation frequency, 100 kHz, modulation a mplitude, 5 G, microwave power, 6.33 mW, temperature, 295 K, 10 scans).

Figure 3.3. HRMS study: (a) wide range data, and (b) isotope distributions of $[CpNi(Xantphos)]^+$. $[Ni(Xantphos)_2+2Na]^{2+}$ (ESI+, m/z) calcd for $C_{78}H_{64}Na_2NiO_2P_4^{2+}$ ($[M+2Na]^{2+}$) 630.1500, found 630.1638, $[CpNi(Xantphos)]^+$ (ESI+, m/z) calcd for $C_{44}H_{37}NiOP_2$ ($[M]^+$) 701.1667, found 701.1671.

Figure 4.1. ^1H NMR (400 MHz, $CDCl_3$) of the compound **2i**.

Figure 4.2. ^1H NMR (400 MHz, $CDCl_3$) of the compound **2h**.

Figure 4.3. ^1H NMR (400 MHz, $CDCl_3$) of the compound **3ba**.

Figure 4.4. ^1H NMR (400 MHz, $CDCl_3$) of the compound **3ca**.

Figure 4.5. ^1H NMR (400 MHz, $CDCl_3$) of the compound **3ga**.

Figure 4.6. ^1H NMR (400 MHz, $CDCl_3$) of the compound **3ha**.

Figure 4.7. ^1H NMR (400 MHz, $CDCl_3$) of the compound **3ia**.

Figure 4.8. ^1H NMR (400 MHz, $CDCl_3$) of the compound **3bb**.

Figure 4.9. ^1H NMR (400 MHz, $CDCl_3$) of the compound **3bc**.

Figure 4.10. ^1H NMR (400 MHz, $CDCl_3$) of the compound **3bd**.

Figure 4.11. ^1H NMR (400 MHz, $CDCl_3$) of the compound **3be**.

Figure 4.12. ^1H NMR (400 MHz, $CDCl_3$) of the compound **3bf**.

Figure 4.13. ^1H NMR (400 MHz, $CDCl_3$) of the compound **3bi**.

List of Tables

Table 3.1. Optimization of reaction conditions.[a]

Table 3.2. Nickel catalyst screening.[a]

Table 3.3. Metallocene catalyst screening.[a]

Table 3.4. Ligand screening.[a]

Table 3.5. Base/additive screening.[a]

Table 3.6. Crystal Data and Structure Refinement of **3ah**.

Table 3.7. Crystal Data and Structure Refinement of **3ja**.

Table 4.1. Optimization of reaction conditions.

List of Schemes

Scheme 1.1. Representative examples of click reaction.

Scheme 1.2. (A) Schematic representation of convergent dendrimer synthesis. (B) Examples of click polymerization using various monomers such as AB_2, A_2+B_3, A_2+B_2.

Scheme 3.1. Synthesis of 1,5-disubstituted 1,2,3-triazoles.

Scheme 3.2. Substrate scope of the NiAAC.[a]

Scheme 3.3. Expanded scope with respect to non-natural carbohydrates and amino acids.[a]

Scheme 3.4. Attempted NiAAC reactions with unprotected sugar **1l′** and **1m′**.

Scheme 3.5. Tentative reaction mechanism of the NiAAC.

Scheme 3.6. Preparation of organic azides.

Scheme 3.7. Possible transformations of Ni complexes based on the experimental results and literature precedent.

Scheme 4.1. Schematic representation of precedent and this works in synthesis of 4-cyano-1,5-disubstitutd 1,2,3-triazoles.

Scheme 4.2. Substrate scope of nickel catalyzed azide−cyanoalkyne cycloaddition[a]

Scheme 4.3. Reactivity comparison test between cyanoalkyne and terminal alkyne.

Scheme 4.4. Schematic representation of chemoselective sequential double click reactions.

Scheme 4.5. Preparation of propynenitriles.

Scheme 4.6. Preparation of propynenitriles **2h** and **2i**.

Abbreviation

APC	Antigen-presenting Cell
CD	Cluster of Differentiation
CFSE	Carboxyfluorescein Succinimidyl Ester
Cp	Cyclopentadienyl
Cp*	Pentamethylcyclopentadienyl
CTL	Cytotoxic T Lymphocyte
DAPI	4′,6-Diamidino-2-phenylindole
DBU	1,8-Diazabicyclo[5.4.0]undec-7-ene
DC	Dendritic Cell
DCM	Dichloromethane
DFT	Discrete Fourier Transform
DIPEA	*N*,*N*-Diisopropylethylamine
DI water	Deionized water
DLS	Dynamic Light Scattering
DMF	Dimethylformamide
DMSO	Dimethyl Sulfoxide
EPR	Electron Paramagnetic Resonance
ESI-MS	Electrospray Ionization Mass Spectrometry
FACS	Fluorescence-activated Cell Sorting
HBTU	*N*,*N*,*N*′,*N*′-Tetramethyl-O-(1*H*-benzotriazol-1-yl)uronium hexafluorophosphate
HIV	Human Immunodeficiency Virus
HRMS	High-resolution Mass Spectrometry
HSQC	Heteronuclear Single-quantum Correlation Spectroscopy

MeOH	Methanol
MHC	Major Histocompatibility Complex
MRI	Magnetic Resonance Imaging
NHC	*N*-Heterocyclic Carbene
NH_4OH	Ammonium Hydroxide
NMR	Nuclear Magnetic Resonance
NOESY	Nuclear Overhauser Effect Spectroscopy
NP	Nanoparticle
OVA	Ovalbumin
PAMP	Pathogen-associated Molecular Pattern
PBS	Phosphate-buffered Saline
PDI	Poly Dispersity Index
PE	Phycoerythrin
TBAF	Tetrabutylammonium Fluoride
TBPB	*tert*-Butyl Peroxybenzoate
TCR	T-cell Receptor
TEM	Transmission Electron Microscopy
THF	Tetrahydrofuran
TLC	Thin Layer Chromatography
TLR	Toll-like Receptor
TMS	Trimethylsilyl
UV	Ultraviolet
XRD	X-Ray Diffraction

Chapter I

Introduction

1.1. Click Chemistry

The concept of "click chemistry" was firstly devised by K. Barry Sharpless with several criteria to categorize powerful and selective cross-coupling reactions. Click reactions should be modular, give a broad substrate scope, afford excellent yields, and be stereospecific. By these principles, reactions have furnished simple reaction conditions, product isolation (non-chromatographic methods), readily available reagents, and benign solvents such as water.[1] Corresponding rigid acceptance standards secure facile accessibility to interdisciplinary studies. It exerts tremendous influence on various scientific fields including material science, pharmaceutical science, and chemical biology. Exponentially increased numbers of publication containing the concept have proved their impact and versatility (Figure 1.1).

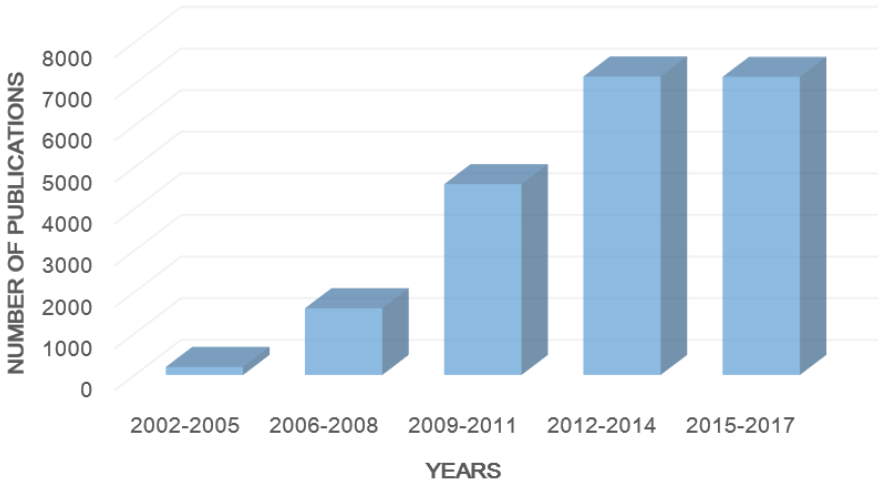

Figure 1.1. Graphic representation of click chemistry publications in 2002 – 2017.

1.1.1 Reactions

Generally, there are four types of practical click reactions: (i) strained ring (epoxide, aziridine) opening by nucleophiles, (ii) non-aldol type carbonyl chemistry forming amides, oximes and isoureas, (iii) addition of thiols to carbon–carbon multiple bonds (thiol-ene/yne reaction), and (iv) cycloaddition including Huisgen cycloaddition and Diels-Alder reaction (Scheme 1.1).

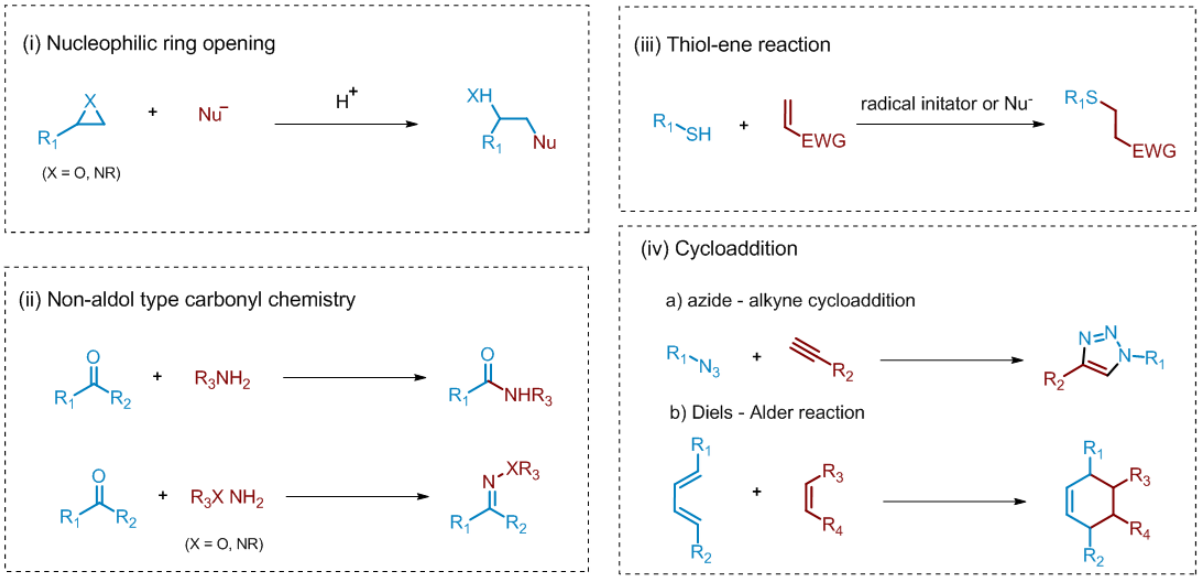

Scheme 1.1. Representative examples of click reaction.

Nucleophilic substitution could be applied in various strained rings such as epoxides, aziridines, and aziridinium ions.[2-4] Strong strain energy called spring-loaded electrophiles are stored in three membered heterocycles, subsequent nucleophilic attack facilitates ring opening under mild conditions easily with released energy. Nucleophiles including azides, nitriles, and acetates are potential candidates to be inserted with high yield in alcohol or water solvents. Non-aldol type carbonyl chemistry affords high yields, and chemoselectivity under aqueous solvents. Primary amines could be coupled with carbonyl functional group for amide or isourea formation. Hydroxyl amine or hydrazine can undergo nucleophilic attack on carbonyl compounds, eliciting the formation of corresponding oximes or hydrazones.[5,6] Reactions are mainly applied in polymer synthesis and bioconjugate chemistry.[7,8]

Thiol-ene chemistry has been broadly studied and applied in early 2000. Two pathways are popular adding free-radicals by light or radical initiator like 2,2'-azobis(isobutyronitrile), and Michael addition in the presence of nucleophiles or bases.[9,10] Usage of unique starting materials and mechanism occupied a certain area in photo-click chemistry and biomolecule conjugation including thiol group.

Azide−alkyne cross coupling and Diels-Alder reactions are representative pericyclic reactions in click chemistry. Diels-Alder reaction, introduced by Otto Diels and Kurt Alder, is a [4+2] cycloaddition to form six membered rings by conjugation of electron-rich dienes and electron-deficient dienophiles without any additional reagents. Substrate candidates are broad including furan, 1,3-cyclopentadiene, tetrazine for dienes, and maleimide, vinyl ketones, cyclooctene for dienophiles (Figure 1.2). Its high yields, regio- and stereo-selectivity fulfill requirements to be click reaction, but competition with retro Diels-Alder reaction at high temperature remains challenges.[11]

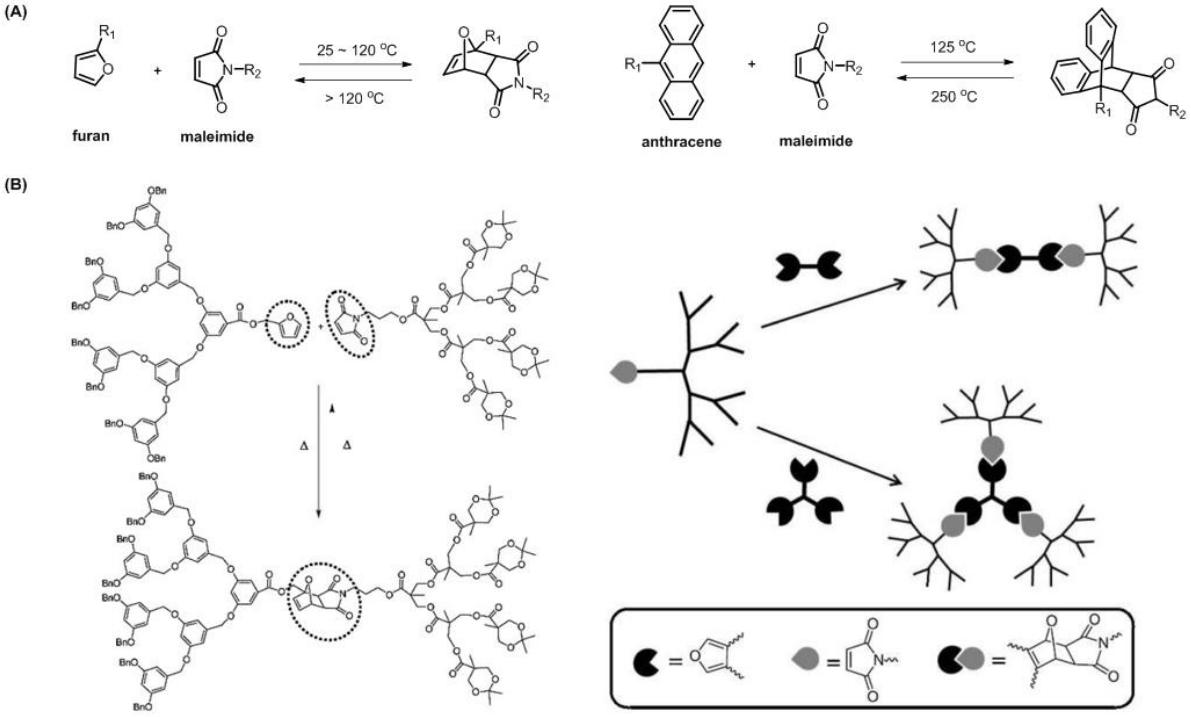

Figure 1.2. (A) Well-known Diels-Alder reactions, (B) Schematic representation of polymer synthesis.[12]

Copper (I)-catalyzed Azide−Alkyne Cycloaddition (CuAAC), firstly reported by Morten Meldal,[13] and K. Barry Sharpless[14] independently on 2002, is 1,3-dipolar cycloaddition to access 1,4-disubstituted 1,2,3-triazoles. CuAAC is one of premier click reaction, satisfying all strict criteria with excellent functional group tolerence. Active catalytic species to achieve corresponding cycloaddition are copper (I) species, which is unstable in air conditions. Alternatively, combination of copper (II) species and reducing agents such as sodium ascorbate is a typical route to make Cu^{1+} *in situ*. With the continuous and profound studies, reaction conditions and possible entries are enhanced, and many relevant triazole

synthetic methods are developed to be applied in chemical biology. Detailed description of CuAAC about mechanism are stated on section 1.2.1, and I would briefly explain a metal-free cycloaddition in this section.

Although CuAAC is a powerful method in click chemistry toolbox, existence of copper metal could be potential hindrance in biological study because of its toxicity. Metal-free click chemistry is developed to solve cytotoxicity issue. Strain-Promoted Azide−Alkyne Cycloaddition (SPAAC), a representative biorthogonal reaction, is designed by Carolyn R. Bertozzi in 2004.[15] Reaction utilized cyclooctyne, which has massive angle deformation 163°, giving intrinsic ring strain nearly 18 kcal/mol.[16] These high ring strain facilitates azide conjugation in physiological temperature without copper species. The absence of toxic metals affords *in vivo* metabolic studies including labeling fluorescence or drugs to complex cells. But the approach has still suffered from slow reaction kinetics, poor solubility, and regiospecificity. Development of useful cyclooctynes from aliphatic or fluoro-containing to dibenzoannulated form have studied to reduce reaction time and increase solubility for SPAAC versatility (Figure 1.3).[16,17]

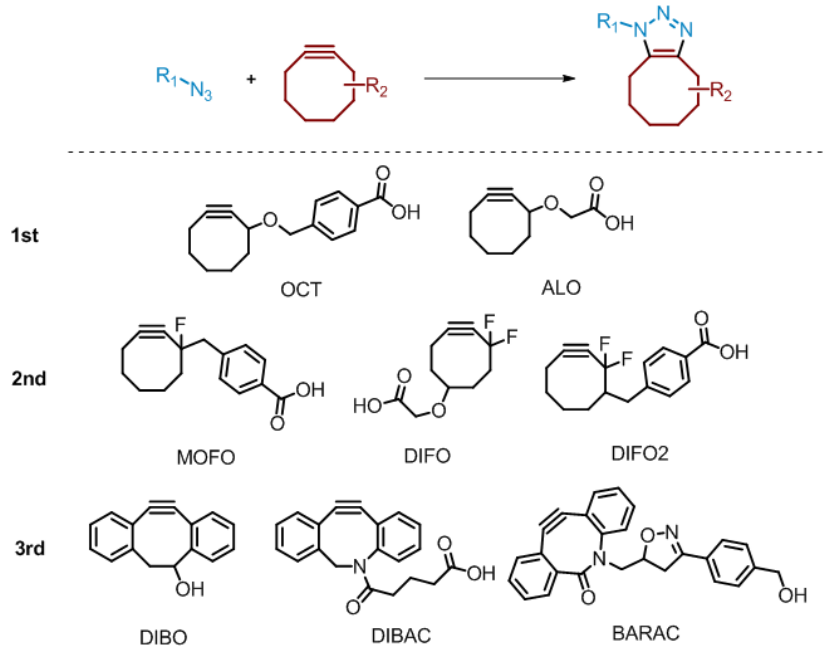

Figure 1.3. Schematic representation of SPAAC and well-known cyclooctynes.

1.1.2. Applications

As the concept of click chemistry implies, there are enormous applications through wide scientific fields. Roughly, I could categorize applications as three major fields, material science, medicinal chemistry, and bioconjugate chemistry. Click reactions fulfill essential elements in polymer synthesis such as simplified experimental procedure and isolation with high yield. Conceptually, step-growth polymerization, self-oligomerization and cross-coupling, depicted in Scheme 1.2, are frequently achieved by the introduction of CuAAC. Step-growth approaches require two distinct functional groups or one functional group with different reactivity. Converting halogen group to azide is a core step to attain step-growth (Scheme 1.2A). Thiol−ene chemistry also gets attention in metal and solvent-free conditions with various forms including star,[18] and branched[19] oligomers.

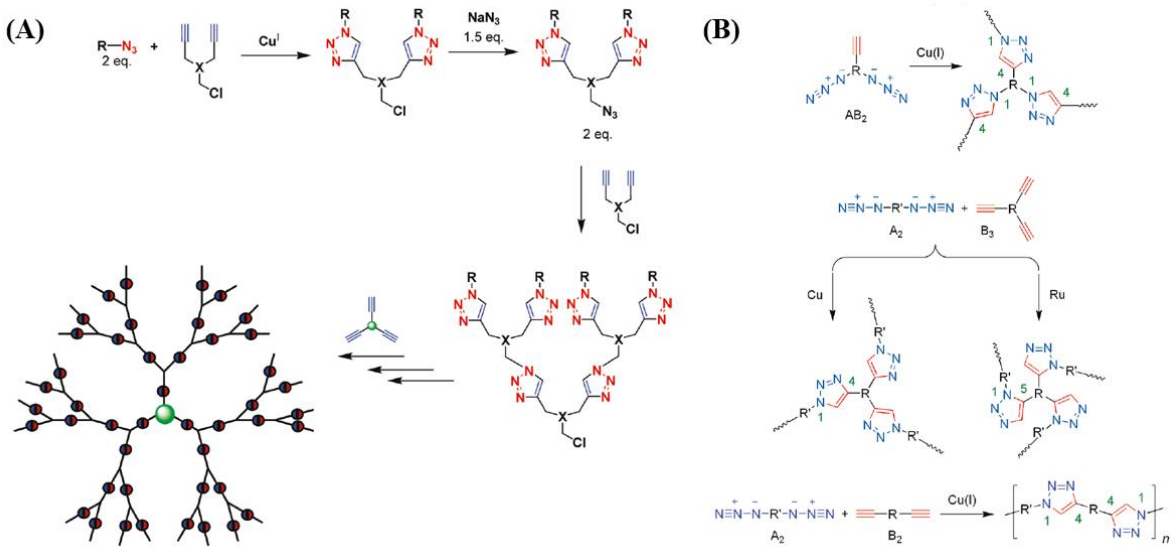

Scheme 1.2. (A) Schematic representation of convergent dendrimer synthesis.[20,21] (B) Examples of click polymerization using various monomers such as AB_2, A_2+B_3, A_2+B_2.[22]

As the potential of molecular machine become realized,[23,24] preparation of interlocked molecules such as rotaxanes, and catenanes gets spotlighted in supramolecular chemistry. Based on conceptual methodologies (capping, clipping, active metal template), various covalent reactions including ring-closing olefin metathesis[25] have contributed to building architectures. Click reactions are powerful surrogates because of their intrinsic properties (e.g., orthogonality, high yielding, and functional group tolerance). CuAAC is a favorably invited reaction in building and modifying interlocked molecules.

Active-metal template for rotaxane synthesis by CuAAC was achieved in 2006 (Figure 1.4A).[26] Tetrakis(acetonitrile)copper(I) hexafluorophosphate was chelated to nitrogen-containing macrocycles. Following azides and alkynes were coordinated to the copper complex, eliciting interlocked molecules after desorption of metal complex. Various substrates have been studied to reduce non-interlocked triazoles.[27] Similar methodology under high temperature was applied in the synthesis of [2]catenanes, but relatively low yields are still challenges.[28]

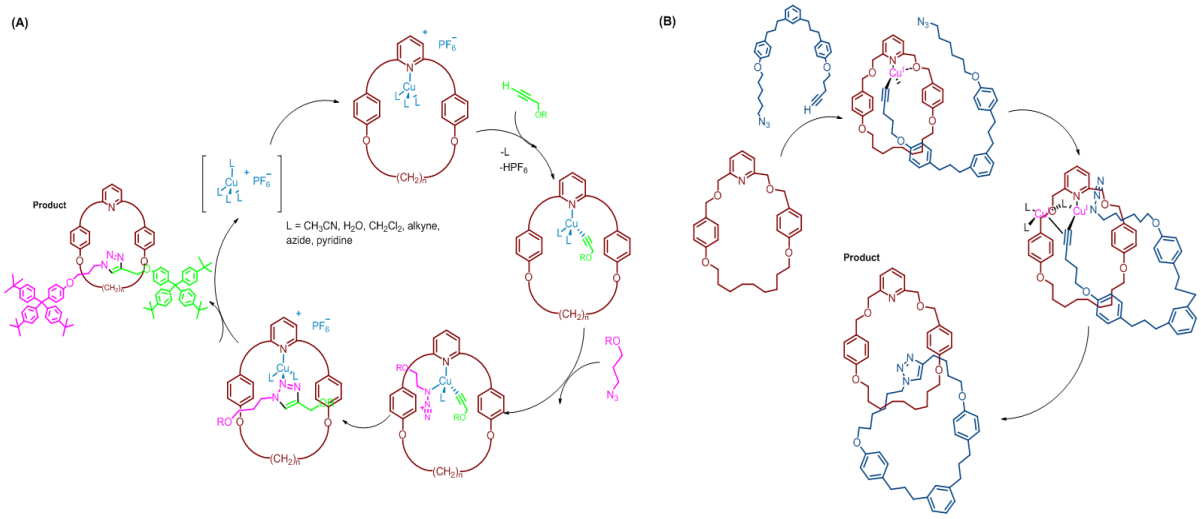

Figure 1.4. Schematic synthetic representations of (A) rotaxane,[27] and (B) catenane.[28]

A concept of bioorthogonal chemistry, focusing reactions in living systems, has many overlapped portions with click chemistry.[29] It emphasizes biological inertness and compatibility with basis of high yield, selectivity, and speed. Those chemistry have shown great performance in bioconjugate chemistry which makes covalent bonds *in vivo* or *in vitro* between chemicals and biomolecular frameworks to study cellular events by tracking biomolecular probes, and make enhanced or multifunctional complexes. Various biomolecules including protein, glycans, lipids, genes, or even cells are candidates to be conjugated in reaction toolbox (e.g., Staudinger ligation, aldehyde condensation, CuAAC, SPAAC, Diels-Alder reaction) with profound consideration of purposes, selectivity, toxicity, rate, and circumstances.

After choosing suitable reaction, next step is an installation of biorthogonal motifs to biomolecules among several methods. Direct chemical modification is a straightforward method introducing biorthogonal motifs directly. Introduction of linkers is also an alternative method linking amino acid residues (e.g., lysine, cysteine) and clickable functional groups.[30] *N*-hydroxysuccinimide (NHS) could connect between lysine and orthogonal motif, and maleimide could connect cysteine and corresponding

motif.[31] Non-specific modification because of their intrinsic abundance is a critical issue. Other option is introduction of unnatural amino acids. Amino acids having orthogonal motifs could be expressed through solid-phase peptide synthesis or metabolic labeling. Unnatural amino acid–specific mutant aminoacyl-tRNA synthetase (UAARS)/tRNA pairs help mutagenesis with genetically encoded amino acids. Techniques have been developed to widen substrates starting from small functional groups to large motifs, cyclooctynes.[32,33]

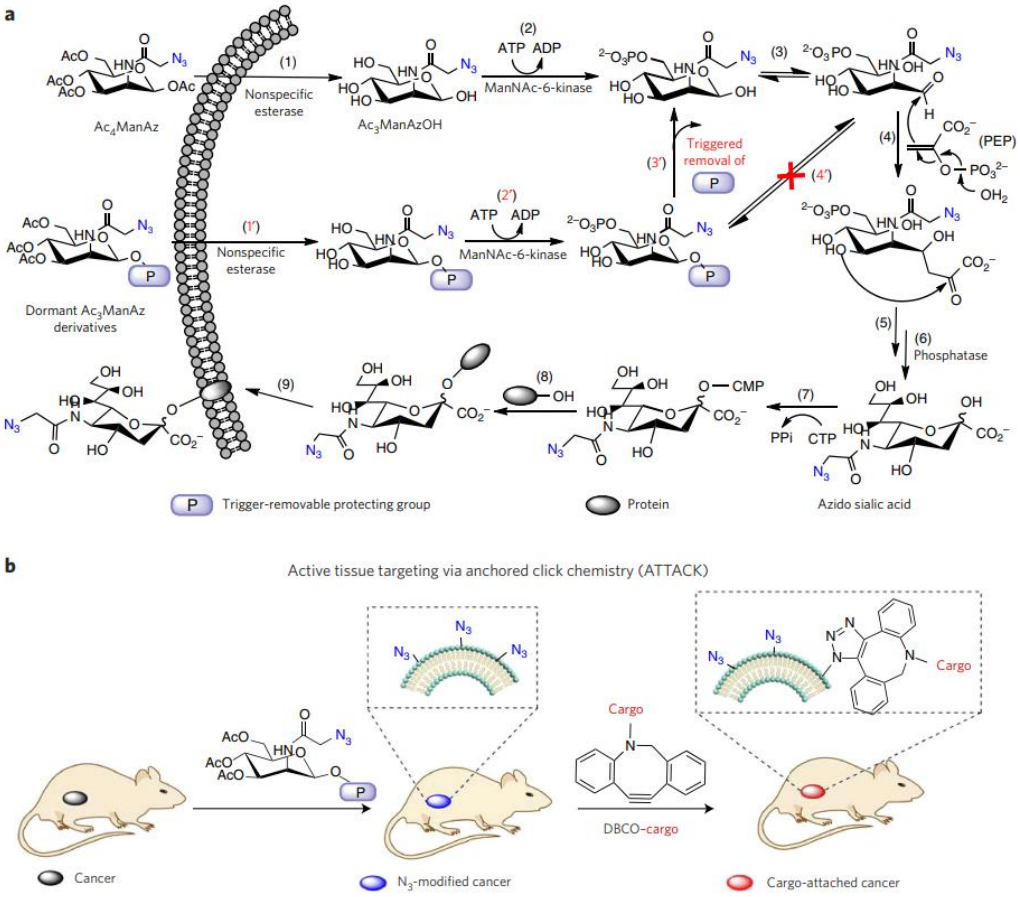

Figure 1.5. Schematic representation of metabolic labeling and SPAAC.[34]

By the metabolic engineering, unnatural moieties could be introduced onto cell surface easily. Figure 1.5 showed metabolic labeling of tetra acetyl-N-azidoacetylmannosamine.[34] With the skillful derivative preparation, chemical reporters could be decorated only on tumor cell. SPAAC including cargoes such as drugs or dyes are conjugated specifically on the cell surfaces having azides, and complete target delivery process.

1.2. 1,2,3-triazoles

1,2,3-triazoles are five-membered heterocycles, containing three nitrogen and two carbon atoms. Aromatic cores are chemically stable towards hydrolysis, oxidative, and reductive conditions. A hydrogen bond donor (C-H bond in a triazole) and two hydrogen bond acceptors (lone pairs of nitrogen in a triazole) induce high dipole moments,[35,36] resulting in strong hydrogen bonds and π stacking interactions. There are many examples employing corresponding properties in functional material synthesis[37-40] and especially on medicinal chemistry. 1,2,3-triazoles are representative non-classical bioisosters of the amide group (Figure 1.6).[41-43] 1,4-disubstituted triazoles have slightly longer distance and strong dipole moments compared to *trans* amide bonds, but their resembled structures motivated triazoles as potential surrogates of corresponding amides. Similar relationship exists between 1,5-disubstituted triazoles and *cis* amide bonds. Figure 1.6B shows synthetic attempts in peptidomimetics to surrogate amino acids by artificial conjugation.[44-47] There are several synthetic 1,2,3-triazoles for amide-bond isosteres, and bioactive molecules for anti-cancer, anti-viral, anti-bacterial, anti-microbial activities. (Figure 1.7 and 1.8).[48,49]

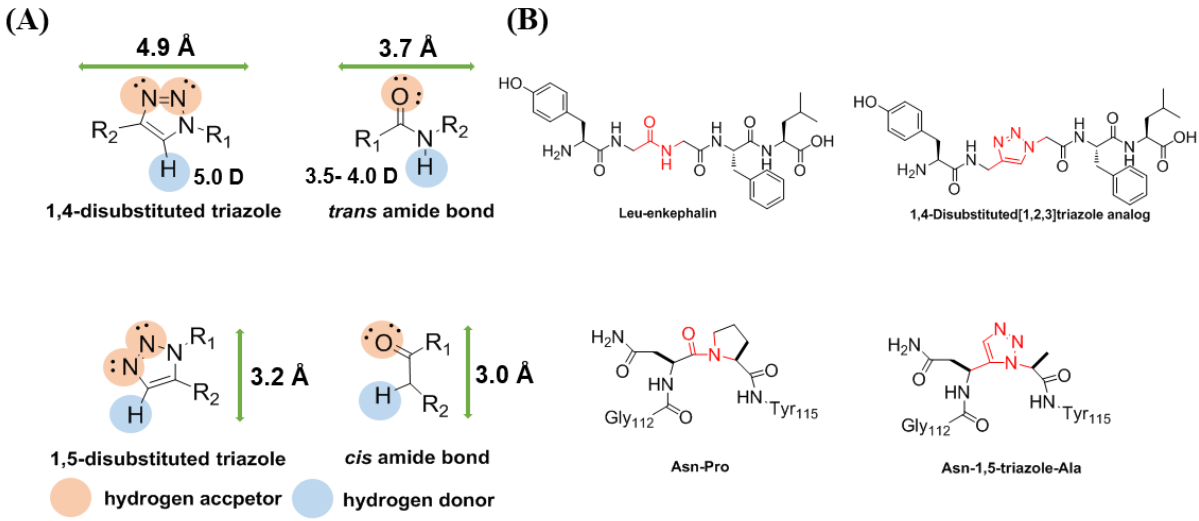

Figure 1.6. (A) Structures of 1,4- and 1,5-disubstituted triazoles, and *trans* and *cis* amide bonds. (B) Examples of surrogating peptide bonds to triazoles.[44,45]

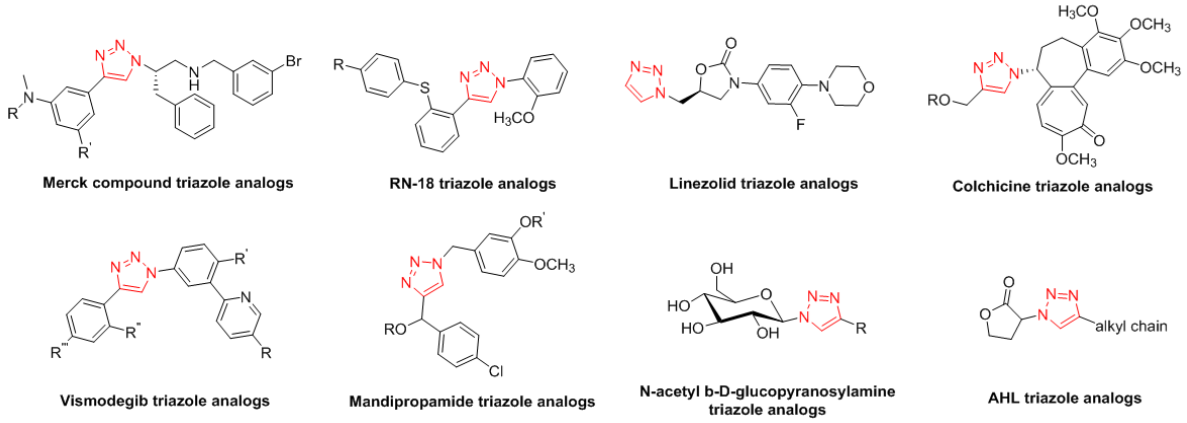

Figure 1.7. Structures of 1,2,3-triazoles to depict amide bonds.[48]

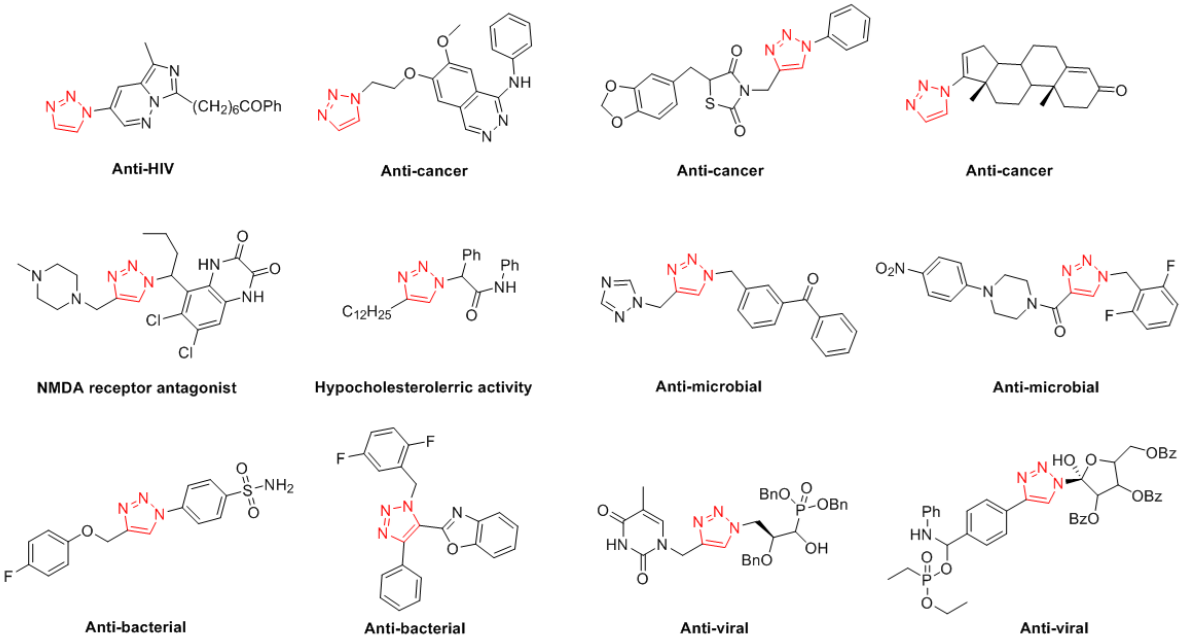

Figure 1.8. Examples of 1,2,3-triazoles eliciting high bio-activities.[49]

Lots of versatile potential of the 1,2,3-triazole motifs elicits the development of facile synthetic methods conducted under simple reagents and conditions. Azides and alkynes are universal building blocks to access 1,2,3-triazoles, leading to massive progress over 50 years (Figure 1.9). Huisgen cycloaddition is almost firstly established approach by Rolf Huisgen in 1960s.[50,51] Triazoles could be formed by simple heating two starting materials, but reaction has suffered from poor selectivity, generating 1,4-disubstituted isomers and corresponding 1,5-isomers as 1 : 1 ratio. Strategies using metal catalysts could conquer the challenging regiocontrol, producing pure 1,4-isomers by copper, and 1,5-isomers by ruthenium.

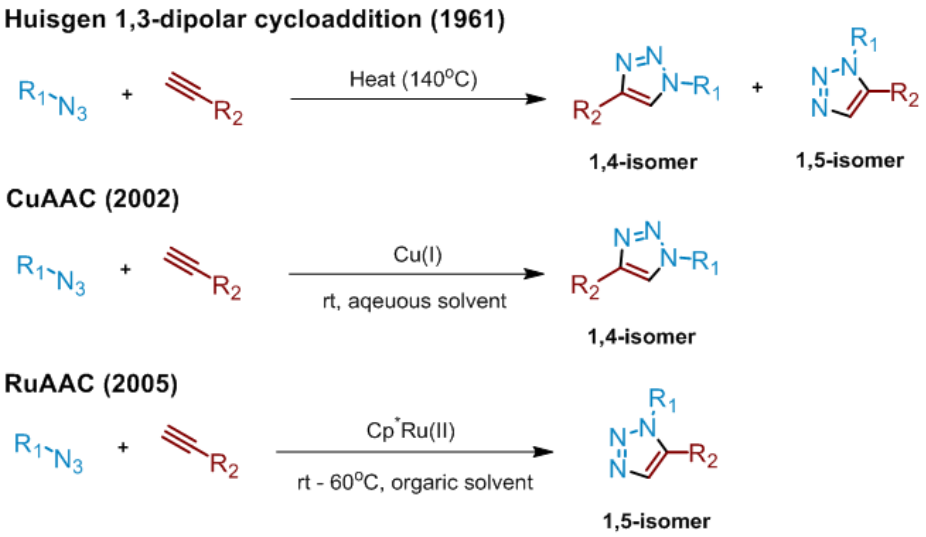

Figure 1.9. Remarkable synthetic approaches in azide−alkyne cycloaddition.

1.2.1. Synthesis of 1,4-disubstituted 1,2,3-triazoles

To access 1,4-disubstituted triazoles, there are two main streams utilizing metal catalysts or metal free approaches to avoid toxicity of the metal. In metal-free methodology, Amine and α,α-dichlorotosylhydrazone can be conjugated by the help of base, or I_2 and *tert*-butyl peroxybenzoate (TBPB), encouraged from Sakai reaction.[52-54] Enamine/enolate (in situ generated by mixing aldehyde and secondary amine/tertiary amine) also induce cross coupling with aryl azides under mild conditions.[55,56] These approaches are suffered from the narrow substrate scope. For general and handy manipulation, different metal catalysts are screened to develop an alternative methodology.

As I mentioned above, CuAAC has become popular in various disciplines because of their convenience and effectivity. Figure 1.10 portraits proposed mechanistic cycles based on density functional theory (DFT) calculation and experimental evidence about intermediates.

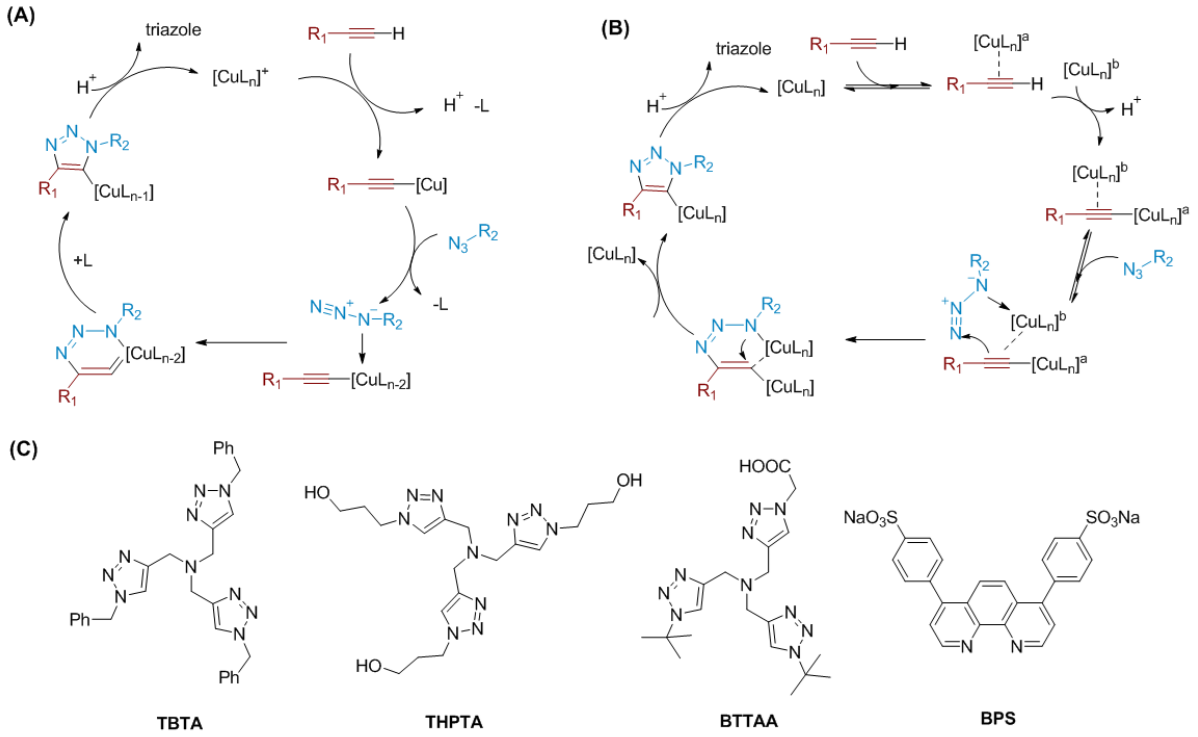

Figure 1.10. Proposed mechanism of CuAAC explained by (A) mononuclear and (B) dinuclear copper intermediate, (C) Representative water soluble chelating ligands.

Reactive copper(I)-acetylides are conjugated with organic azide, following formation of 1,4-disubstituted triazoles, but the matter is numbers of copper participated in. At the early stage, trials to explain CuAAC with one copper metal were predominant. It's quite straightforward process, substituting a copper complex by deprotonation of the alkyne in the presence of base.[14,57] However later studies based on kinetic study,[58] and mass analysis[59] suggested the possibility that two different copper centers are participated as σ-bound ligand and π-complexation during CuAAC.[60] Weak π-complexation could help decrease of electron density of copper-acetylide, overcoming an activation barrier. Valery V. Fokin showed experimental evidence that existence of exogenous copper(I) could elicit azide and copper-acetylide conjugation.[61] But it's still dangerous to select dinuclear mechanism as the only answer because there is an opposite example, explained by mononuclear pathway.[62]

Copper(I) salts catalyze azide−alkyne cycloaddition under the inert atmosphere and organic solvents. To facilitate copper-acetylide complex and stabilization, nitrogen bases such as trimethylamine, 2,6-lutidine, and *N*,*N*-diisopropylethylamine are mandatory, even if homo-coupled alkynes are formed as side products. There are many examples utilizing copper such as CuI,[13] CuBr,[63] $[CuBr•SMe_2]_2$,[64] and CuTC.[65] *In situ* preparation of copper(I) species by mixing copper(II) metals $CuSO_4•5H_2O$ and reducing agents, sodium ascorbate could supply opportunity to relieve the efforts to exclude air and moisture. Application to aerobic conditions are performed with addition of chelating ligands based on tris(triazolymethyl)amine derivatives and sulfonated bathophenanthrolines, which stabilize oxidation state of copper(I) metal, and accelerate cycloaddition reactions (Figure 1.10C).[66-69]

$Cu(OAc)_2$ are potential surrogates of $CuSO_4$ in certain circumstances. On the basis of two precedent observations that copper(II) become active copper(I) in alcoholic media[70] and copper(II) complex could preferably chelated to azide having auxiliary nitrogen donors, 2-picolylazide and alkynes are conjugated exceptionally rapidly in catalytic $Cu(OAc)_2$ and alcohol solvents.[71,72] Furthermore, chemoselective sequential CuAAC could be easily accomplished under mild conditions (Figure 1.11).[73]

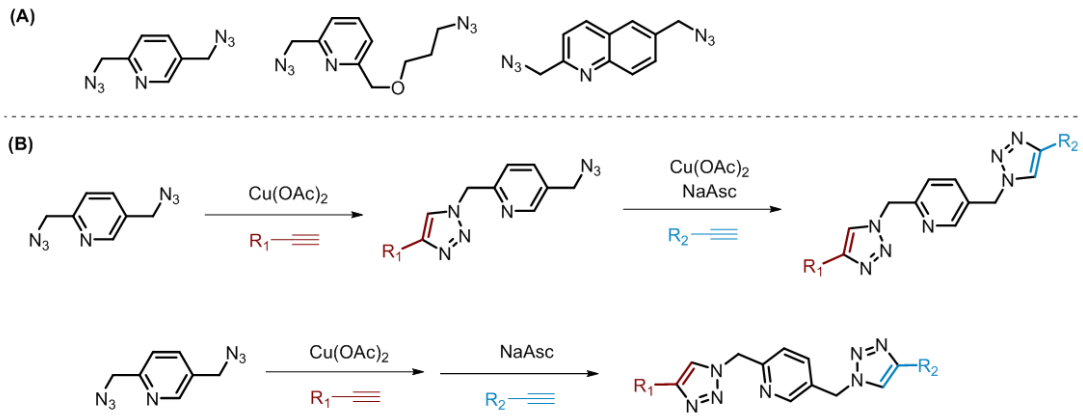

Figure 1.11. (A) Unsymmetrical biazide preparation. (B) Schematic representation of sequential CuAAC.

Wide investigation to surrogate copper metal found different metals such as gold (on Au(111)),[74] ruthenium (e.g., $RuH_2(CO)(PPh_3)_3$, $RuCl_2(PPh_3)_3$),[75,76] and Raney nickel.[77] Silver catalyzed azide−alkyne cycloaddition (AgAAC) showed remarkable results.[78,79] Silver(I) metal-P,O ligand complex (AgOAc with 2-diphenylphosphino-*N*,*N*,-diisopropylcarboxamide) could induce deprotonation of alkyne, resulting in silver(I) acetylide. After that, similar mechanistic pathway could

be drawn as copper cycles. Combination of $AgN(CN)_2$ and *N*,*N*-diisopropylethylamine (DIPEA) relieved reaction conditions with the broad substrate scope under water/ethylene glycol co-solvents.[80]

1.2.2. Synthesis of 1,5-disubstituted 1,2,3-triazoles

Traditionally, metal acetylides, formed by stoichiometric lithium, magnesium, or zinc addition, could be cyclized with organic azide under inert atmosphere.[81-83] But huge amounts of byproduct and harsh reaction conditions strongly require enhanced methodology to access 1,5-disubstituted triazoles. Various methodology have competed and challenged to get the title "biocompatible" by escaping usage of heavy metal. By mimicking *cis*-locked amide bonds, polymer-bound α-keto stabilized phosphorus ylides could spontaneously conjugate aryl azides.[84,85] High yield, selectivity, and exclusion of artificial alkyne are advantageous, but poor functional group tolerance on azide has limited its widespread application. In 1,5-diaryl-substituted 1,2,3-triazole preparation, base promoted azide alkyne cycloaddition could be best option with high yield, and no byproduct. Aryl acetylenes become aryl acetylides with hydroxide or alkoxide in DMSO, following nucleophilic attacks on aryl azides to form triazoles. There is a multicomponent cascade reaction of amine, propynone, tosyl azide, and base by Michael addition/deacylative diazo transfer/cyclization sequence.[86]

Compared to CuAAC, there were no general methods in exclusive preparation of 1,5-disubstituted triazoles. In 2005, ruthenium-catalyzed azide−alkyne cycloaddition (RuAAC) was founded by Valery V. Fokin and Guochen Jia.[87] After screening various ruthenium(II) metals, they found pentamethyl-cyclopentadienyl ruthenium complex (e.g., $Cp^*RuCl(PPh)_3$, $Cp^*RuCl(COD)$, $[Cp^*RuCl]_4$) catalyzed cross coupling, showing functional group tolerance with high yield and selectivity. Continuous studies have extend a substrate scope and reaction conditions, including catalyst species, amounts (1% to 10%), temperature (rt to 80℃), and solvents (e.g., benzene, dioxane, THF, DMF).[88-93]

Both computational calculation based on DFT and experimental analysis including NMR, MS, XRD have complementary supported proposed RuAAC mechanism (Figure 1.12).[88,94] Alkynes and azides are introduced by displacement of two spectator L type ligands forming intermediate **a** with electron-rich ligand Cp^*, which stabilizes higher formal oxidation states. Figure 1.12B represents four possible metal complexes in alkyne and azide coordination. Complex **a** is a most favored orientation, when electronic and steric issues are considered, resulting lowest-energy pathway calculation. Following oxidative coupling to form a ruthenacycle and reductive elimination could finish the catalytic cycle of RuAAC. Steven P. Nolan suggested systemic study of general unsaturated 16 electrons ruthenium complex $Cp^*Ru(L)X$.[95] They provided guidelines in choosing L- and X-type ligands that phosphine ligands are

more helpful compared to NHC ligands and Cl^- group dramatically accelerates reaction rates.

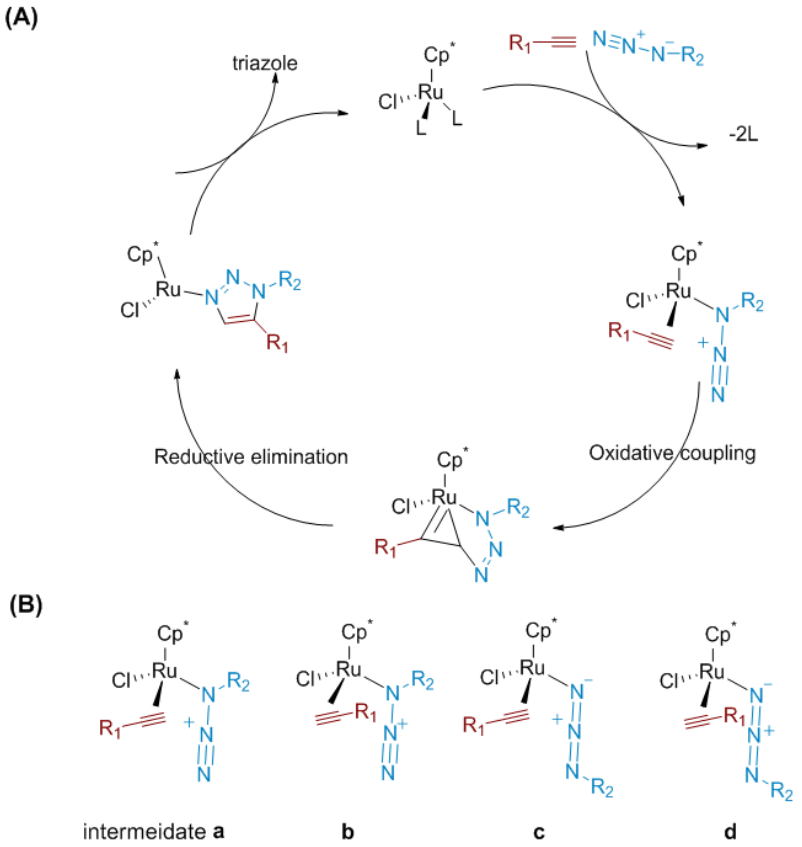

Figure 1.12. Proposed mechanism of RuAAC of (A) whole catalytic cycle and (B) possible orientation of azide and alkyne coordination.

Polymer chemistry gets benefits from methodological studies in preparation of 1,5-disubstituted triazoles. RuAAC produces 1,5-isomer structures, different from corresponding CuAAC products, eliciting various polymer structures. Building blocks such as two terminal alkynes and two azides could form triazoles under elevated temperatures. Hyperbranched structures by cross coupling are also reported, but loading different cargoes in polymer is still at the initial stage (Figure 1.13).[96-98] RuAAC also promotes vigorous investigations in pharmacophores based on target-oriented and diversity-oriented approaches. But in comparison with CuAAC, harsh conditions (e.g., temperature, aprotic solvent) suppressed its active applications in interdisciplinary researches.

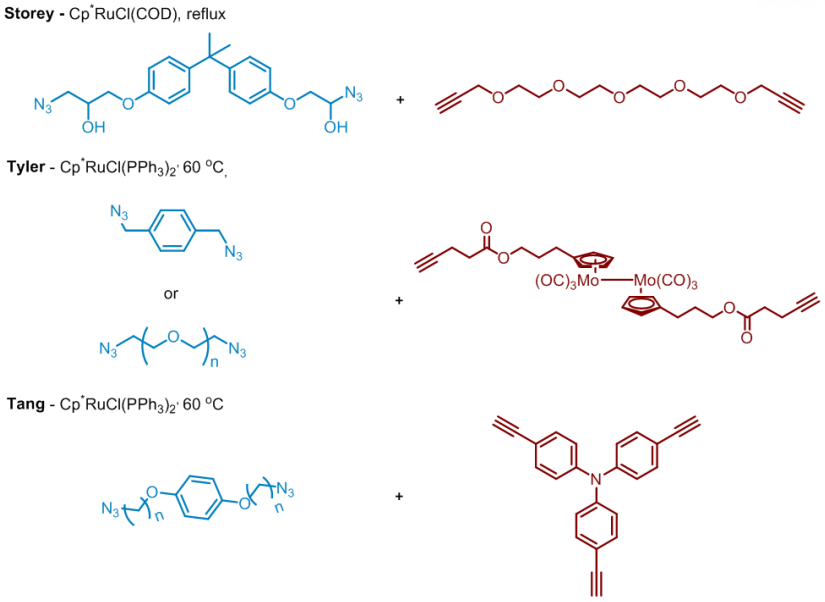

Figure 1.13. Examples of polymerization via RuAAC.

1.3. References

1. Kolb, H. C., Finn, M. G., Sharpless, K. B. *Angew. Chem. Int. Ed.* **2001**, 40, 2004-2021.

2. Kim, Y., Ha, H.-J., Yun, S. Y., Lee, W. K. *Chem. Commun.* **2008**, 4363-4365.

3. Kumaraswamy, G., Ankamma, K., Pitchaiah, A. *J. Org. Chem.* **2007**, 72, 9822-9825.

4. Lin, P.-y., Bellos, K., Stamm, H., Onistschenko, A. *Tetrahedron* **1992**, 48, 2359-2372.

5. Dirksen, A., Dawson, P. E. *Bioconjugate Chem.* **2008**, 19, 2543-2548.

6. Bahta, M., Liu, F., Kim, S.-E., Stephen, A. G., Fisher, R. J., Burke Jr, T. R. *Nature Protoc.* **2012**, 7, 686-702.

7. Kölmel, D. K., Kool, E. T. *Chem. Rev.* **2017**, 117, 10358-10376.

8. Collins, J., Xiao, Z., Müllner, M., Connal, L. A. *Polym. Chem.* **2016**, 7, 3812-3826.

9. Mather, B. D., Viswanathan, K., Miller, K. M., Long, T. E. *Prog. Polym. Sci.* **2006**, 31, 487-531.

10. Hoyle, C. E., Bowman, C. N. *Angew. Chem., Int. Ed.* **2010**, 49, 1540-1573.

11. Nicolaou, K. C., Snyder, S. A., Montagnon, T., Vassilikogiannakis, G. *Angew. Chem. Int. Ed.* **2002**, 41, 1668-1698.

12. Franc, G., Kakkar, A. K. *Chem – Eur. J.* **2009**, 15, 5630-5639.

13. Tornøe, C. W., Christensen, C., Meldal, M. *J. Org. Chem.* **2002**, 67, 3057-3064.

14. Rostovtsev, V. V., Green, L. G., Fokin, V. V., Sharpless, K. B. *Angew. Chem. Int. Ed.* **2002**, 41, 2596-2599.

15. Agard, N. J., Prescher, J. A., Bertozzi, C. R. *J. Am. Chem. Soc*. **2004**, 126, 15046-15047.

16. Dommerholt, J., Rutjes, F. P. J. T., van Delft, F. L. *Top. Curr. Chem.* **2016**, 374, 16-35.

17. Mbua, N. E., Guo, J., Wolfert, M. A., Steet, R., Boons, G.-J. *ChemBioChem* **2011**, 12, 1912-1921.

18. Rim, C., Son, D. Y. *Tetrahedron Lett.* **2009**, 50, 4161-4163.

19. Rissing, C., Son, D. Y. *Organometallics* **2008**, 27, 5394-5397.

20. Wu, P., Feldman, A. K., Nugent, A. K., Hawker, C. J., Scheel, A., Voit, B., Pyun, J., Fréchet, J. M. J., Sharpless, K. B., Fokin, V. V. *Angew. Chem. Int. Ed.* **2004**, 43, 3928-3932.

21. Sumerlin, B. S., Vogt, A. P. *Macromolecules* **2010**, 43, 1-13.

22. Qin, A., Lam, J. W. Y., Tang, B. Z. *Macromolecules* **2010**, 43, 8693-8702.

23. Ballardini, R., Balzani, V., Credi, A., Gandolfi, M. T., Venturi, M. *Acc. Chem. Res.* **2001**, 34, 445-455.

24. Erbas-Cakmak, S., Leigh, D. A., McTernan, C. T., Nussbaumer, A. L. *Chem. Rev.* **2015**, 115, 10081-10206.

25. Grubbs, R. H. *Angew. Chem. Int. Ed.* **2006**, 45, 3760-3765.

26. Aucagne, V., Hänni, K. D., Leigh, D. A., Lusby, P. J., Walker, D. B. *J. Am. Chem. Soc.* **2006**, 128, 2186-2187.

27. Aucagne, V., Berná, J., Crowley, J. D., Goldup, S. M., Hänni, K. D., Leigh, D. A., Lusby, P. J., Ronaldson, V. E., Slawin, A. M. Z., Viterisi, A., Walker, D. B. *J. Am. Chem. Soc.* **2007**, 129, 11950-11963.

28. Goldup, S. M., Leigh, D. A., Long, T., McGonigal, P. R., Symes, M. D., Wu, J. *J. Am. Chem. Soc.* **2009**, 131, 15924-15929.

29. Prescher, J. A., Bertozzi, C. R. *Nat. Chem. Biol.* **2005**, 1, 13-21.

30. van Dongen, S. F. M., Teeuwen, R. L. M., Nallani, M., van Berkel, S. S., Cornelissen, J. J. L. M., Nolte, R. J. M., van Hest, J. C. M. *Bioconjugate Chem.* **2009**, 20, 20-23.

31. Baslé, E., Joubert, N., Pucheault, M. *Chemistry & Biology* **2010**, 17, 213-227.

32. Liu, C. C., Schultz, P. G. *Annu. Rev. Biochem.* **2010**, 79, 413-444.

33. Yu, Z., Pan, Y., Wang, Z., Wang, J., Lin, Q. *Angew. Chem. Int. Ed.* **2012**, 51, 10600-10604.

34. Wang, H., Wang, R., Cai, K., He, H., Liu, Y., Yen, J., Wang, Z., Xu, M., Sun, Y., Zhou, X., Yin, Q., Tang, L., Dobrucki, I. T., Dobrucki, L. W., Chaney, E. J., Boppart, S. A., Fan, T. M., Lezmi, S., Chen, X., Yin, L., Cheng, J. *Nat. Chem. Biol.* **2017**, 13, 415-424.

35. Abboud, J.-Luis M., Foces-Foces, C., Notario, R., Trifonov, Rostislav E., Volovodenko, Anna P., Ostrovskii, Vladimir A., Alkorta, I., Elguero, J. *Eur. J. Org. Chem.* **2001**, 3013–3024.

36. "4.01-1,2,3-Triazoles": W.-Q. Fan, A. R. Katritzky in Comprehensive Heterocyclic Chemistry II: Five-Membered Rings with More than Two Heteroatoms and Fused Carbocyclic Derivatives, Vol. 4

(Eds.: A. R. Katritzky, C. W. Rees, E. F. V. Scriven), Pergamon, Washington DC, 1996, pp. 1-126.

37. Juríček, M., Kouwer, P. H. J. Rowan, A. E. *Chem. Commun.* **2011**, 47, 8740-8749.

38. Marrocchi, A., Facchetti, A., Lanari, D., Santoro, S., Vaccaro, L. *Chem. Sci.* **2016**, 7, 6298-6308.

39. Bakhshi, H., Yeganeh, H., Mehdipour-Ataei, S., Solouk, A., Irani, S. *Macromolecules* **2013**, 46, 7777-7788.

40. Díaz, D. D., Cid, J. J., Vázquez, P., Torres, T. *Chem. - Eur. J.* **2008**, 14, 9261-9273.

41. Bock, V. D., Hiemstra, H., van Maarseveen, J. H. *Eur. J. Org. Chem.* **2006**, 51–68.

42. Tron, G. C., Pirali, T., Billington, R. A., Canonico, P. L., Sorba, G., Genazzani, A. A. *Med. Res. Rev.* **2008**, 28, 278-308.

43. Chow, H.-F., Lau, K.-N., Ke, Z., Liang, Y., Lo, C.-M. *Chem. Commun.* **2010**, 46, 3437-3453.

44. Proteau-Gagné, A., Rochon, K., Roy, M., Albert, P.-J., Guérin, B., Gendron, L., Dory, Y. L. *Bioorganic Med. Chem. Lett.* **2013**, 23, 5267-5269.

45. Tam, A., Arnold, U., Soellner, M. B., Raines, R. T. *J. Am. Chem. Soc.* **2007**, 129, 12670-12671.

46. Bachl, J., Mayr, J., Sayago, F. J., Cativiela, C., Díaz *Chem. Commun.* **2015**, 51, 5294-5297.

47. Kracker, O., Góra, J., Krzciuk-Gula, J., Marion, A., Neumann, B., Stammler, H.-G., Nieß, A., Antes, I., Latajka, R., Sewald, N. *Chem. - Eur. J.* **2018**, 24, 953-961.

48. Bonandi, E., Christodoulou, M. S., Fumagalli, G., Perdicchia, D., Rastelli, G., Passarella, D. *Drug Discov. Today* **2017**, 22, 1572-1581.

49. Dheer, D., Singh, V., Shankar, R. *Bioorg. Chem.* **2017**, 71, 30-54.

50. Huisgen, R. *Proc. Chem. Soc.* **1961**, 0, 357-396.

51. Huisgen, R. *Angew. Chem., Int. Ed.* **1963**, 2, 633-645.

52. Sakai, K., Hida, N., Kondo, K. *Bull. Chem. Soc. Jpn.* **1986**, 59, 179-183.

53. van Berkel, S. S., Brauch, S., Gabriel, L., Henze, M., Stark, S., Vasilev, D., Wessjohann, L. A., Abbas, M., Westermann, B. *Angew. Chem., Int. Ed.* **2012,** 51, 5343-5346.

54. Cai, Z.-J., Lu, X.-M., Zi, Y., Yang, C., Shen, L.-J., Li, J., Wang, S.-Y., Ji, S.-J. *Org. Lett.* **2014,** 16, 5108-5111.

55. Ramachary, D. B., Shashank, A. B., Karthik, S. *Angew. Chem.* **2014,** 126, 10588-10592.

56. Jia, Q., Yang, G., Chen, L., Du, Z., Wei, J., Zhong, Y., Wang, J. *Eur. J. Org. Chem.* **2015**, 3435-3440.

57. Himo, F., Lovell, T., Hilgraf, R., Rostovtsev, V. V., Noodleman, L., Sharpless, K. B., Fokin, V. V. *J. Am. Chem. Soc.* **2005**, 127, 210-216.

58. Ahlquist, M., Fokin, V. V. *Organometallics* **2007**, 26, 4389-4391.

59. Iacobucci, C., Reale, S., Gal, J.-F., De Angelis, F. *Angew. Chem., Int. Ed.* **2015**, 54, 3065-3068.

60. Rodionov, V. O., Fokin, V. V., Finn, M. G. *Angew. Chem., Int. Ed.* **2005**, 44, 2210-2215.

61. Worrell, B. T., Malik, J. A., Fokin, V. V. *Science* **2013,** *340* (6131), 457-460.

62. Deraedt, C., Pinaud, N., Astruc, D. *J. Am. Chem. Soc.* **2014**, 136, 12092-12098.

63. Meldal, M. *Macromol. Rapid Commun.* **2008**, 29, 1016-1051.

64. Isobe, H., Fujino, T., Yamazaki, N., Guillot-Nieckowski, M., Nakamura, E. *Org. Lett.* **2008**, 10, 3729-3732.

65. Raushel, J., Fokin, V. V. *Org. Lett.* **2010**, 12, 4952-4955.

66. Wang, Q., Chan, T. R., Hilgraf, R., Fokin, V. V., Sharpless, K. B., Finn, M. G. *J. Am. Chem. Soc.* **2003**, 125, 3192-3193.

67. Hong, V., Steinmetz, N. F., Manchester, M., Finn, M. G. *Bioconjugate Chem.* **2010**, 21, 1912-1916.

68. Soriano del Amo, D., Wang, W., Jiang, H., Besanceney, C., Yan, A. C., Levy, M., Liu, Y., Marlow, F. L., Wu, P., *J. Am. Chem. Soc.* **2010**, 132, 16893-16899.

69. Kaltgrad, E., Sen Gupta, S., Punna, S., Huang, C.-Y., Chang, A., Wong, C.-H., Finn, M. G., Blixt, O. *ChemBioChem* **2007**, 8, 1455-1462.

70. Kirai, N., Yamamoto, Y. *Eur. J. Org. Chem.* **2009**, 1864-1867.

71. Brotherton, W. S., Michaels, H. A., Simmons, J. T., Clark, R. J., Dalal, N. S., Zhu, L. *Org. Lett.* **2009**, 11, 4954-4957.

72. Kuang, G.-C., Michaels, H. A., Simmons, J. T., Clark, R. J., Zhu, L. *J. Org. Chem.* **2010**, 75, 6540-6548.

73. Yuan, Z., Kuang, G.-C., Clark, R. J., Zhu, L. *Org. Lett.* **2012**, 14, 2590-2593.

74. Díaz Arado, O., Mönig, H., Wagner, H., Franke, J.-H., Langewisch, G., Held, P. A., Studer, A., Fuchs, H. *ACS Nano* **2013**, 7, 8509-8515.

75. Liu, P. N., Siyang, H. X., Zhang, L., Tse, S. K. S., Jia, G. *J. Org. Chem.* **2012**, 77, 5844-5849.

76. Liu, P. N., Li, J., Su, F. H., Ju, K. D., Zhang, L., Shi, C., Sung, H. H. Y., Williams, I. D., Fokin, V. V., Lin, Z., Jia, G. *Organometallics* **2012**, 31, 4904-4915.

77. Surya Prakash Rao, H., Chakibanda, G. *RSC Advances* **2014**, 4, 46040-46048.

78. McNulty, J., Keskar, K., Vemula, R. *Chem. - Eur. J.* **2011**, 17, 14727-14730.

79. McNulty, J., Keskar, K. *Eur. J. Org. Chem.* **2012**, 5462-5470.

80. Ali, A. A., Chetia, M., Saikia, B., Saikia, P. J., Sarma, D. *Tetrahedron Lett.* **2015**, 56, 5892-5895.

81. Akimova, G. S., Chistokletov, V. N., Petrov, A. A. *Zh. Org. Khim.* **1968**, 4, 389-394.

82. Krasinski, A., Fokin, V. V., Sharpless, K. B. *Org. Lett.* **2004**, 6, 1237-1240.

83. Smith, C. D., Greaney, M. F. *Org. Lett.* **2013**, 15, 4826-4829.

84. Ahsanullah, Rademann, J. *Angew. Chem., Int. Ed.* **2010**, 49, 5378-5382.

85. Ahsanullah, Schmieder, P., Kühne, R. *Angew. Chem., Int. Ed.* **2009**, 48, 5042-5045.

86. Cheng, G., Zeng, X., Shen, J., Wang, X., Cui, X., *Angew. Chem., Int. Ed.* **2013**, 52, 13265-13268.

87. Zhang, L., Chen, X., Xue, P., Sun, H. H. Y., Williams, I. D., Sharpless, K. B., Fokin, V. V., Jia, G. *J.*

Am. Chem. Soc. **2005**, 127, 15998-15999.

88. Boren, B. C., Narayan, S., Rasmussen, L. K., Zhang, L., Zhao, H., Lin, Z., Jia, G., Fokin, V. V. *J. Am. Chem. Soc.* **2008**, 130, 8923-8930.

89. Pribut, N., Veale, C. G. L., Basson, A. E., van Otterlo, W. A. L., Pelly, S. C. *Bioorg. Med. Chem. Lett.* **2016**, 26, 3700– 3704.

90. Oakdale, J. S., Sit, R. K., Fokin, V. V. *Chem. - Eur. J.* **2014**, 20, 11101– 11110.

91. Shen, Q., Han, E. J., Huang, Y. G., Chen, Q. Y., Guo, Y. *Synthesis* **2015**, 47, 3936– 3946.

92. Chemama, M., Fonvielle, M., Arthur, M., Valery, J. M., Etheve- Quelquejeu, M. *Chem. - Eur. J.* **2009**, 15, 1929–1938.

93. Imperio, D., Pirali, T., Galli, U., Pagliai, F., Cafici, L., Canonico, P. L., Sorba, G., Genazzani, A. A.,Tron, G. C. *Bioorg. Med. Chem.* **2007**, 15, 6748–6757.

94. Boz, E., Tüzün, N. Ş. *J. Orgonmet. Chem.* **2013**, 724, 167-176.

95. Lamberti, M., Fortman, G. C., Poater, A., Broggi, J., Slawin, A. M. Z., Cavallo, L., Nolan, S. P. *Organometallics* **2012**, 31, 756-767.

96. Brei, M. R., Hunter Cooke, R., III, Hanson, D. J., Gray, C. T., Storey, R. F. *J. Macromol. Sci., Part A: Pure Appl.Chem.* **2016**, 53, 413– 423.

97. Brady, S. E., Shultz, G. V., Tyler, D. R. *J. Inorg. Organomet. Polym. Mater.* **2010**, 20, 511– 518.

98. Qin, A. J., Lam, J. W. Y., Jim, C. K. W., Zhang, L., Yan, J. J., Haussler, M., Liu, J. Z., Dong, Y. Q.,Liang, D. H., Chen, E., Jia, G., Tang, B. Z. *Macromolecules* **2008**, 41, 3808– 3822

Chapter II

Covalent Conjugation of Small-Molecule Adjuvants to Nanoparticles Induces Robust Cytotoxic T Cell Responses via DC Activation

2.1. Abstract

Specific recognitions of pathogen associated molecular patterns by Toll-like receptors (TLRs) initiate dendritic cell (DC) activation, which is critical for coordinating innate and adaptive immune responses. Imidazoquinolines as small-molecule TLR7 agonists often suffer from prompt dissemination and short half-life in the bloodstream, preventing their localization to the corresponding receptors and effective DC activation. We postulated that covalent incorporation of imidazoquinoline moieties onto the surface of biocompatible nanoparticles (~30 nm size) would enhance their chemical stability, cellular uptake efficiency, and adjuvanticity. The fully synthetic adjuvant-nanocomplexes led to successful DC activation at lower nanomolar doses compared with free small molecule agonists. Once a model antigen such as ovalbumin was used for immunization, we found that the nanocomplexes promoted an unusually strong cytotoxic T lymphocyte response, revealing their unique immunostimulatory capacity benefiting from multivalency and efficient transport to endosomal TLR7. This chapter is reproduced from *Bioconjugate Chem.* **2016**, 27, 9, 2007-2013.

2.2. Introduction

Dendritic cells (DCs) are the most potent antigen-presenting cells (APCs), which coordinate between the innate and adaptive immune systems.[1] They are specialized to engulf and process antigens and

subsequently present epitopes to elicit robust immune responses.[2–4] APCs express various types of pattern recognition receptors including lectins or TLRs to distinguish between self- and non-self-structures. Recognition of pathogen associated molecular patterns (PAMPs) by TLRs generally induces DC activation.[5–7] Activated DCs present foreign epitopes of antigens onto major histocompatibility complexes (MHCs), and increase the expression of costimulatory molecules (CD80, CD86) to help cognate interaction with T cell receptor (TCR). The expression of chemokine receptor CCR7 leads DCs to migrate into lymph nodes, where naïve T cells are transformed into functional T lymphocytes including cytotoxic T lymphocytes (CTLs).[8,9]

TLR7, located within endosomal compartment, is a promising adjuvant target site for DC-mediated immunization. It recognizes nucleotide-derived compounds, including single-stranded RNA or low-molecular-weight imidazoquinoline derivatives, such as R837 (imiquimod) and R848 (resiquimod).[5,8,10] Yet, promotion of robust CTL responses by small molecule adjuvants is highly challenging due to their prompt dissemination through diffusion.[8,11–13] To overcome these hurdles, polymeric or inorganic nanoparticles (NPs) encapsulating imidazoquinolines have been introduced to enhance stability and biodistribution of TLR7 agonists, consequently improving DC activation efficiency.[14–17] Here, we describe the first synthetic approach for preparing covalently linked imidazoquinoline-nanoconjugates for inducing robust CTL responses (Figure 2.1). Our design can entirely avoid the potential time-based release of small-molecule agonists from the noncovalently functionalized nanocarriers through the interactions between cell membranes and engineered NPs. However, the challenges associated with our approach are twofold. First, the design of nanocomplexes requires multistep reactions to achieve a molecularly well-defined structure. Second, the synthetic nanocomplexes should effectively initiate TLR-mediated DC activation and subsequently induce T cell immunity. To validate our working hypothesis, we designed alkyne-functionalized imidazoquinoline derivatives and covalently conjugated them with biocompatible NPs to examine their role in DC activation and generation of CTL response.

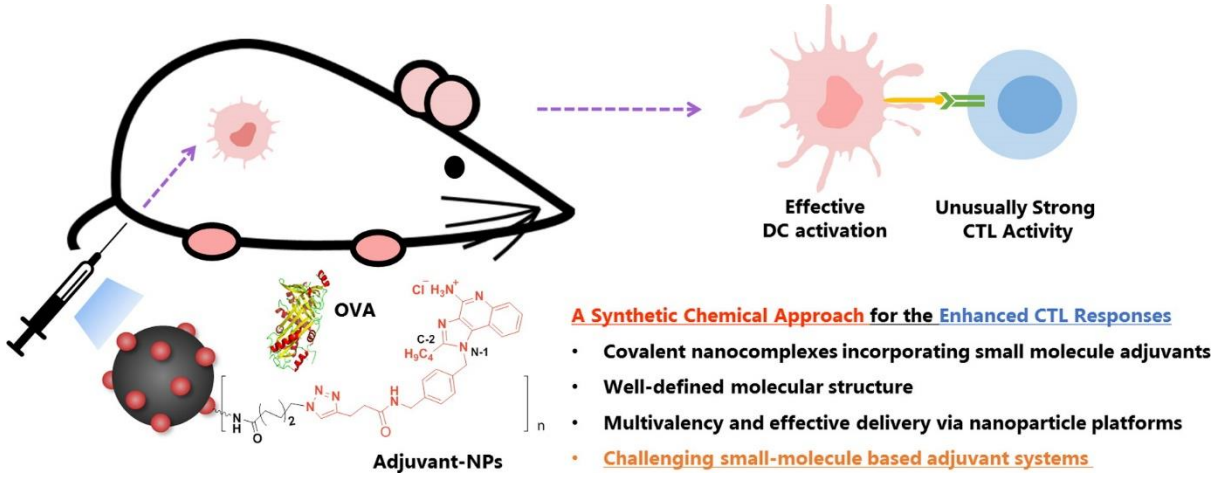

Figure 2.1. General attributes of Adjuvant-NPs in inducing DC activation and a robust CTL response.

2.3. Results and discussion

Although live-attenuated vaccines can elicit long-term immunity, they have a potential risk of infection, and are practically not suitable vaccine candidates against pathogens such as influenza, HIV, or Ebola virus.[18] In contrast, subunit vaccines provide superior safety profiles and allow tunable design at the molecular level to elicit predictable immune responses. However, they are short-lived and poorly immunogenic. Thus, immunostimulatory adjuvants are required to generate potent T cell immunity.[8,18] The advent of engineered nanocomplexes loaded with imidazoquinoline analogues opens up new opportunities to effectively target TLR7, yet investigations have been established on the basis of noncovalent encapsulation chemistry. Although CpG oligodeoxynucleotide-NP complexes have been previously demonstrated,[19,20] NPs covalently incorporating the small-molecule cognate ligands without repeating monomer units have not been reported so far.

To synthesize well-defined molecular adjuvant-nanocomplexes, we designed and prepared an imidazoquinoline analogue (Adjuvant **1**) with a terminal alkyne moiety to couple with azide coated iron oxide NPs (see Figure 2.2a). Adjuvant **2** was synthesized from 2,4-quinolinediol as previously described by the David group.[21−24] Based on the previous structure−activity relationship studies,[21,25−28] n-butyl group was introduced at C-2 position to increase TLR7 agonistic potency. Further, an alkyne functionality as a versatile anchor was placed at N-1 position for next-stage chemical reactions, since the site modification does not significantly compromise agonistic potency. Molecular structure of TLR7 agonist, Adjuvant **1**, was confirmed by ^{1}H and ^{13}C nuclear magnetic resonance (NMR) spectra (Figure 2.2b and c). As a conjugation platform displaying multivalency, water-soluble and surface-engineered iron oxide NPs were selected because of their biocompatibility, facile surface modification, monodisperse size, biomolecule-free structure, and enhanced stability. In addition, they can be potentially applied as multifunctional agents for diagnostic/therapeutic purposes (e.g., magnetic resonance imaging (MRI) or photothermal therapy).[29−34] Biocompatible NPs with monodisperse size ranges of ~30 nm can be used as nanocarriers in vivo, which are optimal for internalization by immature DCs by facilitating endolysosomal pathway, and can be trafficked into the draining lymph nodes, thereby enhancing their adjuvanticity.[11,20,35−38] Amine-surface-modified iron oxide NPs (Amine-NPs) were then reacted with Spacer **3** with an activated ester moiety, to afford Azide-NPs, since azido functionality can be readily installed and is highly orthogonal and versatile for further transformations. Finally, Adjuvant **1** was conjugated by CuI-catalyzed Huisgen 1,3-dipolar cycloaddition reaction, and treated with 0.1 M Tris buffer (pH 6) to form Adjuvant-NPs (for details, see Experimental).

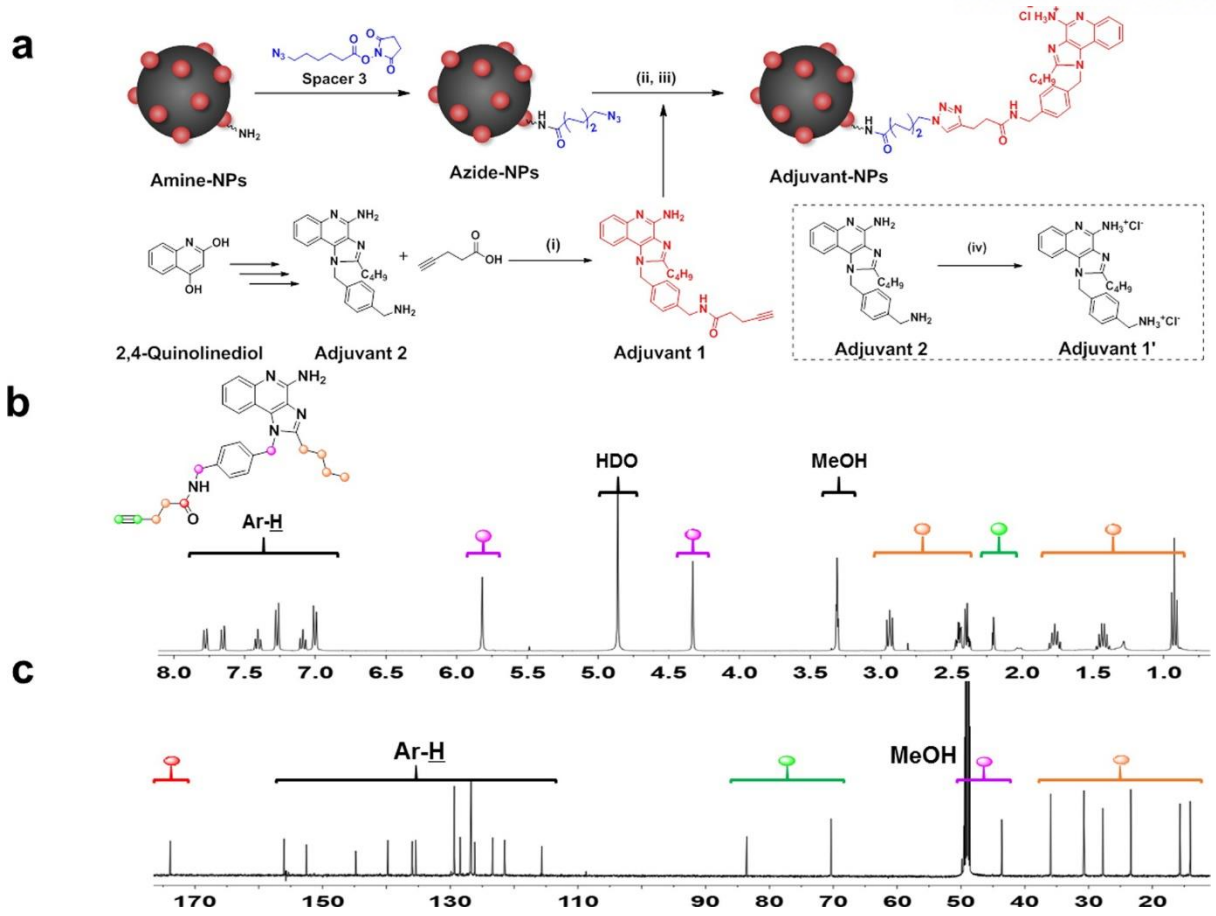

Figure 2.2. Synthetic scheme of Adjuvant-NPs (i) HBTU, TEA, DCM, (ii) $CuSO_4 \cdot 5H_2O$, sodium ascorbate, DMF, (iii) 0.1 M Tris buffer (pH 6), and (iv) diluted hydrogen chloride solution. (b,c) ^{1}H and ^{13}C NMR spectra (MeOD) of Adjuvant **1**.

Core and hydrodynamic sizes of the synthetic nanocomplexes were determined by transmission electron microscopy (TEM) and dynamic light scattering (DLS) analyses, respectively (Figure 2.3a and b). TEM imaging revealed spherical and monodisperse particles with ~11 nm core diameters of Adjuvant-NPs without any signs of particle aggregation, even after multistep chemical modifications. DLS data analysis showed an effective diameter of 31.6 nm and a narrow size distribution with polydispersity index (PDI) = 0.258. Previously NPs having ~30 nm size were demonstrated to be efficiently taken up by DCs.[19,20] Moreover, we carried out spectroscopic studies to examine the effectiveness of imidazoquinoline conjugation. UV−vis spectrum of Adjuvant-NPs showed distinct imidazoquinoline peaks at about 225, 246, and 321 nm with slight peak shifts (Figure 2.3c). To quantify the loading level, a fluorescence assay was conducted (Figure 2.3d), since iron oxide NPs are weakly fluorescent. NHS-fluorescein is an amine reactive fluorescent probe bearing an activated ester moiety, thus, fluorophores

can be appended to Adjuvant-NPs to generate Fluorescein-Adjuvant-NPs. Based on the standard curve of NHS-fluorescein and iron concentration of NPs, the loading amount of imidazoquinolines in Adjuvant-NPs was estimated to be 0.139 μmol/[mg Fe] (Figure 2.12 and 2.13).

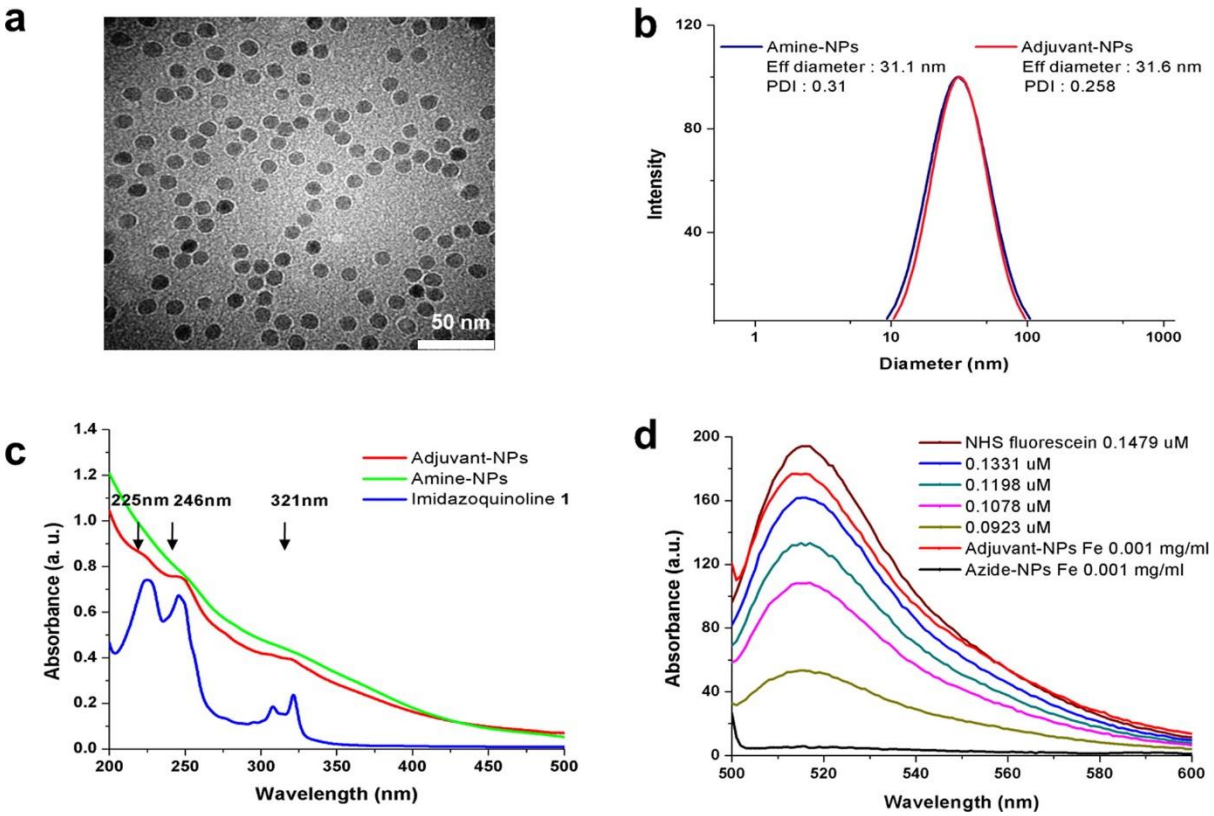

Figure 2.3. Characterization of Adjuvant-NPs. (a) TEM image of Adjuvant-NPs, (b) DLS analysis, (c) UV−vis spectra, and (d) fluorescence spectra.

Further, we evaluated DC activation efficacies by using synthetic TLR7 agonists. Adjuvant-NPs or free Adjuvant **1′** were intraperitoneally injected into mice, and their DCs were harvested 18 h later. DC activation markers including CD80, CD86, MHC I, and CCR7 were stained with phycoerythrin (PE)-conjugated antibodies and analyzed by flow cytometry. R848,[10] Adjuvant-NPs, or Adjuvant **1′** effectively increased the expression levels of the markers (Figure 2.4-2.7). Highly water-soluble Adjuvant **1′** acted as an effective stimulant of DC activation at 115.6 nmol or even at a concentration as low as 69.4 nmol (Figure 2.5). Amine-NPs showed weak self-adjuvant effect (Figure 2.7). Remarkably, 13.9 nmol of Adjuvant-NPs (concentration in loading levels of cognate ligands) and 115.6 nmol of free Adjuvant **1′** induced comparable immunostimulatory activities. This is attributed to the enhanced avidity as well as effective internalization of the nanocomplexes to the endosomal TLR7 of DCs. IL-12p40 is known as one of important pro-inflammatory cytokines secreted from activated DCs to educate naïve $CD8^+$ T cells.[39] The secreted IL-12p40 levels of the Adjuvant-NP treated group were significantly higher than those of groups that were treated with PBS or Amine-NPs (Figure 2.8a). Adjuvant **1′** also induced the production of the secreted IL-12p40 at an almost identical level. To directly detect the antigen-specific $CD8^+$ T cell response, we carried out MHC I tetramer assays and observed increased populations of OT-1 peptide-specific $CD8^+$ T cells in the groups treated with Adjuvant **1′** or Adjuvant-NPs compared to those of Amine-NPs (Figure 2.8b). These data suggested that Adjuvant-NPs induce efficient DC activation leading to the effective presentation of antigenic peptides on MHC I and subsequent antigen-specific CTL effect.

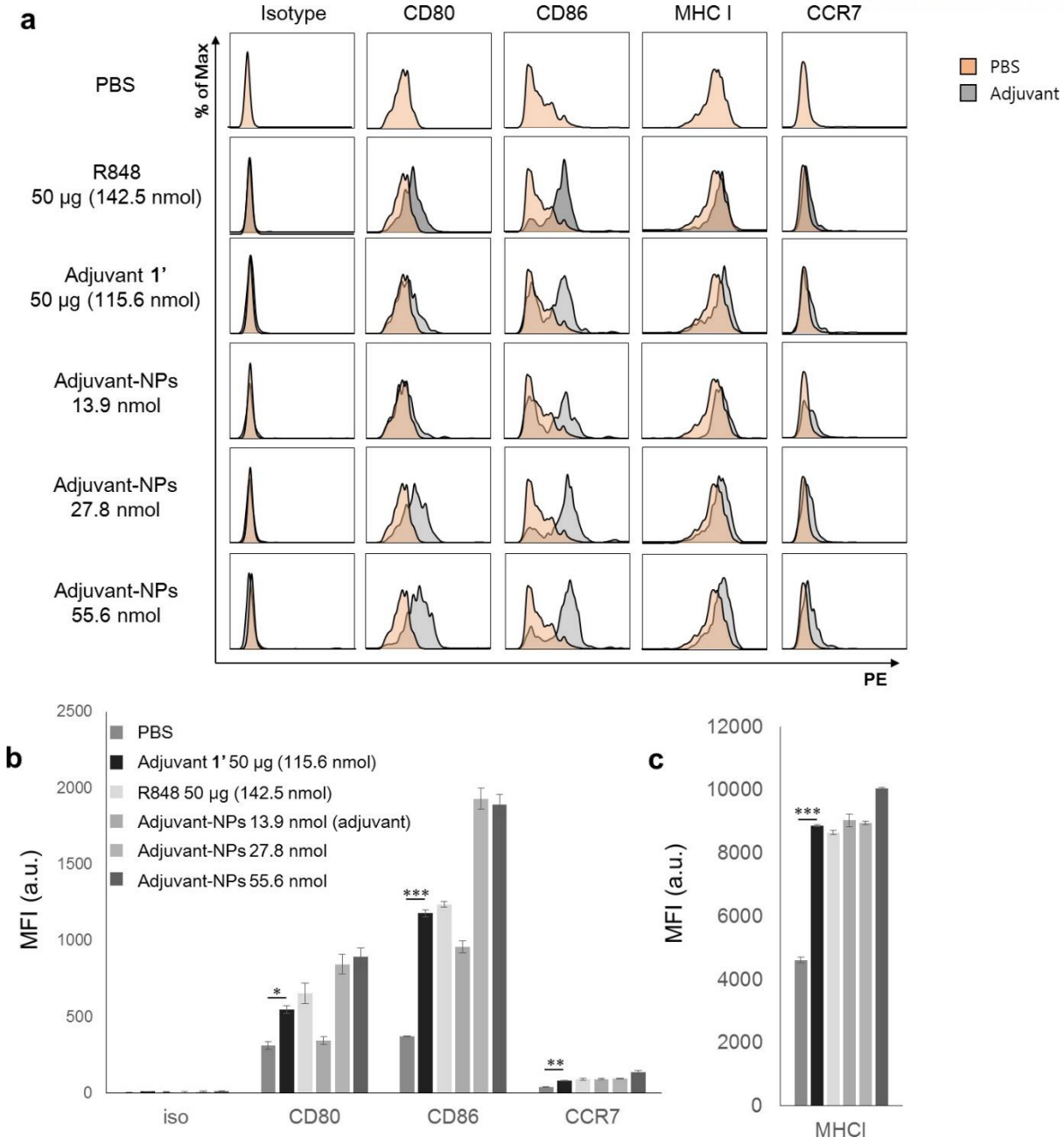

Figure 2.4. Adjuvant effects on in vivo DC activation: (a) flow cytometry analyses, and (b,c) the mean fluorescence intensity (MFI) levels of DC activation markers (CD80, CD86, CCR7, and MHC I). The P values of <0.05(*), <0.01(**), and <0.001(***) were considered significant.

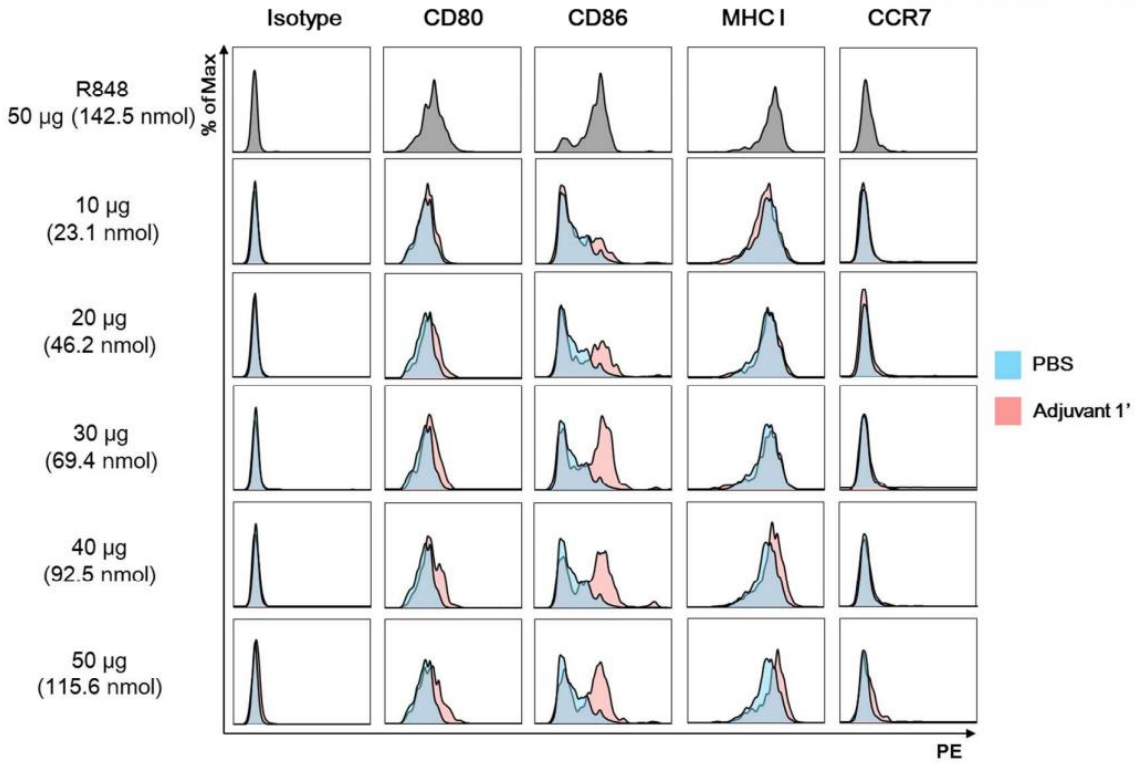

Figure 2.5. DC activation tests at various concentration of Adjuvant **1′**.

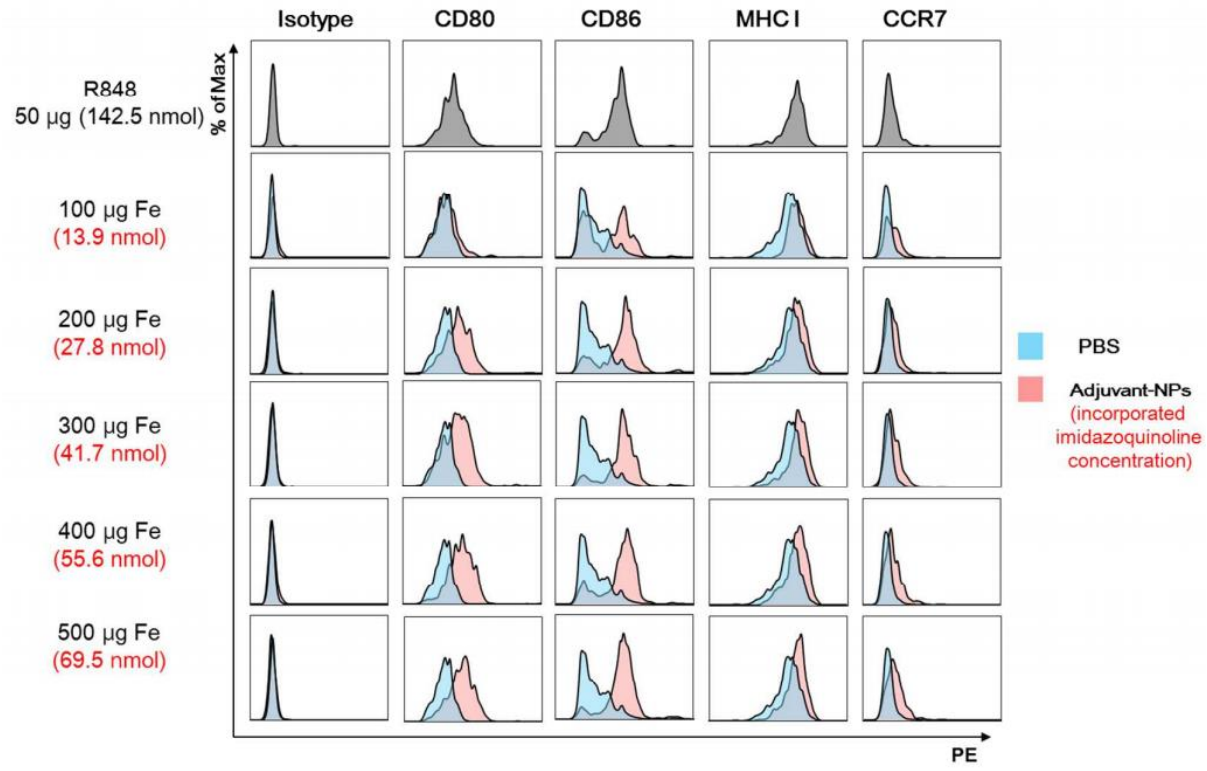

Figure 2.6. DC activation tests at various concentration of Adjuvant-NPs.

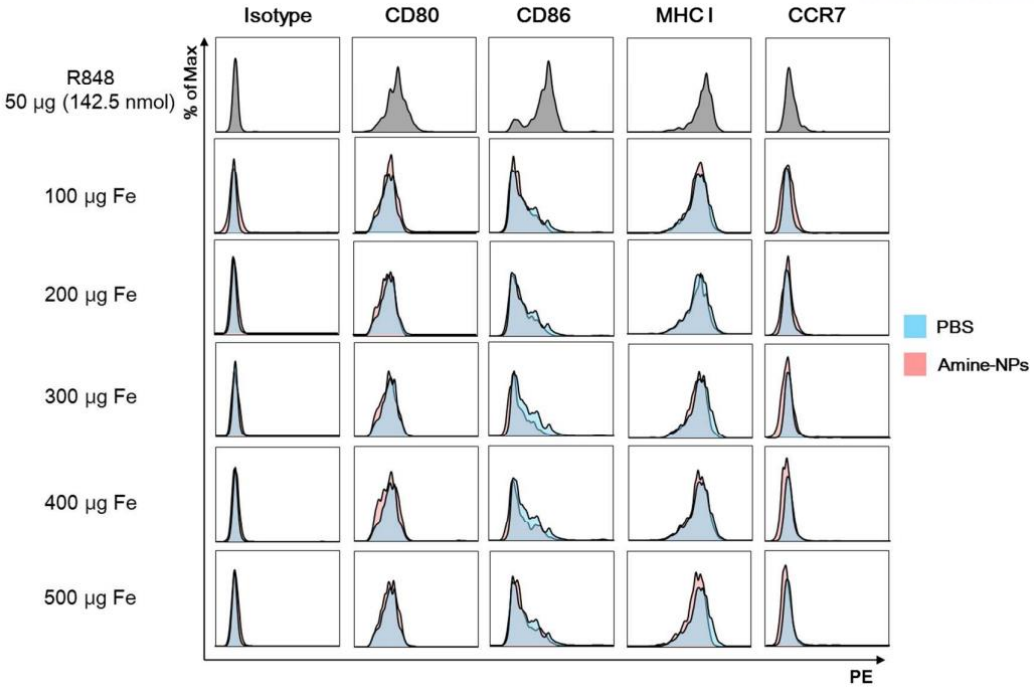

Figure 2.7. DC activation tests at various concentration of Amine-NPs.

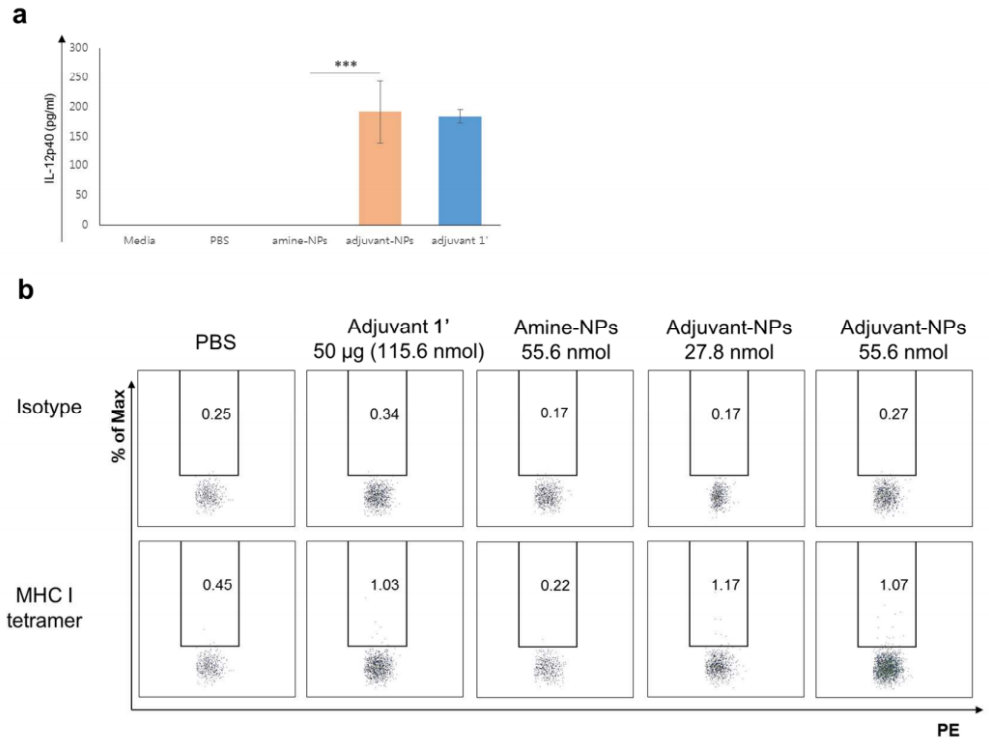

Figure 2.8. (a) IL-12p40 secretion of Adjuvant-NPs in DCs. Samples were analyzed by ELISA after 48 hours culture. The P values < 0.001(***) were considered significant. (b) Flow cytometry analyses of OT-1 peptide specific T cell receptor expressing $CD8^+$ T cells.

Since TLR7 is expressed inside endosomal compartments of DCs, effective delivery of antigens and adjuvants into DCs is indispensable for their proper maturation and subsequent immune response. However, free small molecules hardly localize to TLRs, thus, they require effective delivery vehicles.

To examine cellular internalization of the nanocomplexes and their appropriate localization in DCs, we prepared Fluorescein-Adjuvant-NPs as probes (see Experimental) and studied their uptake using confocal fluorescence microscopy (Figure 2.9a). The complexes were cultured with immature DCs in vitro in the presence of ovalbumin (OVA) as a model antigen. After 18 h, the cells were fixed, and the nuclei and low pH endosomes were stained with DAPI and LysoTracker, respectively. Fluorescent confocal cell images clearly demonstrated that Fluorescein-Adjuvant-NPs were localized within endosomes thanks to their suitable particle size (～30 nm) (Figure 2.9b and 2.10),[19,20] which can assist imidazoquinoline cognate agonists effectively interact with TLR7 within DC endosomes.

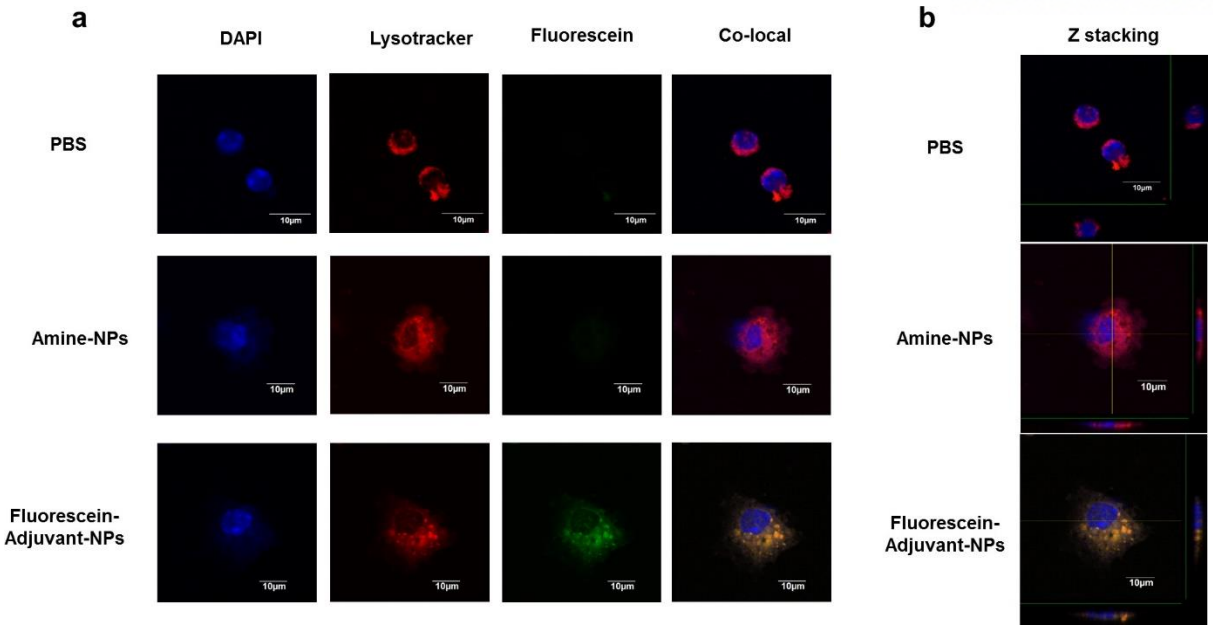

Figure 2.9. (a,b) Fluorescence imaging studies to examine the internalization of Fluorescein-Adjuvant-NPs in DCs. Samples were characterized by confocal fluorescent microscopy.

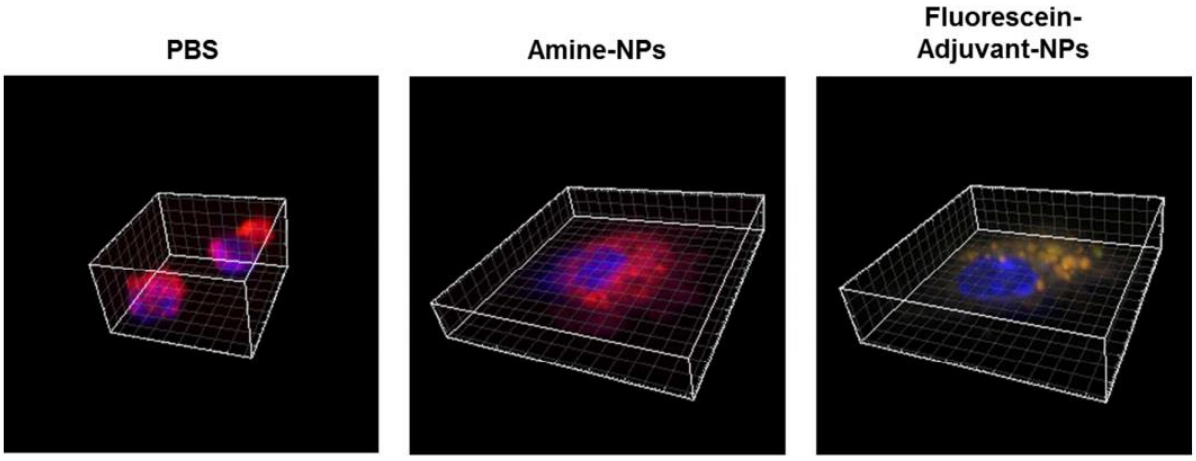

Figure 2.10. Z-stacking 3D Fluorescence images to examine the internalization of Fluorescein-Adjuvant-NPs in DCs.

The efficient DC activation and nanocomplex internalization prompted us to test whether these mature DCs can elicit sufficient cytotoxic $CD8^+$ T cell responses. We performed an in vivo CTL assay based on the carboxyfluorescein diacetate succinimidyl ester (CFSE) assay to monitor OVA-specific T cell proliferation.[40,41] Mice were intraperitoneally immunized with 25 μg of OVA protein as an antigen in

the presence of PBS, R848, Amine-NPs, or Adjuvant-NPs as TLR7 agonists. Groups of mice were primarily immunized for 2 weeks, and additionally boosted for 1 week. After immunization, mice were intravenously injected with 50:50 mixtures of OT-1 peptidepulsed ($CFSE^{hi}$) and unpulsed ($CFSE^{low}$) syngeneic splenocytes to evaluate OVA-specific CTL activity. The population of OT-1 peptide pulsed target cells was analyzed by flow cytometry. It is speculated that if OT-1 specific T cells are effectively stimulated by matured DCs with OVA protein and adjuvants, the percentage of OT-1 peptide-pulsed ($CFSE^{hi}$) syngeneic splenocytes would be lysed and their population decreased because of T cell cytotoxicity (Figure 2.11a). Remarkably, injection of Adjuvant-NPs with 27.8 nmol of adjuvant together with OVA protein caused 84% target cell lysis. In contrast, small-molecule R848 (28.5 or 142.5 nmol) or Amine-NPs showed negligible to poor (0−25%) cytotoxic responses (Figure 2.11b). It is speculated that superior $CD8^+$ T cell efficacy of Adjuvant-NPs at low doses of imidazoquinoline moiety is associated with the enhanced avidity of fully synthesized multivalent Adjuvant-NPs and effective DC internalization.

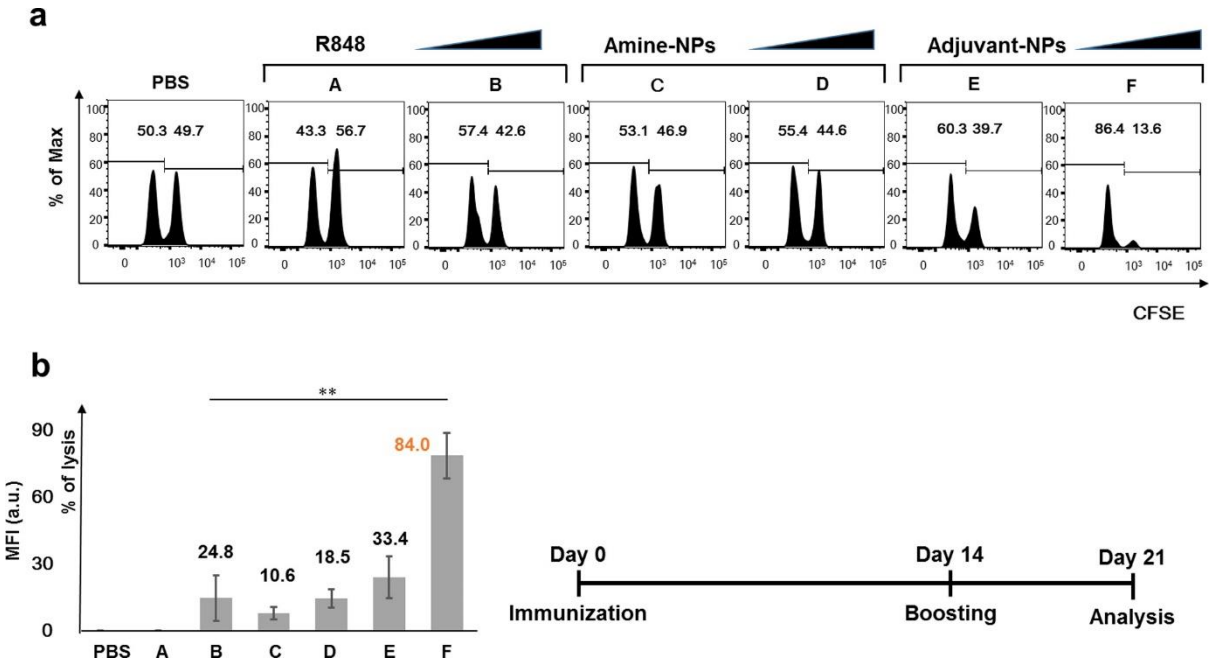

Figure 2.11. In vivo CTL assay on splenocytes. (a) Percentages of OT-1 peptide unpulsed $CFSE^{low}$ (left) and that of pulsed $CFSE^{high}$ (right) were analyzed by flow cytometry. Each group was stimulated with indicated adjuvants: Sample A: R848 10 μg, 28.5 nmol, sample B: R 848 50 μg, 142.5 nmol, sample C: amine-NPs 100 μg Fe, sample D: amine NPs 200 μg Fe, sample E: Adjuvant-NPs (100 μg Fe, 13.9 nmol of imidazoquinoline), sample F: Adjuvant-NPs (200 μg Fe, 27.8 nmol of imidazoquinoline) along with OVA protein. (b) Conversion of the percentages of $CFSE^{high}$ based on the negative control of PBS treated group. The P values of <0.01(**) were considered significant.

2.4. Conclusion

We chemically synthesized structurally well-defined molecular adjuvant-nanoparticle conjugates through multistep reactions and investigated their potency of immunostimulatory activity. The nanocomplexes displaying multiple low-molecular-weight ligands were efficiently internalized by immature DCs, and they subsequently enhanced in vivo DC activation by facilitating multivalent interactions between imidazoquinoline moieties and endosomal TLR7. In addition, they induced increased expression levels of activation markers in the low nanomolar range. Their cellular localization was validated by fluorescent labeling of the nanocomplexes. Co-administration of the synthetic adjuvant-nanocomplexes and OVA protein elicited unusually robust antigen-specific cytotoxic T cell responses. Considering the significant challenges generating cell-mediated immunity via small-molecule based adjuvant systems, we believe that our synthetic approach can provide a versatile platform for the rational designing of next-generation vaccines.

2.5. Experimental

Reagents

N,N,N′,N′-Tetramethyl-*O*-(1*H*-benzotriazol-1-yl)uronium hexafluorophosphate (HBTU, 98%), 4-pentynoic acid (95%), copper(II) sulfate pentahydrate (98%), (+)-sodium L-ascorbate (98%), and *N*-hydroxysuccinimide (NHS, 98%) was purchased from Sigma-Aldrich. Amine-functionalized iron oxide (Fe_3O_4) magnetic nanoparticles (aqueous solution, 5 mg/mL Fe) were supplied by Ocean nanotech. Triethylamine (TEA, 99%) was obtained from Alfa Aesar. NHS-fluorescein (5/6-carboxyfluorescein succinimidyl ester) was purchased from Thermo Scientific.

Instruments

Proton nuclear magnetic resonance and carbon nuclear magnetic resonance spectra were recorded by an Agilent 400-MR DD2 and an Agilent VNMRS 600. Low resolution mass spectra were measured by a Bruker HCT Basic System with electrospray ionization (ESI) source. High resolution mass spectra were measured by an ABI API-3000 ESI mass spectrometer. Fluorescence spectra were measured by using an Agilent Cary Eclipse fluorescence spectrophotometer. UV-Vis spectra were recorded by a Jasco V-670 spectrometer. Dynamic light scattering (DLS) was measure by a Brookhaven Instrument Corporation’s NanoDLS. Transmission electron microscopy (TEM) images were taken by a JEOL JEM-1400.

Synthesis of Adjuvant 1

Adjuvant **2**[21] (400 mg, 1.11 mmol) and TEA (547 μL, 3.89 mmol, 3.5 equiv) were dissolved in DCM (80 mL). 4-Pentynoic acid (142 mg, 1.45 mmol, 1.3 equiv) and HBTU (549 mg, 1.45 mmol, 1.3 equiv) were added at 0 °C, and the solution left to stir overnight at room temperature. The reaction mixture was concentrated in vacuo and the residue was purified by flash column chromatography (DCM:MeOH:NH_4OH = 9.5:0.5:0.1) to yield the title compound as a clear oil (261 mg, 53%). ^{1}H NMR (400 MHz, MeOD) δ_H 0.92 (t, J 7.4 Hz, 3H), 1.42 (dt, J 14.7, 7.4 Hz, 2H), 1.77 (dt, J 15.4, 7.6 Hz, 2H), 2.20 (t, J 2.6 Hz, 1H), 2.34−2.49 (m, 4H), 4.33 (s, 2H), 5.82 (s, 2H), 7.00 (d, J 8.1 Hz, 2H), 7.09 (m, 1H), 7.27 (d, J 8.1 Hz, 2H), 7.41 (m, 1H), 7.65 (dd, J 8.3, 0.4 Hz, 1H), 7.78 (d, J 7.8 Hz, 1H), ^{13}C NMR (150 MHz, MeOD) δ_C 14.1, 15.7, 23.4, 27.8, 30.7, 35.9, 43.6, 49.5, 70.3, 83.5, 115.7, 121.5, 123.4, 126.2, 126.7, 126.9 128.5 129.4 135.4, 136.0, 139.8, 144.8, 152.5, 156.0, 173.8., HRMS (ESI): Calcd for $C_{27}H_{30}N_5O^+$ $[M + H]^+$: 440.2445, found 440.2445.

Synthesis of Azido-NPs

Spacer **3**[42] (30 mg, 116 μmol) dissolved in DMF was added to the Amine-NPs (1.5 mg Fe). Mixture was stirred at room temperature for a day, then dialyzed in DI water three times to remove nonconjugated molecules in excess.

Synthesis of Adjuvant-NPs

Adjuvant **1** (2.55 mg, 5.80 μmol, 15 equiv) dissolved in DMF, $CuSO_4 \cdot 6H_2O$ (1.45 mg, 5.80 μmol, 15 equiv), and (+)-sodium L-ascorbate (1.15 mg, 5.80 μmol, 15 equiv) was added to Azide-NPs and stirred at room temperature for a day. The reaction mixture was dialyzed in DI water two times and then treated with 0.1 M Tris buffer (pH 6) two times to form the ammonium salt of imidazoquinoline moiety. Solution was filtered through 0.2 μm pore size filter and concentrated to 3 mg/mL Fe, and then dissolved in autoclaved PBS buffer by using centrifugal filter (3000 rpm, 12 min).

Synthesis of Fluorescein-Adjuvant-NPs

For the fluorescence analysis and confocal analysis of DC uptake with nanoparticle, NHS-fluorescein was utilized to append fluorescein to Adjuvant-NPs (Figure 2.12). To a solution of Adjuvant-NPs in PBS buffer was added NHS-fluorescein (0.92 mg, 1.94 μmol, 5 equiv to Amine-NPs (1.5 mg Fe)) and stirred for 1 day at room temperature. NHS-fluorescein in excess was removed by DI water dialysis (for 3 times) and the solution was centrifuged (3000 rpm, 12 min, for 3 times). Then Fluorescein-Adjuvant-NPs were concentrated to 3 mg Fe/mL in autoclaved PBS buffer.

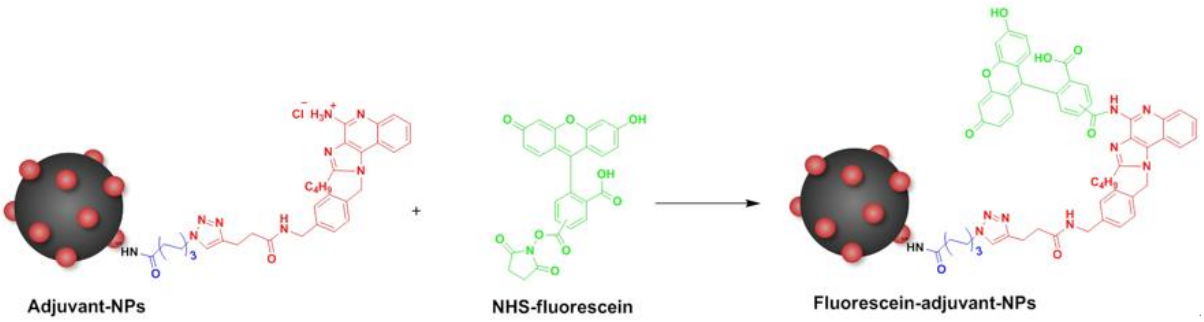

Figure 2.12. Synthesis of Fluorescein-Adjuvant-NPs.

Calculation of loading amount of imidazoquinolines on NPs by fluorescence assay

NHS-fluorescein has specific wavelength of excitation (494 nm) and emission (518 nm). Standard curve was generated by plotting emission absorbance against concentration (Figure 2.13). Azide-NPs showed negligible absorbance level in the range of 500-600 nm. Serial dilutions were done to produce 0.001 mg Fe/mL solution, which gave a y value of 176.4. Based on the calibration curve, the concentration of imidazoquinoline moiety was evaluated as 0.139 μM. Thus, the loading level of TLR 7 agonists on NPs is 0.139 μmol/[mg Fe].

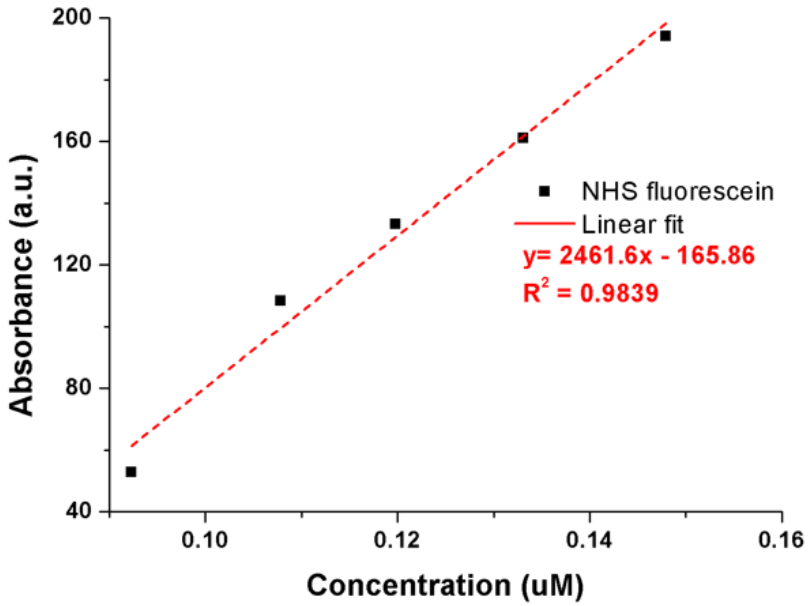

Figure 2.13. A calibration curve of NHS fluorescein.

Immunization studies

Mice

Female C57BL/6 mice were purchased from Taconic. All mice were maintained under specific pathogen-free (SFP) conditions and used at 6-8 weeks with Institutional Animal Care and Use guidelines. The Institutional Animal Care and Use Committee of the Ulsan National Institute of Science and Technology (UNISTIACUC) approved the *in vivo* animal experiments conducted in this study.

DC activation

Mice were injected intraperitoneally (I.P.) with R848 (InvivoGen, San Diego, CA), Adjuvant 1', Amine-NPs, Adjuvant-NPs, or PBS for *in vivo* DC activation. Mice were sacrificed after 18 hours of injection. Whole splenocytes were harvested and stained with CD11c FITC. Cells were subsequently stained with CD80 PE, CD86 PE, MHC II PE, CCR7 PE and isotypes control (supplied by BioLegend). Activation of $CD11c^+$ DC were measured by BD FACS Fortessa and analyzed by FlowJo software (TreeStar).

DC isolation

Spleens were harvested from mice to HBSS buffer (GIBCO), then, ballooning with 400 Mandl U/ml collagenase D (Roche) and tear them into small pieces by 25G needle and 3 ml syringe. $CD11c^+$ cells were positively enriched with magnetic activated cell sorting (MACS, Miltenyi Biotech). Sorted T cells showed >98 % purity, as detected by flow cytometry. All flow cytometry data were acquired by BD FACS Fortessa and analyzed by FlowJo software (TreeStar).

Confocal microscopic imaging of DCs

1×10^6 Cells/ml of immature DCs were isolated and incubated on coverslip in 24 wells plate with indicated PBS or NP 7 with 5 μg of OVA protein as a model antigen onto cover slip for 18 hours at 37 °C. Matured DCs were treated with 50 nM of lysotracker (Thermo-Fisher scientific) to stain the lysosome with red fluorescence for last 2 hours. Nucleus was stained with DAPI and images of green fluorescence of NP and red fluorescence of lysosome were obtained by FV1000 confocal microscopy (Olympus).

***In vivo* cytotoxic T lymphocyte (CTL) assay**

For *in vivo* CTL assay, mice were immunized with 50 μg of OVA protein with indicated adjuvant intraperitoneally, list indicated adjuvants. After 7 days, mice were re-immunized to boost immune responses. Then, mice were intravenously injected with 1:1 mixtures of OT-I peptide-pulsed (5 μM CFSE-labeled, $CFSE^{hi}$) and unpulsed (0.5 μM CFSE-labeled, $CFSE^{low}$) syngeneic splenocytes (7×10^6 of each). 18 Hours later, single cells were harvested form lymph nodes and spleens from each mouse. OT-I specific CTL activity was evaluated by flow cytometry. We repeated *in vivo* CTL assay three times and three mice were used in each group (total 9 mice/experimental set).

MHC I tetramer assay

To investigate OVA epitope (OT-I peptide) specificity induced by adjuvant-NPs vaccination, immunized mice as CTL experiment were sacrificed and single homogenized splenocytes were harvested. Cells were meshed with 70 μm pore strainer, then, re-stimulated with OT-I peptide (1 μM) in 96 well plate (5×10^5 cells/ 200 μl) at humidified incubator for 4 days. OT-I peptide specific T cell receptor expressing T cells were stained with PE-conjugated MHC I tetramer (Glycotope), then analyzed by flow cytometry.

2.6. References

1. Tacken, P. J., de Vries, I. J. M., Torensma, R., and Figdor, C. G., *Nat. Rev. Immunol.* **2007**, 7, 790−802.

2. Palucka, K., and Banchereau, J., *Nat. Rev. Cancer* **2012**, 12, 265−277.

3. Mandal, S., Hammink, R., Tel, J., Eksteen-Akeroyd, Z. H., Rowan, A. E., Blank, K., and Figdor, C. G., *ACS Chem. Biol.* **2015**, 10, 485−492.

4. Mandal, S., Eksteen-Akeroyd, Z. H., Jacobs, M. J., Hammink, R., Koepf, M., Lambeck, A. J. A., van Hest, J. C. M., Wilson, C. J., Blank, K., Figdor, C. G., et al., *Chem. Sci.* **2013**, 4, 4168−4174.

5. O'Neill, L. A. J., Golenbock, D., and Bowie, A. G., *Nat. Rev. Immunol.* **2013**, 13, 453−460.

6. Iwasaki, A., and Medzhitov, R., *Science* **2010**, 327, 291−295.

7. Tom, J. K., Dotsey, E. Y., Wong, H. Y., Stutts, L., Moore, T., Davies, D. H., Felgner, P. L., and Esser-Kahn, A. P., *ACS Cent. Sci.* **2015**, 1, 439−448.

8. Moyle, P. M., and Toth, I., *ChemMedChem* **2013**, 8, 360−376.

9. Palucka, K., Banchereau, J., and Mellman, I., *Immunity* **2010**, 33, 464−478.

10. Hemmi, H., Kaisho, T., Takeuchi, O., Sato, S., Sanjo, H., Hoshino, K., Horiuchi, T., Tomizawa, H., Takeda, K., and Akira, S., *Nat. Immunol.* **2002**, 3, 196−200.

11. Moon, J. J., Huang, B., and Irvine, D. J., *Adv. Mater.* **2012**, 24, 3724−3746.

12. Rajagopal, D., Paturel, C., Morel, Y., Uematsu, S., Akira, S., and Diebold, S. S., *Blood* **2010**, 115, 1949−1957.

13. Warshakoon, H. J., Hood, J. D., Kimbrell, M. R., Malladi, S., Wu, W. Y., Shukla, N. M., Agnihotri, G., Sil, D., and David, S. A., *Hum. Vaccines* **2009**, 5, 381−394.

14. Kasturi, S. P., Skountzou, I., Albrecht, R. A., Koutsonanos, D., Hua, T., Nakaya, H. I., Ravindran, R., Stewart, S., Alam, M., Kwissa, M., et al., *Nature* **2011**, 470, 543−550.

15. Heo, M. B., and Lim, Y. T., *Biomaterials* **2014**, 35, 590−600.

16. Ilyinskii, P. O., Roy, C. J., O'Neil, C. P., Browning, E. A., Pittet, L. A., Altreuter, D. H., Alexis, F., Tonti, E., Shi, J., Basto, P. A., et al., *Vaccine* **2014**, 32, 2882−2895.

17. Tacken, P. J., Zeelenberg, I. S., Cruz, L. J., van Hout-Kuijer, M. A., van de Glind, G., Fokkink, R. G., Lambeck, A. J. A., and Figdor, C. G., *Blood* **2011**, 118, 6836−6844.

18. Coffman, R. L., Sher, A., and Seder, R. A., *Immunity* **2010**, 33, 492−503.

19. de Titta, A., Ballester, M., Julier, Z., Nembrini, C., Jeanbart, L., van der Vlies, A. J., Swartz, M. A., and Hubbell, J. A., *Proc. Natl. Acad. Sci. U. S. A.* **2013**, 110, 19902−19907.

20. Molino, N. M., Anderson, A. K. L., Nelson, E. L., and Wang, S.- W., *ACS Nano* **2013**, 7, 9743−9752.

21. Shukla, N. M., Malladi, S. S., Mutz, C. A., Balakrishna, R., and David, S. A., *J. Med. Chem.* **2010**, 53, 4450−4465.

22. Shukla, N. M., Mutz, C. A., Ukani, R., Warshakoon, H. J., Moore, D. S., and David, S. A., *Bioorg. Med. Chem. Lett.* **2010**, 20, 6384−6386.

23. Shukla, N. M., Lewis, T. C., Day, T. P., Mutz, C. A., Ukani, R., Hamilton, C. D., Balakrishna, R., and David, S. A., *Bioorg. Med. Chem. Lett.* **2011**, 21, 3232−3236.

24. Shukla, N. M., Mutz, C. A., Malladi, S. S., Warshakoon, H. J., Balakrishna, R., and David, S. A., *J. Med. Chem.* **2012**, 55, 1106−1116.

25. Schiaffo, C. E., Shi, C., Xiong, Z., Olin, M., Ohlfest, J. R., Aldrich, C. C., and Ferguson, D. M., *J. Med. Chem.* **2014**, 57, 339−347.

26. Shi, C., Xiong, Z., Chittepu, P., Aldrich, C. C., Ohlfest, J. R., and Ferguson, D. M., *ACS Med. Chem. Lett.* **2012**, 3, 501−504.

27. Ryu, K. A., Stutts, L., Tom, J. K., Mancini, R. J., and Esser-Kahn, A. P. J., *J. Am. Chem. Soc.* **2014**, 136, 10823−10825.

28. Yoo, E., Salunke, D. B., Sil, D., Guo, X., Salyer, A. C. D., Hermanson, A. R., Kumar, M., Malladi, S. S., Balakrishna, R., Thompson, W. H., et al., *J. Med. Chem.* **2014**, 57, 7955−7970.

29. Dobrovolskaia, M. A., and McNeil, S. E., *Nat. Nanotechnol.* **2007**, 2, 469−478.

30. Gupta, A. K., and Gupta, M., *Biomaterials* **2005**, 26, 3995−4021.

31. Na, H. B., Song, I. C., and Hyeon, T., *Adv. Mater.* **2009**, 21, 2133−2148.

32. de Vries, I. J. M., Lesterhuis, W. J., Barentsz, J. O., Verdijk, P., van Krieken, J. H., Boerman, O. C., Oyen, W. J., Bonenkamp, J. J., Boezeman, J. B., Adema, G. J., et al., *Nat. Biotechnol.* **2005**, 23, 1407−1413.

33. Song, X., Gong, H., Yin, S., Cheng, L., Wang, C., Li, Z., Li, Y., Wang, X., Liu, G., and Liu, Z., *Adv. Funct. Mater.* **2014**, 24, 1194−1201.

34. Yang, K., Hu, L., Ma, X., Ye, S., Cheng, L., Shi, X., Li, C., Li, Y., and Liu, Z., *Adv. Mater.* **2012**, 24, 1868−1872.

35. Irvine, D. J., Hanson, M. C., Rakhra, K., and Tokatlian, T., *Chem. Rev.* **2015**, 115, 11109−11146.

36. Leleux, J., and Roy, K., *Adv. Healthcare Mater.* **2013**, 2, 72−94.

37. Mintern, J. D., Percival, C., Kamphuis, M. M. J., Chin, W. J., Caruso, F., and Johnston, A. P. R., *Adv. Healthcare Mater.* **2013**, 2, 940−944.

38. Smith, D. M., Simon, J. K., and Baker, J. R., *Nat. Rev. Immunol.* **2013**, 13, 592−605.

39. Koch, F., Stanzl, U., Jennewein, P., Janke, K., Heufler, C., Kampgen, E., Romani, N., and Schuler, G., *J. Exp. Med.* **1996**, 184, 741−746.

40. Han, J.-A., Kang, Y. J., Shin, C., Ra, J.-S., Shin, H.-H., Hong, S. Y., Do, Y., and Kang, S., *Nanomedicine* **2014**, 10, 561−569.

41. Quah, B. J. C., Warren, H. S., and Parish, C. R., *Nat. Protoc.* **2007**, 2, 2049−2056.

42. Lampkins, A. J., O'Neil, E. J., and Smith, B. D., *J. Org. Chem.* **2008**, 73, 6053−6058.

Chapter III

Nickel-Catalyzed Azide−Alkyne Cycloaddition To Access 1,5-Disubstituted 1,2,3-Triazoles in Air and Water

3.1. Abstract

Transition-metal-catalyzed or metal-free azide−alkyne cycloadditions are methods to access 1,4- or 1,5-disubstituted 1,2,3-triazoles. Although the copper-catalyzed cycloaddition to access 1,4-disubstituted products has been applied to biomolecular reaction systems, the azide−alkyne cycloaddition to access the complementary 1,5-regioisomers under aqueous and ambient conditions remains a challenge due to limited substrate scope or moisture-/air-sensitive catalysts. Herein, we report a method to access 1,5-disubstituted 1,2,3-triazoles using a Cp_2Ni/Xantphos catalytic system. The reaction proceeds both in water and organic solvents at room temperature. This protocol is simple and scalable with a broad substrate scope including both aliphatic and aromatic substrates. Moreover, triazoles attached with carbohydrates or amino acids are prepared via this cycloaddition. This chapter is reproduced from *J. Am. Chem. Soc.* **2017**, 139, 35, 12121-12124.

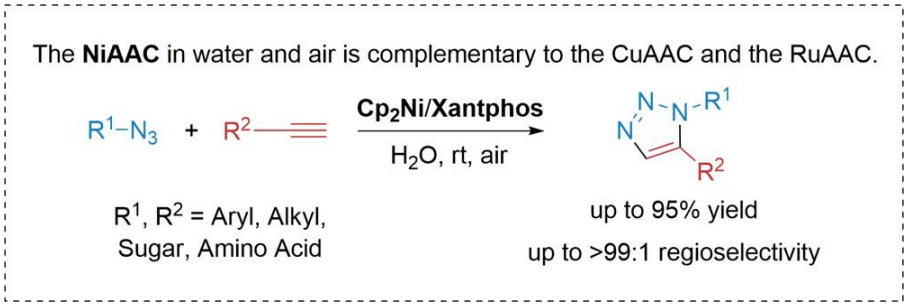

3.2. Introduction

Switching the regiochemical outcome is one of the issues in modular synthetic approaches involving carbon−heteroatom bond-forming processes.[1-3] It is important to impart a high level of regiocontrol to the Huisgen 1,3-dipolar cycloaddition, which assembles two molecular bricks, an organic azide and an alkyne, with ideal atom economy.[1-6] The thermal cycloaddition exhibits high activation barriers and poor regioselectivity at elevated temperatures. Rapid and regioselective formation of 1,4-disubstituted products has been accomplished by the copper-catalyzed azide−alkyne cycloaddition (CuAAC), since

the first reports by the groups of Sharpless and Meldal.[7,8] The main features of this utilized click chemistry include operational simplicity, mild conditions, a broad substrate scope, bioorthogonality, favorable kinetics, and high yields. The transformation proceeds not only in organic solvents but also in aqueous media at room temperature. As the 1,4-disubstituted 1,2,3-triazole scaffold is chemically stable, aromatic, and pharmacologically important, the CuAAC reactions have flourished in medicinal chemistry, materials science, and chemical biology.[1-6, 9-15]

Synthetic pathways complementary to the CuAAC have been developed to access 1,5-disubstituted 1,2,3-triazoles. As illustrated in Scheme 3.1a, a metal acetylide reacts with an organic azide to afford a 4-metalated triazole.[16-19] Subsequent aqueous quenching can lead to product formation.[16,18,19] Kwok et al. introduced a metal-free synthetic route to furnish 1,5-diaryl-1,2,3-triazoles (Scheme 3.1b).[20] Fokin, Jia, and co-workers reported the ruthenium-catalyzed azide−alkyne cycloaddition (RuAAC), obtaining a range of products under inert atmosphere (Scheme 3.1c).[21-23] However, the RuAAC reactions using [Cp*RuCl] complexes are typically sensitive to water and air, and proceed at elevated temperatures.[24,25] These conditions limit their application in biochemical research. The development of methods compatible with aqueous and ambient conditions remains a challenge.[26-30] Herein we report a strategy to access 1,5-disubstituted 1,2,3-triazoles by the nickel-catalysis. Functionalization of carbohydrates and amino acids has been also accomplished via this developed nickel-catalyzed azide−alkyne cycloaddition (NiAAC) in water at room temperature.

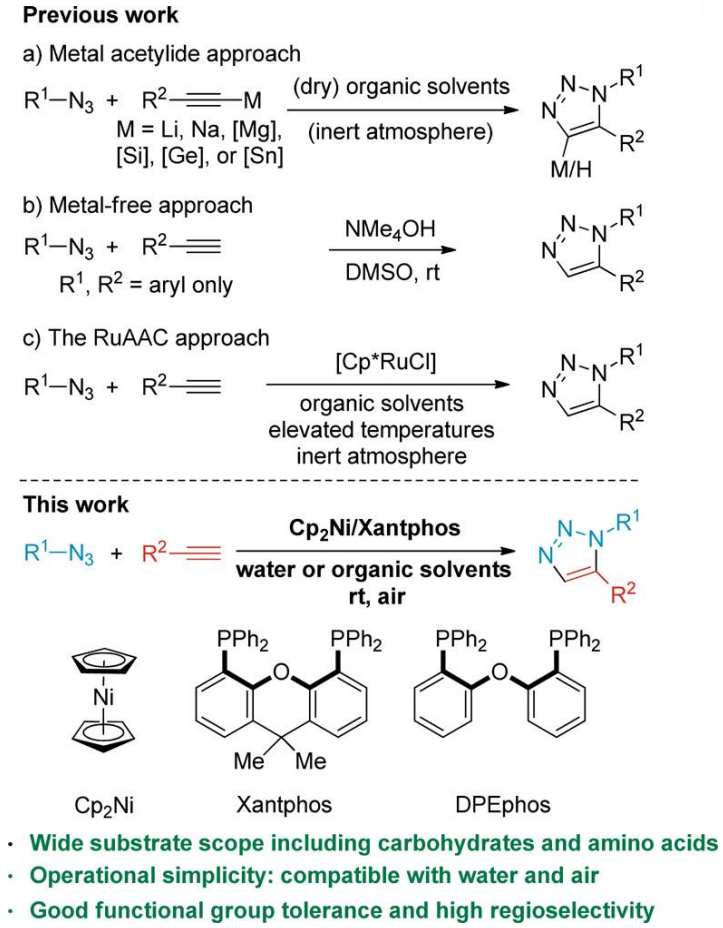

Scheme 3.1. Synthesis of 1,5-disubstituted 1,2,3-triazoles.

3.3. Results and discussion

We initiated our investigation of the NiAAC by treating two simple substrates, benzyl azide **1a** and phenylacetylene **2a**, with a catalytic amount of nickel precatalyst at room temperature without effort to exclude air and moisture (Table 3.1). All reagents including precatalysts, ligands, and solvents were used as-received from standard suppliers with no extra purification steps. After extensive screening of precatalysts, ligands, and additives (Tables 3.2-3.5), the reaction conditions were optimized to achieve high yield and excellent regioselectivity. Under the standard conditions, the desired 1,5-disubstituted triazole **3aa** was isolated in 94% yield with only 6% of **4aa** (entry 1). The regioisomers were separated by flash column chromatography. In the absence of the nickelocene (Cp_2Ni) precatalyst or the bidentate Xantphos ligand, the 1,2,3-triazole core was not formed (entries 2−5). Control experiments showed nickel precatalysts lacking the Cp ligands or other metallocene complexes were ineffective (entries 2−4, see Tables 3.2 and 3.3). Yet, more sterically demanding Cp-based complexes resulted in comparable or

unsatisfactory results (Table 3.3). Replacement of Xantphos with other P- or N-ligands caused diminished or no catalytic activity (Table 3.4). The use of DPEphos as the ligand, which has a similar structure to Xantphos (Table 3.1, entry 6, see also Scheme 3.1), furnished **3aa** in 76% yield. Geometrical constraints such as the rigidity of the backbone and a wide bite angle may play a critical role in determining the reactivity of the NiAAC.[31,32] Among the mild bases screened, Cs_2CO_3 was optimal (Table 3.5). The reaction was less effective when the precatalyst/ligand loading was reduced (Table 3.1, entry 8). Elevated temperatures (entries 9 and 10) lowered the reaction yield and regioselectivity, presumably due to catalyst decomposition or the involvement of the thermal pathway. A shortened reaction time (1.5 h) did not significantly affect the yield (entry 11). The reaction proceeded well in other solvents including DMF, DCM, and even water (entries 12−14) with similar yields and regioselectivity. This NiAAC reaction is highly compatible with water as the sole solvent and can be carried out under air at room temperature.

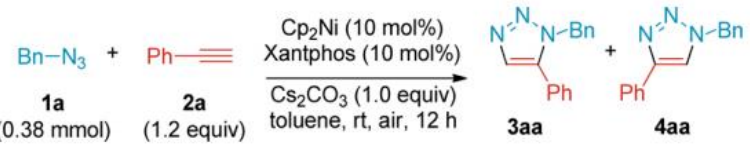

entry	change from above conditions	yield [%][b] 3aa	4aa
1	none	94	6
2	no Cp_2Ni	0	0
3	$NiCl_2{\cdot}6H_2O$ (instead of Cp_2Ni)	0	0
4	Cp_2Ru (instead of Cp_2Ni)	0	0
5	no Xantphos	0	0
6	DPEphos (instead of Xantphos)	76	9
7	no Cs_2CO_3	70	10
8	Cp_2Ni (5 mol %)/Xantphos (5 mol %)	38	4
9	75 °C	55	5
10	100 °C	70	9
11	1.5 h	91	6
12	DMF (instead of toluene)	90	8
13	DCM (instead of toluene)	90	3
14	water (instead of toluene), 1.5 h	91	6

[a]Reaction conditions: **1a** (0.38 mmol), **2a** (0.46 mmol, 1.2 equiv), Cp_2Ni (10 mol %), Xantphos (10 mol %), Cs_2CO_3 (1.0 equiv) in toluene (2.0 mL) at rt under air for 12 h. [b]Isolated yield. Bn, benzyl; Cp, cyclopentadienyl.

Table 3.1. Optimization of reaction conditions.[a]

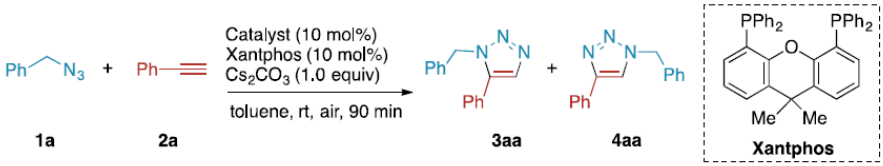

Entry	Catalyst	Ligand	Additive	Yield [%][b]	
				3aa	4aa
1	Nickel(II) acetate tetrahydrate	Xantphos	Cs_2CO_3	0	0
2	Nickel(II) chloride hexahydrate	Xantphos	Cs_2CO_3	0	0
3	Nickel(II) nitrate hexahydrate	Xantphos	Cs_2CO_3	0	0
4	Nickel	Xantphos	Cs_2CO_3	0	0
5	Nickel(II) trifluoromethanesulfonate	Xantphos	Cs_2CO_3	0	0
6	Bis(tricyclohexylphospine)nickel(II) dichloride	Xantphos	Cs_2CO_3	0	0

[a] Reaction conditions: **1a** (0.38 mmol), **2a** (0.46 mmol, 1.2 equiv), catalyst (10 mol%), Xantphos (10 mol%), Cs_2CO_3 (1.0 equiv), toluene (2.0 mL), rt, air, 90 min. [b] Isolated yield.

Table 3.2. Nickel catalyst screening.[a]

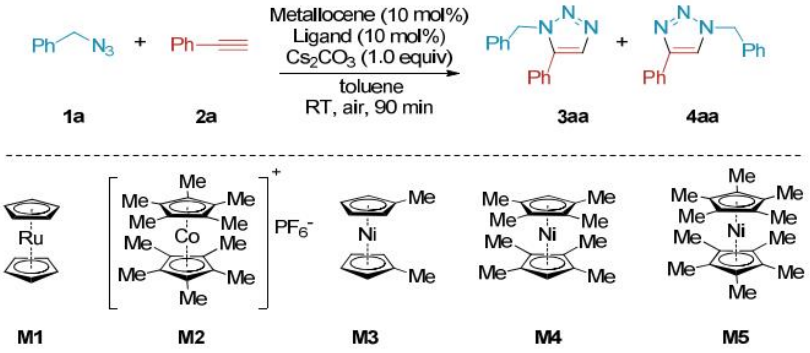

Entry	Catalyst	Ligand	Additive	Yield [%][b]	
				3aa	4aa
1	**M1**	Xantphos	Cs_2CO_3	0	0
2	**M2**	Xantphos	Cs_2CO_3	0	0
3	**M3**	Xantphos	Cs_2CO_3	93	6
4	**M4**	Xantphos	Cs_2CO_3	90	6
5	**M5**	Xantphos	Cs_2CO_3	0	0
6	**M5**	-	Cs_2CO_3	0	0
7	**M5**	Neocuproine	Cs_2CO_3	0	0
8	**M5**	Johnphos	Cs_2CO_3	0	0
9	**M5**	1,4-bisdiphenylphosphinobutane	Cs_2CO_3	0	0

[a] Reaction conditions: **1a** (0.38 mmol), **2a** (0.46 mmol, 1.2 equiv), catalyst (10 mol%), Xantphos (10 mol%), Cs_2CO_3 (1.0 equiv), toluene (2.0 mL), rt, air, 90 min. [b] Isolated yield.

Table 3.3. Metallocene catalyst screening.[a]

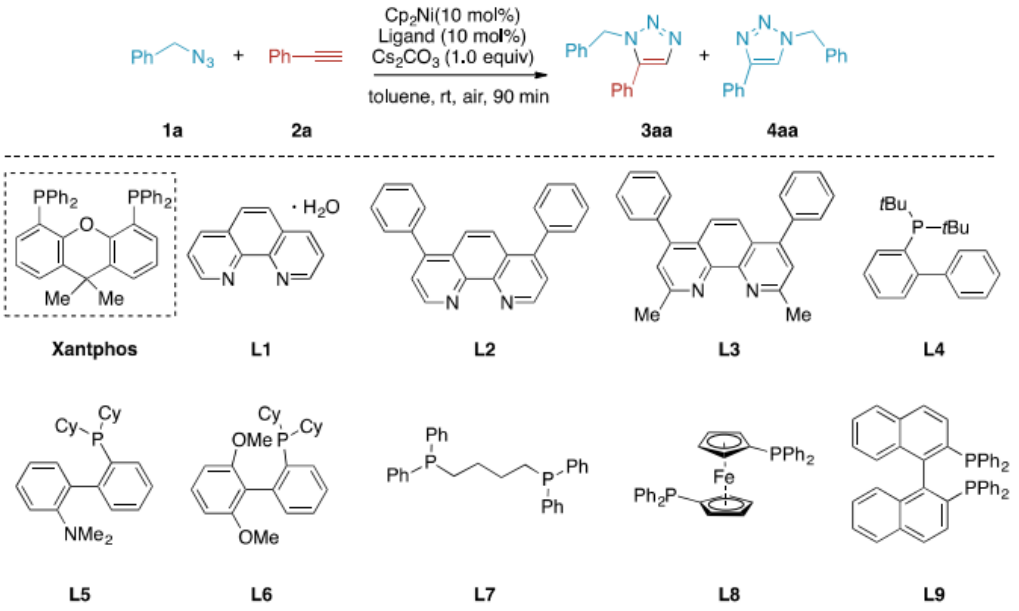

Entry	Catalyst	Ligand	Additive	Yield [%][b]	
				3aa	**4aa**
1	Cp_2Ni	**L1**	Cs_2CO_3	0	0
2	Cp_2Ni	**L2**	Cs_2CO_3	10	2
3	Cp_2Ni	**L3**	Cs_2CO_3	33	3
4	Cp_2Ni	**L4**	Cs_2CO_3	0	0
5	Cp_2Ni	**L5**	Cs_2CO_3	0	0
6	Cp_2Ni	**L6**	Cs_2CO_3	0	0
7	Cp_2Ni	**L7**	Cs_2CO_3	0	0
8	Cp_2Ni	**L8**	Cs_2CO_3	0	0
9	Cp_2Ni	**L9**	Cs_2CO_3	0	0

[a] Reaction conditions: **1a** (0.38 mmol), **2a** (0.46 mmol, 1.2 equiv), Cp_2Ni (10 mol%), Xantphos (10 mol%), Cs_2CO_3 (1.0 equiv), toluene (2.0 mL), rt, air, 90 min. [b] Isolated yield.

Table 3.4. Ligand screening.[a]

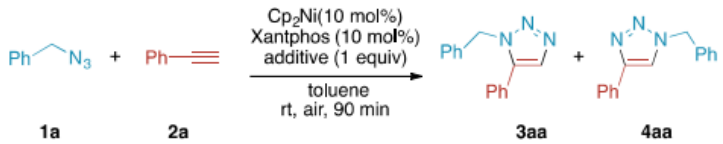

1a 2a 3aa 4aa

Entry	Catalyst	Ligand	Additive	Yield [%][b]	
				3aa	**4aa**
1	Cp_2Ni	Xantphos	Silver acetate	0	0
2	Cp_2Ni	Xantphos	Boc-lie-OH	0	0
3	Cp_2Ni	Xantphos	Potassium phosphate tribasic	77	15
4	Cp_2Ni	Xantphos	Sodium hydroxide	88	6
5	Cp_2Ni	Xantphos	Sodium ascorbate	83	7
6	Cp_2Ni	Xantphos	Cesium pivalate	90	10

[a] Reaction conditions: **1a** (0.38 mmol), **2a** (0.46 mmol, 1.2 equiv), Cp_2Ni (10 mol%), Xantphos (10 mol%), Cs_2CO_3 (1.0 equiv), toluene (2.0 mL), rt, air, 90 min. [b] Isolated yield.

Table 3.5. Base/additive screening.[a]

With the optimized conditions based on the Cp_2Ni/Xantphos catalytic system in hand, the substrate scope and generality of this NiAAC reaction were investigated under aqueous conditions at room temperature (Scheme 3.2). Owing to the poor solubilities of the precatalyst, ligand, and substrates in water, reactions were conducted as aqueous suspensions. Reactions of various azides (**1b** and **1e**−**1k**) produced the corresponding 1,5-disubstituted triazoles in moderate to excellent isolated yields (63−95%) with high regioselectivity ranging from 11.4:1 to >99:1 for **3**/**4**. However, regioselectivity was significantly decreased when phenyl azide **1c** (3.2:1 ratio) or 1-azidoadamantane **1d** was used (4.5:1 ratio). This can be attributed to the steric congestion between the substrates and catalytic Ni species containing Cp and Xantphos ligands. Various functional groups of **1**, including fluorinated arenes and fused cyclic moieties, were compatible with the reaction conditions. The hydroxyl and ester functional groups remained intact during the catalysis, as illustrated in the cases of **3ha** and **3ia**.

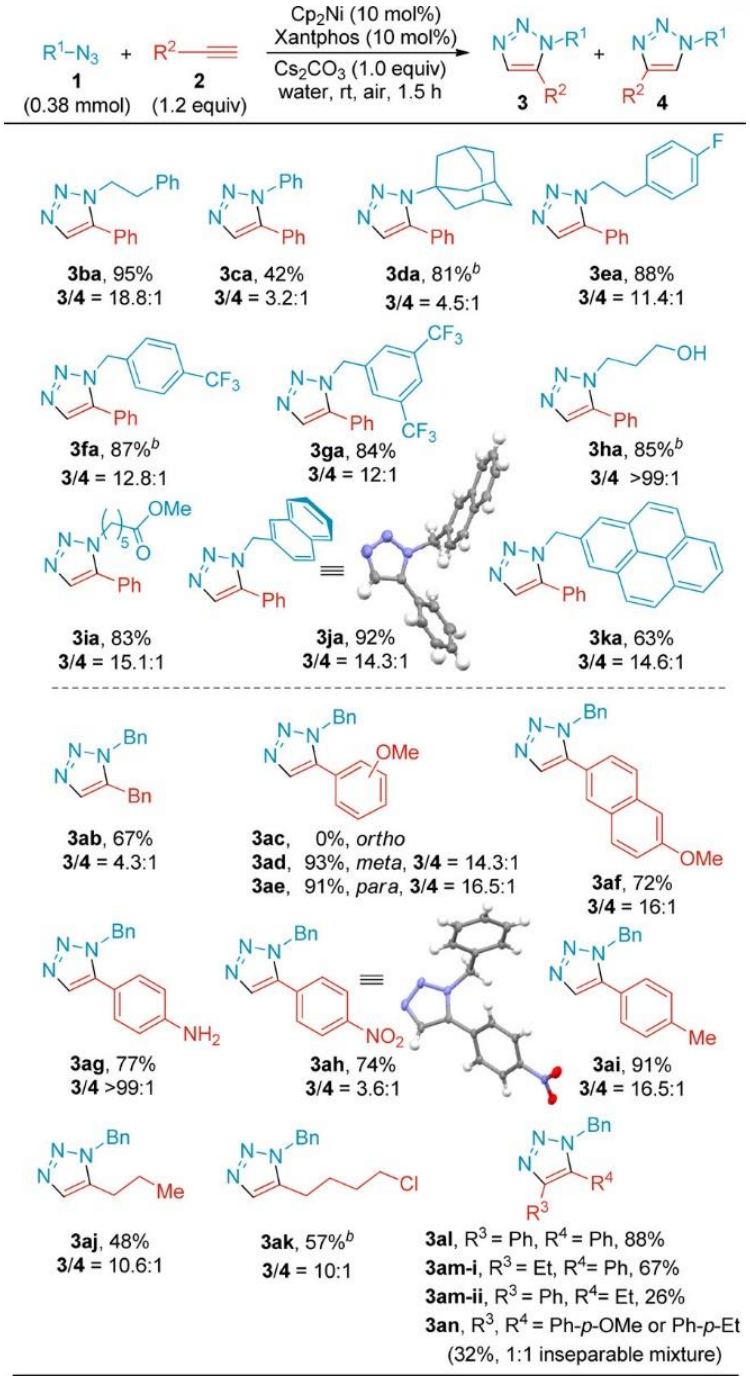

[a]Reaction conditions: **1** (0.38 mmol), **2** (0.46 mmol, 1.2 equiv), Cp_2Ni (10 mol %), Xantphos (10 mol %), Cs_2CO_3 (1.0 equiv) in water (2.0 mL) at rt under air for 1.5 h. Isolated yields of 1,5-products. [b]12 h.

Scheme 3.2. Substrate scope of the NiAAC.[a]

Regarding the organic alkyne partner **2**, aliphatic and aromatic alkynes with diverse functional groups, including methoxy-, amine-, nitro-, chloro-, and methyl moieties, were well-tolerated. Yet, *ortho*-OMe-substituted alkyne **2c** showed no reactivity owing to the steric effect. The NiAAC reaction is favored with less-sterically hindered *meta*- and *para*-substituted substrates **2d** and **2e**. It was reported RuAAC reactions are significantly affected by steric factor of alkynes.[22] However, the contribution of electronic factor cannot be ruled out (**3ab**, **3ag**, and **3ah**). The cycloaddition of the electronically unbiased internal alkyne **2l** afforded **3al** in 88% yield. Unsymmetrical internal alkynes **2m** and **2n** also participated in the NiAAC to give fully substituted triazoles,[21-25,33] albeit with poor regioselectivity. Regiochemical assignments were confirmed by 2D NMR (Figure 3.1),[7,8,25,33] assisted by the ^{13}C chemical shifts of the triazole CH.[34] In addition, single-crystal X-ray crystallographic analyses determined structures of the 1,5-disubstituted triazoles **3ja** and **3ah** (Table 3.6 and 3.7).

To expand the repertoire of the NiAAC, this developed click reaction was explored to include biomolecules such as carbohydrates and amino acids. In particular, glycoconjugates feature unparalleled branched structures, compared with oligopeptides or oligonucleotides, with diverse configurations and glycosidic linkages.[9,35-39] Their effective functionalization has been achieved by producing non-natural glycoconjugates and amino acid derivatives (Scheme 3.3). Both O- and N-linked sugars were well-tolerated in this NiAAC (**3la**–**3oa**). In addition, the cycloaddition reaction could be scaled up to a 1 g of **1m** with an increased reaction yield of 82% (**3ma**). Maltose azide **1p**, a disaccharide moiety, could be incorporated affording the cycloaddition product in 74% yield, albeit in DCM, due to the solubility problem. Finally, both carbohydrate **1o** and amino acid **2o** were subjected to the NiAAC, and non-natural glyco-amino acid **3oo** was successfully prepared in 65% yield, presenting the potential of biomolecule conjugation. However, the attempted NiAAC reactions with unprotected sugars were not successful (Scheme 3.4).

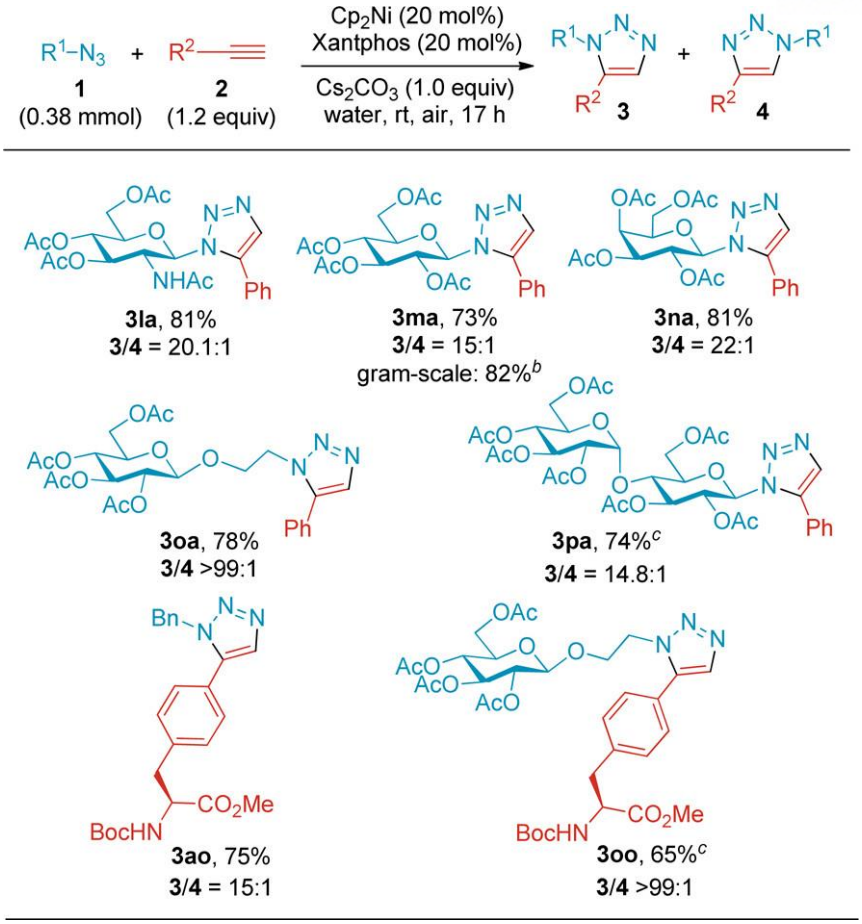

[a]Reaction conditions: **1** (0.38 mmol), **2** (0.46 mmol, 1.2 equiv), Cp_2Ni (20 mol %), Xantphos (20 mol %), Cs_2CO_3 (1.0 equiv) in water (2.0 mL) at rt under air for 17 h. Isolated yields of 1,5-products. [b]**1m** (1.0 g, 2.68 mmol). [c]**1** (0.19 mmol), 12 h in DCM.

Scheme 3.3. Expanded scope with respect to non-natural carbohydrates and amino acids.[a]

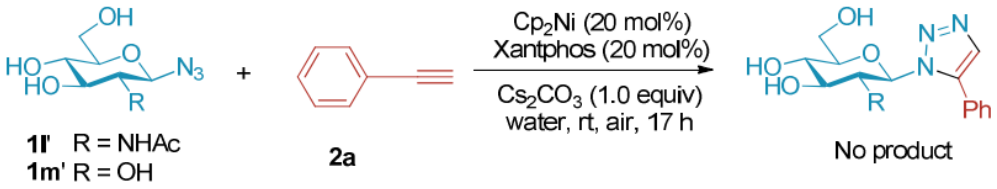

Scheme 3.4. Attempted NiAAC reactions with unprotected sugar **1l′** and **1m′**.

Having established the utility of the Cp_2Ni/Xantphos catalytic system for azide−alkyne cycloaddition, we turned our attention to the Ni species that may be present in solution. Literature indicates that reaction of Cp_2Ni with mono- and bidentate phosphine ligands may, in some cases, give CpNi(P-ligand)$_2$ and Ni(P-ligand)$_4$ complexes.[40-43] The formal one-electron reduction steps of the Ni center (from Ni^{II} to Ni^{I} to Ni^{0}) upon coordination of the phosphine ligands may be explained by successive dissociation of Cp• radicals.[44,45] Indeed, analysis of the reaction between Cp_2Ni and Xantphos by EPR spectroscopy and mass spectrometry gave results consistent with the presence of CpNi(Xantphos) and Ni(Xantphos)$_2$ (see the Experimental). The EPR spectrum of the reaction mixture shows a triplet resonance signal centered at g = 2.088 with a hyperfine splitting constant of a = 104 G (Figure 3.2), as expected for a paramagnetic Ni^{I} center (S = 1/2) coupled to two ^{31}P nuclei.[40,44−47] Moreover, these parameters are similar to those reported for related Ni complexes, such as CpNi-(dppe).[40,44]

Next, the high-resolution ESI mass spectrum (Figure 3.3) of the reaction mixture exhibits the most-abundant peak at *m/z* 701.1671, which is attributed to $[CpNi(Xantphos)]^+$. Measured and calculated isotope distributions were well-matched. In addition, a peak at *m/z* 630.1638 is assigned to $[Ni(Xantphos)_2+2Na]^{2+}$.[41-43] Because the reactions in this study were performed under air, it may seem likely that CpNi(Xantphos), at least in part, undergoes oxidization, giving rise to the corresponding Ni^{II} complex $[CpNi(Xantphos)]^+$ detected in positive ESI mode. Together, these findings agree with the reaction sequences (i) Cp_2Ni → CpNi(Xantphos) → Ni(Xantphos)$_2$ and (ii) CpNi(Xantphos) → $CpNi(Xantphos)^+$. More detailed studies are needed, however, to confirm the presence of these species and to determine which ones are involved in the NiAAC reaction.

On the basis of literature reports[48-50] and our experimental results, a reaction mechanism is suggested as shown in Scheme 3.5. Alkyne and azide coordinate to Ni, forming intermediate **A**, while the spectator ligands (Cp and/or Xantphos) may change their bonding modes to accommodate the new ligands. Because both internal and terminal alkynes participate in this cycloaddition (*vide supra*, see Scheme 3.2), the formation of a nickel−acetylide species is excluded. The C−N bond formation between alkyne and azide giving complex **B** determines 1,5-regioselectivity, analogous to the RuAAC pathway.[22] Subsequent reductive elimination leads to the formation of cyclized target product **3**, while regenerating NiL_n through association (or change of bonding mode) of the spectator ligands.

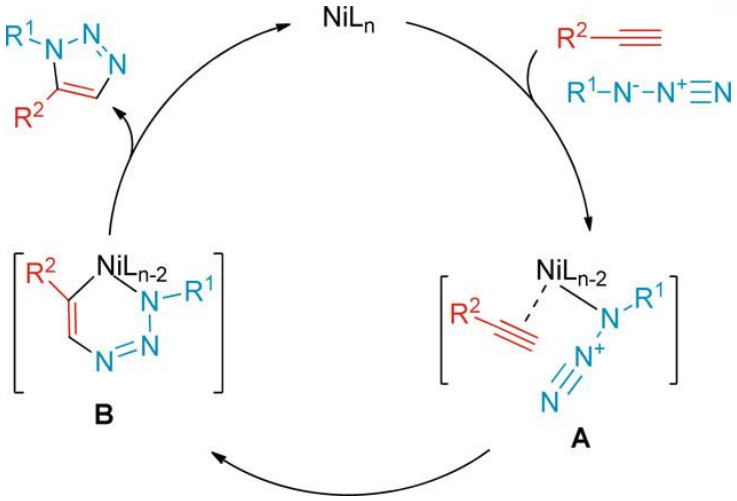

Scheme 3.5. Tentative reaction mechanism of the NiAAC.

3.4. Conclusion

In summary, we developed the nickel-catalyzed azide−alkyne cycloaddition to access 1,5-disubstituted 1,2,3-triazoles from available substrates and inexpensive reagents at room temperature. The Cp_2Ni precatalyst and Xantphos ligand were critical to accomplish the catalytic manifold, insensitive to molecular oxygen and water. This methodology exhibits a broad substrate scope, good functional group tolerance, high yields, and high regioselectivity, complementing the classical copper-catalyzed click chemistry that produces 1,4-disubstituted 1,2,3-triazoles. The synthetic utility of this nickel-catalyzed pathway has been highlighted by the functionalization of carbohydrates and amino acids. Further mechanistic studies of catalyst activation and intermediate formation are underway.

3.5. Experimental

General information

Reactions were monitored by thin-layer chromatography (TLC) using Merck silica gel $60F_{254}$ glass plate with 0.25 mm thickness. The glass plates were visualized by a ultra-violet lamp (254 nm) and stained with potassium permanganate solution. Flash column chromatography was carried out using Merck silica gel 60 (size range: 0.040–0.063 mm). ^{1}H, ^{13}C, and ^{19}F NMR spectra were recorded on a Bruker Avance III HD (400 MHz for proton, 100 MHz for carbon) or an Agilent VNMRS 600 (600 MHz for proton, 150 MHz for carbon). Chemical shifts are given on the δ-scale in ppm, and residual solvent peaks were used as internal standards. High-resolution mass spectrometry (HRMS) data were

measured on a Thermo Scientific Q Exactive Plus Hybrid Quadrupole-Orbitrap mass spectrometer. Single-crystal X-ray analysis was conducted by monochromatic synchrotron X-rays (λ = 0.66 Å, 6D UNIST-PAL beamline) with a Rayonix MX225-HS detector. Electron paramagnetic resonance (EPR) spectra were obtained on a Bruker EMXplus 9.5/12 spectrometer.

Experimental procedures

(CAUTION!) organic and inorganic azides are potentially explosive and toxic. In particular, the use of metal spatula for weighing sodium azide should be avoided.

Synthesis of organic azides: (1b, 1e, 1j),[51] (1a, 1g),[52] 1f,[53] 1h[54]

Organic bromide (1.0 equiv) was treated with sodium azide (1.5 equiv) in DMSO or a mixture of 1:3 water/acetone solution. Solution was stirred at rt or 80 ºC. After 12–24 h, the reaction mixture was diluted with D.I. water, and then extracted with diethyl ether 3 times. The combined organic layer was washed with water and brine, dried over sodium sulfate, and then concentrated *in vacuo*. The corresponding product was purified by flash column chromatography.

Preparation of organic azides

Methyl 6-azidohexanoate **1i**,[55] 1-azidomethylpyrene **1k**,[56] 2-acetamido-2-deoxy-3,4,6-tri-*O*-acetyl-β-D-glucopyranosyl azide **1l**,[57] 2-acetylamido-2-deoxyl-β-D-glucopyranosyl azide **1l'**,[58] 2,3,4,6-tetra-*O*-acetyl-β-D-glucopyranosyl azide **1m**,[59] β-D-glucopyranosyl azide **1m'**,[60] 2,3,4,6-tetra-*O*-acetyl-β-D-galactopyranosyl azide **1n**,[61] 2′-azidoethyl-2,3,4,6-tetra-*O*-acetyl-β-D-glucopyranoside **1o**,[62] and 2,3,6,2′,3′,4′,6′-hepta-*O*-acetyl-β-maltosyl azide **1p**[63] were synthesized according to previously reported methods. Azidobenzene solution **1c** (0.5 M in *tert*-butyl methyl ether) and 1-azidoadamantane **1d** were purchased from Sigma-Aldrich.

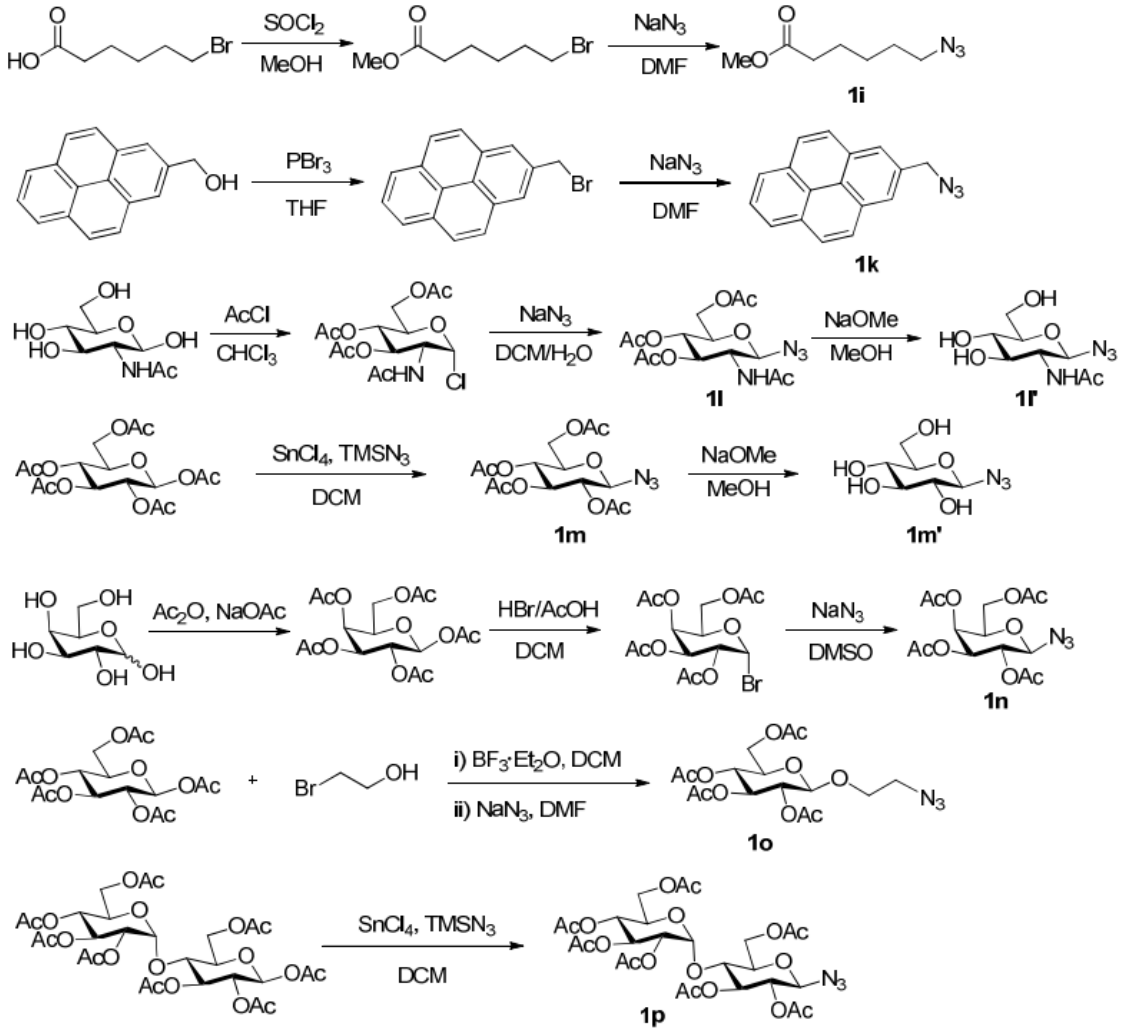

Scheme 3.6. Preparation of organic azides.

Preparation of alkynes

N-Boc-4-ethynyl-L-phenylalanine methyl ester **2o**[64] was synthesized according to previously reported method. Other alkynes were purchased from standard suppliers (Sigma-Aldrich, TCI, and Alfa Aesar).

General Procedure for the NiAAC

To a mixture of nickelocene (10 or 20 mol%) and Xantphos ligand (10 or 20 mol%) in water or organic solvent (2.0 mL), alkyne **2** (1.2 equiv, 0.46 mmol) and cesium carbonate (1.0 equiv, 0.38 mmol) were added at 0 ºC. Then, organic azide **1** (1.0 equiv, 0.38 mmol) was added and the reaction mixture was stirred at rt. After 1.5–17 h, the suspension was diluted with DCM, washed with water, and dried over sodium sulfate. The desired product was purified by flash column chromatography on silica gel.

Characterization data

^{1}H NMR spectra of (**3aa**, **3ba**, **3ha**, **3al**),[23] **3ca**,[65] **3da**,[66] **3ia**,[67] (**3ae**, **3ai**),[68] **3aj**,[69] **3ma**,[70] and **3am** (as a regioisomeric mixture)[71] are in good agreement with the previously reported literature values.

1-(1-Adamantyl)-5-phenyl-1*H*-1,2,3-triazole (**3da**)

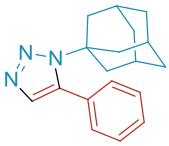

81% yield, brown solid, ^{1}H NMR (600 MHz, $CDCl_3$) δ 7.47 (s, 1H), 7.42 – 7.35 (m, 3H), 7.29 – 7.25 (m, 2H), 2.16 (s, 6H), 2.05 (s, 3H), 1.61 (d, *J* = 12.3 Hz, 3H), 1.55 (d, *J* = 11.9 Hz, 3H), ^{13}C NMR (100 MHz, $CDCl_3$) δ 136.8, 135.5, 130.5, 130.1, 129.2, 128.1, 63.1, 42.9, 35.7, 29.6, HRMS (ESI+) m/z calcd for $C_{18}H_{21}N_3Na$ ($[M+Na]^+$) 302.1627, found 302.1627.

1-(4-Fluorophenethyl)-5-phenyl-1*H*-1,2,3-triazole (**3ea**)

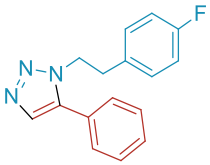

88% yield, brown solid, ^{1}H NMR (600 MHz, $CDCl_3$) δ 7.62 (s, 1H), 7.46–7.37 (m, 3H), 7.08 (d, *J* = 6.5 Hz, 2H), 6.86 (d, *J* = 7.0 Hz, 4H), 4.52 (t, *J* = 7.2 Hz, 2H), 3.14 (t, *J* = 7.2 Hz, 2H), ^{13}C NMR (150 MHz, $CDCl_3$) δ 162.0 (d, *J* = 245.3 Hz), 138.3 (s), 133.0 (s), 132.9 (d, *J* = 3.3 Hz), 130.3 (d, *J* = 8.0 Hz), 129.5 (s), 129.0 (s), 128.8 (s), 127.1 (s), 115.6 (d, *J* = 21.3 Hz), 49.5 (s), 35.8 (s), ^{19}F NMR (376 MHz, $CDCl_3$) δ -115.75 – -115.92 (m), HRMS (ESI+) m/z calcd for $C_{16}H_{15}FN_3$ ($[M+H]^+$) 268.1244, found 268.1242.

5-Phenyl-1-(4-(trifluoromethyl)benzyl)-1*H*-1,2,3-triazole (**3fa**)

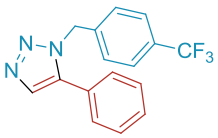

87% yield, white solid, ^{1}H NMR (600 MHz, $CDCl_3$) δ 7.73 (s, 1H), 7.52 (d, *J* = 8.1 Hz, 2H), 7.46 – 7.38 (m, 3H), 7.23 (d, *J* = 6.5 Hz, 2H), 7.17 (d, *J* = 8.0 Hz, 2H), 5.59 (s, 2H). ^{13}C NMR (150 MHz, $CDCl_3$) δ 139.4 (s), 138.3 (s), 133.3 (s), 130.4 (q, *J* = 32.7 Hz), 129.7 (s), 129.1 (s), 128.8 (s), 127.5 (s), 126.6 (s), 125.8 (q, *J* = 3.7 Hz), 123.8 (q, *J* = 272.2 Hz), 51.2 (s), ^{19}F NMR (376 MHz, $CDCl_3$) δ -62.70 (s), HRMS (ESI+) m/z calcd for $C_{16}H_{13}F_3N_3$ ($[M+H]^+$) 304.1056, found 304.1051.

1-(3,5-Bis(trifluoromethyl)benzyl)-5-phenyl-1*H*-1,2,3-triazole (**3ga**)

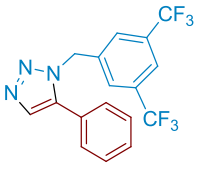

84% yield, yellow oil, ^{1}H NMR (600 MHz, $CDCl_3$) δ 7.76 (s, 1H), 7.73 (s, 1H), 7.51 – 7.41 (m, 5H), 7.21 (d, *J* = 7.1 Hz, 2H), 5.65 (s, 2H), ^{13}C NMR (100 MHz, $CDCl_3$) δ 138.3 (s), 137.7 (s), 133.7 (s), 132.3 (q, *J* = 33.7 Hz), 130.1 (s), 129.4 (s), 128.9 (s), 128.0 (d, *J* = 2.7 Hz), 126.5 (s), 122.9 (q, *J* = 272.9 Hz), 122.5 (dt, *J* = 6.9, 3.4

Hz), 51.0 (s), ^{19}F NMR (376 MHz, $CDCl_3$) δ -63.04 (s), HRMS (ESI+) m/z calcd for $C_{17}H_{11}F_6N_3Na$ ($[M+Na]^+$) 394.0749, found 394.0748.

1-(Naphthalen-2-ylmethyl)-5-phenyl-1*H*-1,2,3-triazole (**3ja**)

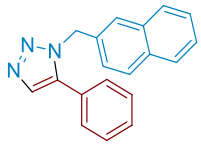

92% yield, brown solid, ^{1}H NMR (600 MHz, $CDCl_3$) δ 7.82 – 7.75 (m, 3H), 7.72 – 7.69 (m, 1H), 7.50 – 7.36 (m, 6H), 7.27 – 7.24 (m, 3H), 5.70 (s, 2H), ^{13}C NMR (100 MHz, $CDCl_3$) δ 138.3, 133.4, 133.2, 133.1, 133.0, 129.6, 129.1, 129.0, 128.9, 128.0, 127.8, 127.0, 126.6, 126.5, 126.3, 124.8, 52.0, HRMS (ESI+) m/z calcd for $C_{19}H_{16}N_3$ ($[M+H]^+$) 286.1338, found 286.1335.

5-Phenyl-1-(pyren-2-ylmethyl)-1*H*-1,2,3-triazole (**3ka**)

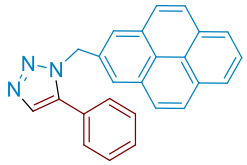

63% yield, brown solid, ^{1}H NMR (400 MHz, $CDCl_3$) δ 8.04 (dd, *J* = 7.6, 3.4 Hz, 2H), 7.97 (d, *J* = 9.2 Hz, 1H), 7.93 – 7.82 (m, 5H), 7.70 (s, 1H), 7.28 – 7.22 (m, 2H), 7.21 – 7.13 (m, 2H), 7.08 (dt, *J* = 5.9, 2.7 Hz, 2H), 6.13 (s, 2H), ^{13}C NMR (100 MHz, $CDCl_3$) δ 138.5, 133.5, 131.3, 131.2, 130.6, 129.6, 129.1, 128.9, 128.5, 128.3, 128.0, 127.8, 127.3, 127.0, 126.2, 125.7, 125.6, 125.5, 124.9, 124.8, 124.6, 121.8, 50.1, HRMS (ESI+) m/z calcd for $C_{25}H_{17}N_3Na$ ($[M+Na]^+$) 382.1314, found 382.1314.

1,5-Dibenzyl-1*H*-1,2,3-triazole (**3ab**)

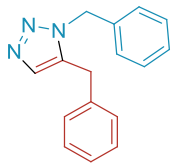

67% yield, yellow solid, ^{1}H NMR (400 MHz, $CDCl_3$) δ 7.38 (s, 1H), 7.27 – 7.16 (m, 6H), 7.04 – 6.90 (m, 4H), 5.32 (s, 2H), 3.76 (s, 2H), ^{13}C NMR (100 MHz, $CDCl_3$) δ 136.0, 134.8, 134.4, 129.1, 129.0, 128.5, 128.4, 127.4, 127.3, 52.0, 29.4, HRMS (ESI+) m/z calcd for $C_{16}H_{15}N_3Na$ ($[M+Na]^+$) 272.1158, found 272.1157.

1-Benzyl-5-(3-methoxyphenyl)-1*H*-1,2,3-triazole (**3ad**)

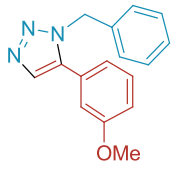

93% yield, yellow oil, ^{1}H NMR (600 MHz, $CDCl_3$) δ 7.72 (s, 1H), 7.35 – 7.22 (m, 4H), 7.08 (d, *J* = 6.6 Hz, 2H), 6.95 (dd, *J* = 8.3, 2.1 Hz, 1H), 6.84 (d, *J* = 7.5 Hz, 1H), 6.71 (s, 1H), 5.54 (s, 2H), 3.68 (s, 3H), ^{13}C NMR (100 MHz, $CDCl_3$) δ 159.8, 138.1, 135.7, 133.3, 130.1, 128.9, 128.2, 128.1, 127.1, 121.2, 115.4, 114.2, 55.3, 51.9, HRMS (ESI+) m/z calcd for $C_{16}H_{16}N_3O$ ($[M+H]^+$) 266.1287, found 266.1285.

1-Benzyl-5-(6-methoxynaphthalen-2-yl)-1*H*-1,2,3-triazole (**3af**)

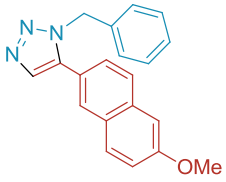

72% yield, yellow oil, ^{1}H NMR (600 MHz, $CDCl_3$) δ 7.81 (s, 1H), 7.77 (d, *J* = 8.4 Hz, 1H), 7.66 – 7.61 (m, 2H), 7.32 – 7.10 (m, 8H), 5.59 (s, 2H), 3.94 (s, 3H), ^{13}C NMR (100 MHz, $CDCl_3$) δ 158.8, 138.5, 135.8, 134.8, 133.5, 129.8, 129.0, 128.5, 128.3, 127.7, 127.3, 126.5, 121.8, 120.1, 105.7, 55.5, 52.0, HRMS (ESI+) m/z calcd for $C_{20}H_{18}N_3O$ ($[M+H]^+$) 316.1444, found 316.1439.

4-(1-Benzyl-1*H*-1,2,3-triazol-5-yl)aniline (**3ag**)

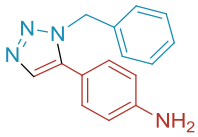

77% yield, brown oil, ^{1}H NMR (600 MHz, $CDCl_3$) δ 7.64 (s, 1H), 7.29 – 7.22 (m, 3H), 7.08 (d, *J* = 6.5 Hz, 2H), 7.00 (d, *J* = 8.5 Hz, 2H), 6.65 (d, *J* = 8.5 Hz, 2H), 5.49 (s, 2H), 3.98 (s, 2H), ^{13}C NMR (100 MHz, $CDCl_3$) δ 147.9, 138.6, 135.9, 132.8, 130.0, 128.8, 128.0, 127.1, 116.0, 115.0, 51.5, HRMS (ESI+) m/z calcd for $C_{15}H_{15}N_4$ ($[M+H]^+$) 251.1291, found 251.1291.

1-Benzyl-5-(4-nitrophenyl)-1*H*-1,2,3-triazole (**3ah**)

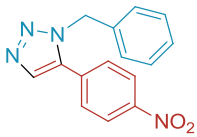

74% yield, yellow solid, ^{1}H NMR (600 MHz, $CDCl_3$) δ 8.24 (d, *J* = 8.7 Hz, 2H), 7.82 (s, 1H), 7.43 (d, *J* = 8.7 Hz, 2H), 7.32–7.25 (m, 3H), 7.07–7.01 (m, 2H), 5.59 (s, 2H), ^{13}C NMR (100 MHz, $CDCl_3$) δ 148.3, 136.1, 135.0, 134.2, 133.4, 129.8, 129.1, 128.6, 127.0, 124.2, 52.4, HRMS (ESI+) m/z calcd for $C_{15}H_{13}N_4O_2$ ($[M+H]^+$) 281.1033, found 281.1030.

1-Benzyl-5-(4-chlorobutyl)-1*H*-1,2,3-triazole (**3ak**)

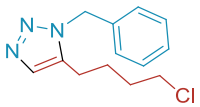

57% yield, brown solid, ^{1}H NMR (400 MHz, $CDCl_3$) δ 7.49 (s, 1H), 7.35 – 7.27 (m, 3H), 7.18 – 7.10 (m, 2H), 5.50 (s, 2H), 3.44 (t, *J* = 6.1 Hz, 2H), 2.52 (t, *J* = 7.3 Hz, 2H), 1.75 – 1.63 (m, 4H), ^{13}C NMR (100 MHz, $CDCl_3$) δ 136.7, 135.0, 132.8, 129.1, 128.5, 127.2, 51.8, 44.3, 31.7, 25.2, 22.5, HRMS (ESI+) m/z calcd for $C_{13}H_{17}ClN_3$ ($[M+H]^+$) 250.1105, found 250.1102.

1-Benzyl-4-(4-ethylphenyl)-5-(4-methoxyphenyl)-1*H*-1,2,3-triazole and 1-benzyl-5-(4-ethylphenyl)-4-(4-methoxyphenyl)-1*H*-1,2,3-triazole (**3an**): an inseparable regioisomeric 1:1 mixture

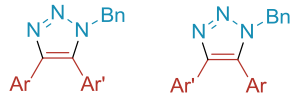

32% yield, brown solid, ^{1}H NMR (400 MHz, $CDCl_3$) δ 7.46 – 7.37 (m, 4H), 7.22 – 7.10 (m, 8H), 7.05 – 6.92 (m, 10H), 6.88 – 6.82 (m, 2H), 6.76 – 6.68 (m, 2H), 5.31 (s, 4H), 3.78 (s, 3H), 3.69 (s, 3H), 2.64 (q, *J* = 7.6 Hz, 2H), 2.52 (q, *J* = 7.6 Hz, 2H), 1.21 (t, *J* = 7.6 Hz, 3H), 1.12 (t, *J* = 7.6 Hz, 3H), ^{13}C NMR (100 MHz, $CDCl_3$) δ 160.6, 159.3, 146.0, 144.7, 144.4, 143.8, 135.7, 133.5, 133.4, 131.6, 130.2, 128.8, 128.7, 128.6, 128.2, 128.1, 128.0, 127.6, 126.7, 125.2, 123.8, 119.9, 114.7, 114.0, 55.5, 55.3, 52.0, 28.8, 28.7, 15.5, 15.4, HRMS (ESI+) m/z calcd for $C_{24}H_{24}N_3O$ ($[M+H]^+$) 370.1919, found 370.1915.

1-(2′-Acetamido-2′-deoxy-3′,4′,6′-tri-*O*-acetyl-β-D-glucopyranosyl)-5-phenyl-1*H*-1,2,3-triazole (**3la**)

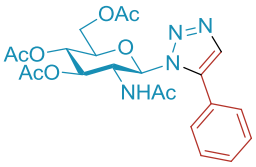

81% yield, white solid, ^{1}H NMR (400 MHz, $CDCl_3$) δ 7.69 (s, 1H), 7.50 (s, 5H), 6.36 (d, *J* = 9.7 Hz, 1H), 5.99 (d, *J* = 7.3 Hz, 1H), 5.87 (t, *J* = 9.8 Hz, 1H), 5.12 (t, *J* = 9.7 Hz, 1H), 4.46 (td, *J* = 10.0, 7.4 Hz, 1H), 4.24 (dd, *J* = 12.4, 5.8 Hz, 1H), 4.15 (dd, *J* = 12.4, 2.0 Hz, 1H), 3.97 (ddd, *J* = 10.0, 5.7, 2.0 Hz, 1H), 2.10 (s, 3H), 2.05 (s, 3H), 2.04 (s, 3H), 1.73 (s, 3H), ^{13}C NMR (100 MHz, $CDCl_3$) δ 170.9, 170.6, 170.2, 169.7, 140.1, 133.6, 130.2, 129.2, 129.1, 126.0, 82.3, 74.5, 71.2, 68.8, 62.4, 54.4, 23.2, 20.9, 20.8, 20.7, HRMS (ESI+) m/z calcd for $C_{22}H_{26}N_4NaO_8$ ($[M+Na]^+$) 497.1642, found 497.1640.

5-Phenyl-1-(2′,3′,4′,6′-tetra-*O*-acetyl-β-D-glucopyranosyl)-1*H*-1,2,3-triazole (**3ma**)

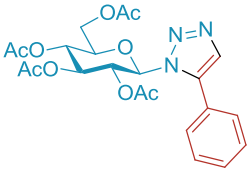

73% yield, white solid, ^{1}H NMR (400 MHz, $CDCl_3$) δ 7.70 (s, 1H), 7.50 (s, 5H), 5.92 (t, *J* = 9.4 Hz, 1H), 5.61 (d, *J* = 9.5 Hz, 1H), 5.28 (t, *J* = 9.4 Hz, 1H), 5.18 (t, *J* = 9.7 Hz, 1H), 4.25 (dd, *J* = 12.5, 5.5 Hz, 1H), 4.17 (dd, *J* = 12.4, 2.2 Hz, 1H), 3.90 (ddd, *J* = 9.8, 5.5, 2.2 Hz, 1H), 2.09 (s, 3H), 2.02 (s, 3H), 1.97 (s, 3H), 1.79 (s, 3H), ^{13}C NMR (100 MHz, $CDCl_3$) δ 170.5, 170.3, 169.3, 168.3, 139.5, 133.5, 130.2, 129.2, 129.2, 126.1, 83.6, 74.8, 73.4, 69.5, 67.7, 62.0, 20.8, 20.6, 20.5, 20.3, HRMS (ESI+) m/z calcd for $C_{22}H_{25}N_3NaO_9$ ($[M+Na]^+$) 498.1483, found 498.1483.

5-(Phenyl)-1-(2′,3′,4′,6′-tetra-*O*-acetyl-β-D-galactopyranosyl)-1*H*-1,2,3-triazole (**3na**)

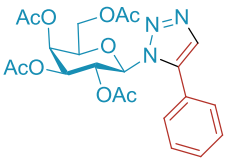

81% yield, yellowish solid, ^{1}H NMR (400 MHz, $CDCl_3$) δ 7.67 (s, 1H), 7.56 – 7.43 (m, 5H), 5.87 (t, *J* = 9.8 Hz, 1H), 5.68 (d, *J* = 9.4 Hz, 1H), 5.43 (d, *J* = 3.2 Hz, 1H), 5.10 (dd, *J* = 10.2, 3.3 Hz, 1H), 4.19 – 4.09 (m, 3H), 2.06 (s, 3H), 2.04 (s, 3H), 1.92 (s, 3H), 1.79 (s, 3H), ^{13}C NMR (100 MHz, $CDCl_3$) δ 170.3, 170.1,

170.0, 168.3, 139.2, 134.0, 129.9, 129.6, 128.8, 126.3, 85.0, 73.8, 71.5, 67.0, 66.9, 61.6, 20.7, 20.6, 20.5, 20.3, HRMS (ESI+) m/z calcd for $C_{22}H_{25}N_3NaO_9$ ([M+Na]$^+$) 498.1483, found 498.1478.

1-(1′-Ethyl-2′,3′,4′,6′-tetra-*O*-acetyl-β-D-glucopyranosyl)-5-phenyl-1*H*-1,2,3-triazole (**3oa**)

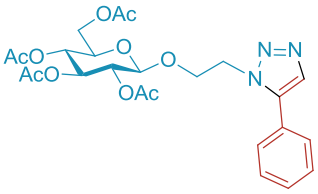

78% yield, white solid, ^{1}H NMR (400 MHz, $CDCl_3$) δ 7.65 (s, 1H), 7.53 – 7.43 (m, 3H), 7.44 – 7.38 (m, 2H), 5.11 (t, *J* = 9.5 Hz, 1H), 5.01 (t, *J* = 9.7 Hz, 1H), 4.91 (dd, *J* = 9.5, 8.0 Hz, 1H), 4.52 – 4.40 (m, 3H), 4.31 (dt, *J* = 10.2, 4.3 Hz, 1H), 4.25 – 4.18 (m, 2H), 4.04 (dd, *J* = 12.3, 2.3 Hz, 1H), 3.64 (ddd, *J* = 9.9, 4.7, 2.3 Hz, 1H), 2.04 (s, 3H), 1.99 (s, 3H), 1.94 (s, 3H), 1.80 (s, 3H), ^{13}C NMR (100 MHz, $CDCl_3$) δ 170.66, 170.16, 169.48, 169.31, 139.18, 132.75, 129.64, 129.29, 129.15, 126.68, 101.02, 72.72, 71.92, 70.89, 68.36, 68.17, 61.77, 47.44, 20.79, 20.64, 20.61, 20.53, HRMS (ESI+) m/z calcd for $C_{24}H_{29}N_3NaO_{10}$ ([M+Na]$^+$) 542.1745, found 542.1750.

1-(2′,3′,6′,2″,3″,4″,6″-Hepta-*O*-acetyl- β-maltosyl)-5-phenyl-1*H*-1,2,3-triazole (**3pa)**

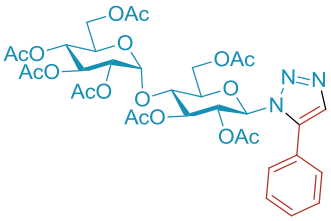

74% yield, white solid, ^{1}H NMR (400 MHz, $CDCl_3$) δ 7.72 (s, 1H), 7.57 – 7.45 (m, 5H), 5.92 (t, *J* = 9.5 Hz, 1H), 5.55 (d, *J* = 9.5 Hz, 1H), 5.44 (d, *J* = 4.0 Hz, 1H), 5.32 (td, *J* = 9.5, 2.6 Hz, 2H), 5.03 (t, *J* = 9.9 Hz, 1H), 4.85 (dd, *J* = 10.5, 4.0 Hz, 1H), 4.49 (dd, *J* = 12.2, 2.4 Hz, 1H), 4.30 – 4.22 (m, 2H), 4.13 (t, *J* = 9.3 Hz, 1H), 4.05 (dd, *J* = 12.4, 2.1 Hz, 1H), 3.98 (ddd, *J* = 10.2, 4.0, 2.2 Hz, 1H), 3.89 (ddd, *J* = 9.6, 5.3, 2.5 Hz, 1H), 2.14 (s, 3H), 2.09 (s, 3H), 2.01 (s, 3H), 1.99 (s, 3H), 1.98 (s, 3H), 1.97 (s, 3H), 1.76 (s, 3H), ^{13}C NMR (100 MHz, $CDCl_3$) δ 170.6, 170.6, 170.5, 170.4, 170.0, 169.5, 168.8, 139.7, 133.2, 130.3, 129.4, 129.0, 126.1, 95.9, 82.8, 76.3, 75.0, 72.7, 70.1, 70.0, 69.3, 68.8, 68.1, 63.0, 61.7, 21.0, 20.9, 20.8, 20.7, 20.6, 20.5, 20.3, HRMS (ESI+) m/z calcd for $C_{34}H_{41}N_3NaO_{17}$ ([M+Na]$^+$) 786.2328, found 786.2315.

Methyl (*S*)-3-(4′-(1″-benzyl-1*H*-1,2,3-triazol-5″-yl)phenyl)-2-((*tert*-butoxycarbonyl)amino)propanoate (**3ao**)

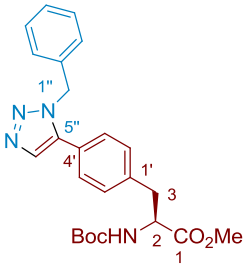

75% yield, brown oil, ^{1}H NMR (400 MHz, $CDCl_3$) δ 7.64 (s, 1H), 7.23 – 7.17 (m, 3H), 7.10 (s, 4H), 7.02 – 6.93 (m, 2H), 5.46 (s, 2H), 4.99 (d, *J* = 8.0 Hz, 1H), 4.54 (dd, *J* = 13.6, 6.1 Hz, 1H), 3.65 (s, 3H), 3.11 (dd, *J* = 13.8, 5.6 Hz, 1H), 2.99 (dd, *J* = 13.8, 6.3 Hz, 1H), 1.34 (s, 9H), ^{13}C NMR (100 MHz, $CDCl_3$) δ 172.1, 155.1, 137.9, 137.9, 135.5, 133.4, 130.0, 129.0, 128.9, 128.2, 127.2, 125.7, 80.2, 54.4, 52.5, 51.9, 38.2, 28.4, HRMS (ESI+) m/z calcd for $C_{24}H_{28}N_4NaO_4$ ([M+Na]$^+$) 459.2002, found 459.2006.

Methyl (*S*)-3-(4′-(1″-(1‴-ethyl-2‴,3‴,4‴,6‴-tetra-*O*-acetyl-β-D-glucopyranosyl)-1*H*-1,2,3-triazol-5″-yl)phenyl)-2-((*tert*-butoxycarbonyl)amino)propanoate (**3oo**)

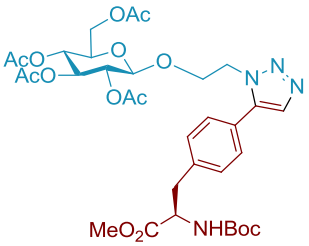

65% yield, yellow solid, ^{1}H NMR (400 MHz, $CDCl_3$) δ 7.59 (s, 1H), 7.30 (d, *J* = 8.0 Hz, 2H), 7.20 (d, *J* = 7.2 Hz, 2H), 5.01 (ddd, *J* = 19.3, 16.6, 9.5 Hz, 3H), 4.86 (dd, *J* = 9.4, 8.1 Hz, 1H), 4.57 (d, *J* = 6.8 Hz, 1H), 4.44 – 4.34 (m, 3H), 4.27 (dd, *J* = 9.2, 5.2 Hz, 1H), 4.17 (dt, *J* = 15.1, 5.1 Hz, 2H), 4.01 (dd, *J* = 12.3, 2.1 Hz, 1H), 3.70 (s, 3H), 3.60 (ddd, *J* = 9.8, 4.6, 2.2 Hz, 1H), 3.14 (dd, *J* = 13.8, 5.4 Hz, 1H), 3.03 (dd, *J* = 13.6, 6.0 Hz, 1H), 2.01 (s, 3H), 1.94 (s, 3H), 1.90 (s, 3H), 1.73 (s, 3H), 1.36 (s, 9H), ^{13}C NMR (100 MHz, $CDCl_3$) δ 172.2, 170.7, 170.2, 169.5, 169.3, 155.2, 139.0, 138.0, 132.8, 130.2, 129.4, 125.4, 101.1, 80.2, 72.8, 72.0, 70.9, 68.4, 68.2, 61.8, 54.4, 52.5, 47.5, 38.3, 28.4, 20.9, 20.7, 20.6, 20.5, HRMS (ESI+) m/z calcd for $C_{33}H_{44}N_4NaO_{14}$ ([M+Na]$^+$) 743.2746, found 743.2750.

2D NMR: NOESY/HSQC Study

The regiochemical patterns of substituted 1,2,3-triazoles were determined by ^{1}H–^{1}H NOESY spectra, as depicted in Figure 3.6. Additionally, the triazole CH of **3** exhibits characteristic ^{13}C chemical shift within ~133 ± 3 ppm.[34] The regiochemistry of triazoles (**3da**, **3ea**, **3fa**, **3ga**, **3ja**, **3ka**, **3ab**, **3ad**, **3af**, **3ag**, **3ah**, **3ak**, **3am**, **3la**, **3ma**, **3na**, **3oa**, **3pa**, **3ao**, and **3oo**) was confirmed by 2D NMR (NOESY and/or HSQC) studies (400 MHz, 298 K, $CDCl_3$).

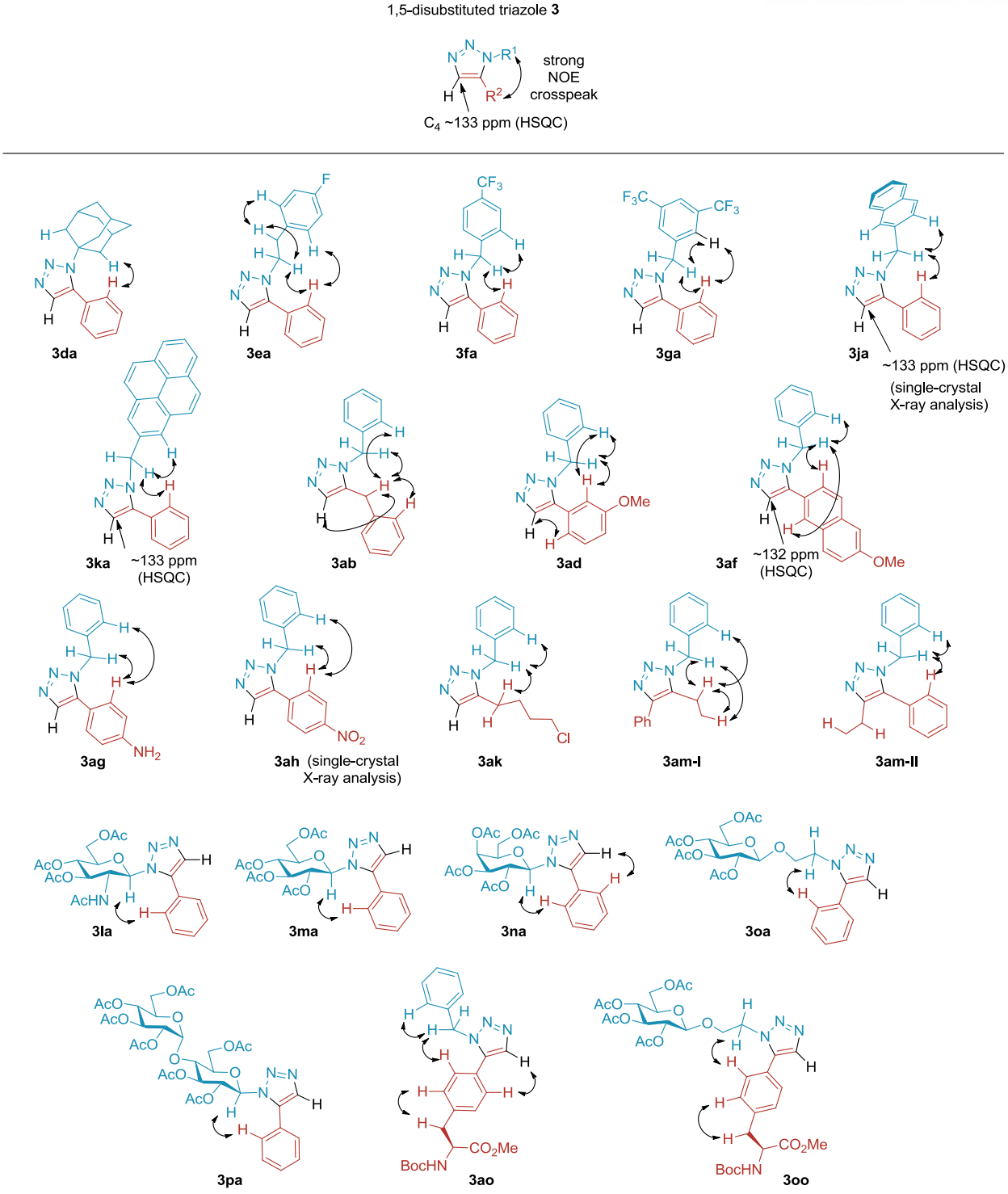

Figure 3.1. 2D NMR (^{1}H–^{1}H NOESY and HSQC) spectroscopic studies.

X-ray Data of 3ah and 3ja

The crystal was mounted under oil on a loop and X-ray diffraction data were collected with monochromatic synchrotron X-rays (λ = 0.66 Å, 6D UNIST-PAL beamline) with a Rayonix MX225-HS detector. The crystal structure was solved by direct method using SHELXTL package. All non-hydrogen atoms were refined with anisotropic displacement parameters. The hydrogen atoms were located at geometrically calculated positions. Crystal data are summarized in Tables 3.6 and 3.7.

Table 3.6. Crystal Data and Structure Refinement of **3ah**.

Identification code	**3ah**	
Empirical formula	$C_{15}H_{12}N_4O_2$	
Formula weight	280.29	
Temperature	123 K	
Crystal system	Monoclinic	
Space group	*P2₁*	
Unit cell dimensions	a = 6.8000(14) Å	α = 90°
	b = 11.502(2) Å	β = 99.74(3)°
	c = 8.4630(17) Å	γ = 90°
Volume	652.4(2) $Å^3$	
Z	2	
Density (calculated)	1.427 g/cm^3	
Absorption coefficient	0.099 mm^{-1}	
F(000)	123	
Theta range for data collection	2.442 to 31.490°.	
Index ranges	-9<=h<=9, -16<=k<=16, -12<=l<=12	
Reflections collected	7695	
Independent reflections	4282 [R(int) = 0.1151]	
Completeness to theta = 25.242°	100.0 %	
Refinement method	Full-matrix least-squares on F^2	
Data / restraints / parameters	4282 / 1 / 190	
Goodness-of-fit on F^2	1.153	
Final R indices [I>2sigma(I)]	R_1 = 0.0628, wR_2 = 0.1664	
R indices (all data)	R_1 = 0.0733, wR_2 = 0.1726	
Largest diff. peak and hole	0.430 and -0.751 e^- $Å^{-3}$	

Table 3.7. Crystal Data and Structure Refinement of **3ja**.

Identification code	**3ja**	
Empirical formula	$C_{19}H_{15}N_3$	
Formula weight	285.34	
Temperature	100 K	
Crystal system	Monoclinic	
Space group	*P2₁*	
Unit cell dimensions	a = 8.1940(16) Å	α = 90°
	b = 6.0730(12) Å	β = 104.96(3)°
	c = 15.178(3) Å	γ = 90°
Volume	729.7(3) $Å^3$	
Z	2	
Density (calculated)	1.299 g/cm^3	
Absorption coefficient	0.079 mm^{-1}	
F(000)	310	
Theta range for data collection	2.573 to 31.531°.	
Index ranges	-12<=h<=12, -0<=k<=8, -22<=l<=22	
Reflections collected	4332	
Independent reflections	2564 [R(int) = 0.0971]	
Completeness to theta = 25.242°	97.6 %	
Refinement method	Full-matrix least-squares on F^2	
Data / restraints / parameters	2564 / 1 / 199	
Goodness-of-fit on F^2	1.203	
Final R indices [I>2sigma(I)]	R_1 = 0.0566, wR_2 = 0.1853	
R indices (all data)	R_1 = 0.0818, wR_2 = 0.2176	
Largest diff. peak and hole	0.603 and -0.602 e^- $Å^{-3}$	

Identification of Ni complexes by EPR spectroscopy and HRMS

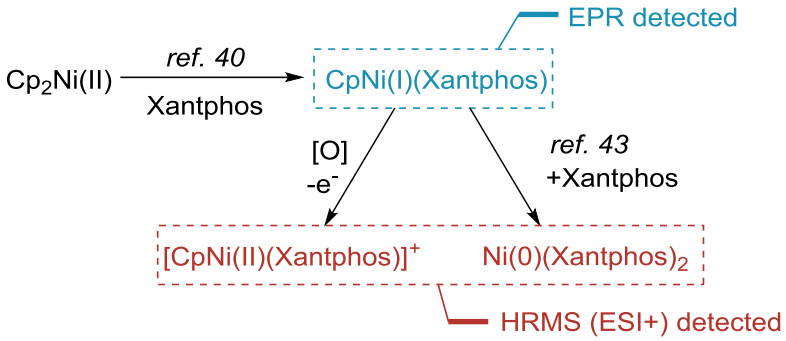

Scheme 3.7. Possible transformations of Ni complexes based on the experimental results and literature precedent.

EPR spectroscopy

Sample preparation: A solution of Cp_2Ni (0.1 mmol) and Xantphos (0.1 mmol) in toluene (2 mL) was stirred at 20 ºC for 1 h, during which the color of the reaction mixture changed from deep green to brown. After filtration, samples were taken from the filtrate.

EPR spectroscopy: EPR spectra were obtained on a Bruker EMXplus 9.5/12 spectrometer at 295 K. Typical EPR spectral parameters were an X-band microwave frequency of 9.385 GHz, a modulation frequency of 100 kHz, a modulation amplitude of 5 G, and a microwave power of 6.33 mW.

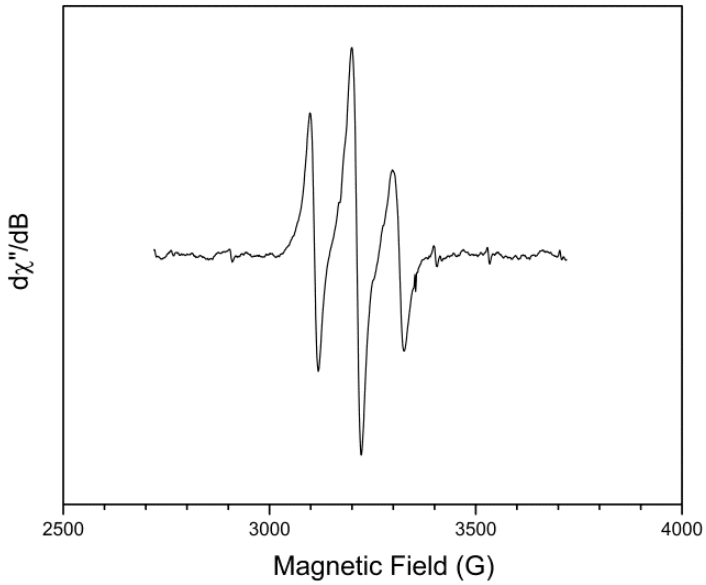

Figure 3.2. EPR spectrum of a sample from the reaction between Cp_2Ni and Xantphos in toluene (X-band microwave frequency, 9.385 GHz, modulation frequency, 100 kHz, modulation amplitude, 5 G, microwave power, 6.33 mW, temperature, 295 K, 10 scans).

The EPR spectrum of the product mixture shows a triplet resonance signal centered at g = 2.088 with a hyperfine splitting constant of a = 104 G. These parameters are similar to those reported for related Ni complexes, such as NiCp(dppe) (g = 2.068, a = 122 G),[40] suggesting that CpNi(Xantphos) was formed.

HRMS Study

HRMS (ESI+) spectra were obtained on a Thermo Scientific Q Exactive Plus Hybrid Quadrupole-Orbitrap mass spectrometer. We prepared samples by diluting the EPR sample with HPLC-grade methanol. After filtration, sample was taken from the filtrate.

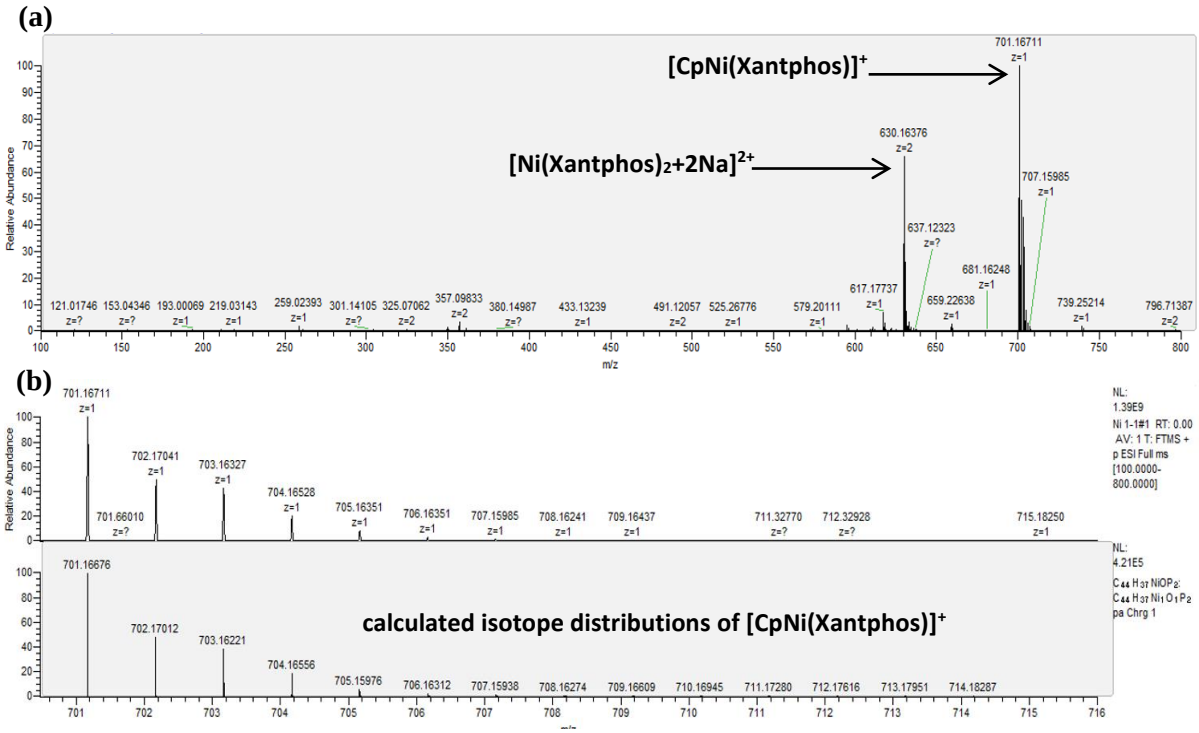

Figure 3.3. HRMS study: (a) wide range data, and (b) isotope distributions of $[CpNi(Xantphos)]^+$. $[Ni(Xantphos)_2+2Na]^{2+}$ (ESI+, m/z) calcd for $C_{78}H_{64}Na_2NiO_2P_4^{2+}$ ($[M+2Na]^{2+}$) 630.1500, found 630.1638, $[CpNi(Xantphos)]^+$ (ESI+, m/z) calcd for $C_{44}H_{37}NiOP_2$ ($[M]^+$) 701.1667, found 701.1671.

3.6. References

1. Meldal, M., Tornoe, C. W. *Chem. Rev.* **2008**, 108, 2952-3015.

2. Kolb, H. C., Finn, M. G., Sharpless, K. B. *Angew. Chem., Int. Ed.* **2001**, 40, 2004-2021.

3. Becer, C. R., Hoogenboom, R., Schubert, U. S. *Angew. Chem., Int. Ed.* **2009**, 48, 4900-4908.

4. Hein, J. E., Fokin, V. V. *Chem. Soc. Rev.* **2010**, 39, 1302-1315.

5. Moses, J. E., Moorhouse, A. D. *Chem. Soc. Rev.* **2007**, 36, 1249-1262.

6. Kumar, A. S., Ghule, V. D., Subrahmanyam, S., Sahoo, A. K. *Chem. - Eur. J.* **2013**, 19, 509-518.

7. Rostovtsev, V. V., Green, L. G., Fokin, V. V., Sharpless, K. B. *Angew. Chem., Int. Ed.* **2002**, 41, 2596-2599.

8. Tornoe, C. W., Christensen, C., Meldal, M. *J. Org. Chem.* **2002**, 67, 3057-3064.

9. Tiwari, V. K., Mishra, B. B., Mishra, K. B., Mishra, N., Singh, A. S., Chen, X. *Chem. Rev.* **2016**, 116, 3086-3240.

10. Kim, W. G., Choi, B., Yang, H.-J., Han, J.-A., Jung, H., Cho, H., Kang, S., Hong, S. Y. *Bioconjugate Chem.* **2016**, 27, 2007-2013.

11. Zhou, Q., Gui, J., Pan, C.-M., Albone, E., Cheng, X., Suh, E. M., Grasso, L., Ishihara, Y., Baran, P. S. *J. Am. Chem. Soc.* **2013**, 135, 12994-12997.

12. Besanceney-Webler, C., Jiang, H., Zheng, T., Feng, L., Soriano del Amo, D., Wang, W., Klivansky, L. M., Marlow, F. L., Liu, Y., Wu, P. *Angew. Chem., Int. Ed.* **2011**, 50, 8051-8056.

13. Hong, S. Y., Tobias, G., Al-Jamal, K. T., Ballesteros, B., Ali-Boucetta, H., Lozano-Perez, S., Nellist, P. D., Sim, R. B., Mather, S. J., Green, M. L. H., Kostarelos, K., Davis, B. G., Finucane, C. *Nat. Mater.* **2010**, 9, 485-490.

14. Hong, V., Presolski, S. I., Ma, C., Finn, M. G. *Angew. Chem., Int. Ed.* **2009**, 48, 9879-9883.

15. Lutz, J.-F. *Angew. Chem., Int. Ed.* **2007**, 46, 1018-1025.

16. Krasinski, A., Fokin, V. V., Sharpless, K. B. *Org. Lett.* **2004**, 6, 1237-1240.

17. Himbert, G., Frank, D., Regit, M. *Chem. Ber.* **1976**, 109, 370-394.

18. Akimova, G. S., Chistokletov, V. N., Petrov, A. A. *Zh. Org. Khim.* **1968**, 4, 389-394.

19. Boyer, J. H., Mack, C. H., Goebel, N., Morgan, L., Jr. *J. Org. Chem.* **1958**, 23, 1051-1053.

20. Kwok, S. W., Fotsing, J. R., Fraser, R. J., Rodionov, V. O., Fokin, V. V. *Org. Lett.* **2010**, 12, 4217-4219.

21. Johansson, J. R., Beke-Somfai, T., Stalsmeden, A. S., Kann, N. *Chem. Rev.* **2016**, 116, 14726-14768.

22. Boren, B. C., Narayan, S., Rasmussen, L. K., Zhang, L., Zhao, H., Lin, Z., Jia, G., Fokin, V. V. *J. Am. Chem. Soc.* **2008**, 130, 8923-8930.

23. Zhang, L., Chen, X., Xue, P., Sun, H. H. Y., Williams, I. D., Sharpless, K. B., Fokin, V. V., Jia, G. *J. Am. Chem. Soc.* **2005**, 127, 15998-15999.

24. Oakdale, J. S., Fokin, V. V., Umezaki, S., Fukuyama, T. *Org. Synth.* **2013**, 90, 96-104.

25. Johansson, J. R., Lincoln, P., Nordén, B., Kann, N. *J. Org. Chem.* **2011**, 76, 2355-2359.

26. Chalker, J. In *Chemoselective and Bioorthogonal Ligation Reactions: Concepts and Applications*, Algar, W. R., Dawson, P. E., Medintz, I. L., Eds., pp 231−270, Wiley: Weinheim, **2017**.

27. Krall, N., da Cruz, F. P., Boutureira, O., Bernardes, G. J. L. *Nat. Chem.* **2016**, 8, 103-113.

28. Boutureira, O., Bernardes, G. J. L. *Chem. Rev.* **2015**, 115, 2174-2195.

29. McKay, C. S., Finn, M. G. *Chem. Biol.* **2014**, 21, 1075-1101.

30. Sletten, E. M., Bertozzi, C. R. *Angew. Chem., Int. Ed.* **2009**, 48, 6974-6998.

31. Kamer, P. C. J., van Leeuwen, P. W. N. M., Reek, J. N. H. *Acc. Chem. Res.* **2001**, 34, 895-904.

32. Staudaher, N. D., Stolley, R. M., Louie, J. *Chem. Commun.* **2014**, 50, 15577-15580.

33. Ding, S., Jia, G., Sun, J. *Angew. Chem., Int. Ed.* **2014**, 53, 1877-1880.

34. Creary, X., Anderson, A., Brophy, C., Crowell, F., Funk, Z. *J. Org. Chem.* **2012**, 77, 8756-8761.

35. Seeberger, P. H. *Acc. Chem. Res.* **2015**, 48, 1450-1463.

36. Wang, L.-X., Davis, B. G. *Chem. Sci.* **2013**, 4, 3381-3394.

37. Gamblin, D. P., Scanlan, E. M., Davis, B. G. *Chem. Rev.* **2009**, 109, 131-163.

38. Seeberger, P. H., Werz, D. B. *Nature* **2007**, 446, 1046-1051.

39. Seeberger, P. H., Haase, W.-C. *Chem. Rev.* **2000**, 100, 4349-4394.

40. Barefield, E. K., Krost, D. A., Edwards, D. S., Van Derveer, D. G., Trytko, R. L., O'Rear, S. P., Williamson, A. N. *J. Am. Chem. Soc.* **1981**, 103, 6219-6222.

41. Uhlig, E., Walther, H. *Z. Anorg. Allg. Chem.* **1974**, 409, 89-96.

42. Olechowski, J. R., McAlister, C. G., Clark, R. F. *Inorg. Chem.* **1965**, 4, 246-247.

43. Leadbeater, N. E. *J. Org. Chem.* **2001**, 66, 7539-7541.

44. Becalska, A., Debad, J. D., Sanati, H. K., Hill, R. H. *Polyhedron* **1990**, 9, 581-587.

45. Saraev, V. V., Kraikivskii, P. B., Zelinskii, S. N., Vil'ms, A. I., Matveev, D. A., Yunda, A. Yu., Fedonina, A. A., Lammertsma, K. *Russ. J. Coord. Chem.* **2006**, 32, 397-401.

46. Mindiola, D. J., Waterman, R., Jenkins, D. M., Hillhouse, G. L. *Inorg. Chim. Acta* **2003**, 345, 299-308.

47. Kitiachvili, K. D., Mindiola, D. J., Hillhouse, G. L. *J. Am. Chem. Soc.* **2004**, 126, 10554-10555.

48. Tasker, S. Z., Standley, E. A., Jamison, T. F. *Nature* **2014**, 509, 299-309.

49. Montgomery, J. *Angew. Chem., Int. Ed.* **2004**, 43, 3890-3908.

50. Montgomery, J. *Acc. Chem. Res.* **2000**, 33, 467-473.

51. Suzuki, T., Ota, Y., Ri, M., Bando, M., Gotoh, A., Itoh, Y., Tsumoto, H., Tatum, P. R., Mizukami, T., Nakagawa, H., Iida, S., Ueda, R., Shirahige, K., Miyata, N. *J. Med. Chem.* **2012**, 55, 9562-9575.

52. Brittain, W. D. G., Buckley, B. R., Fossey, J. S. *Chem. Commun.* **2015**, 51, 17217-17220.

53. Asano, K., Matsubara, S. *Org. Lett.* **2010**, 12, 4988-4991.

54. Baier, G., Siebert, J. M., Landfester, K., Musyanovych, A. *Macromolecules* **2012**, 45, 3419-3427.

55. Edem, P. E., Czorny, S., Valliant, J. F. *J. Med. Chem.* **2014**, 57, 9564-9577.

56. Park, S. Y., Yoon, J. H., Hong, C. S., Souane, R., Kim, J. S., Matthews, S. E., Vicens, J. *J. Org.*

Chem. **2008**, 73, 8212-8218.

57. Orth, R., Pitscheider, M., Sieber, S. A. *Synthesis* **2010**, 2201-2206.

58. Hong, S. Y., Tobias, G., Ballesteros, B., El Qualid, F., Errey, J. C., Doores, K. J., Kirkland, A. I., Nellist, P. D., Green, M. L. H., Davis, B. G. *J. Am. Chem. Soc.* **2007**, 129, 10966-10967.

59. Thomas, G. B., Rader, L. H., Park, J., Abezgauz, L., Danino, D., DeShong, P., English, D. S. *J. Am. Chem. Soc.* **2009**, 131, 5471-5477.

60. Pastuch-Gawolek, G., Malarz, K., Mrozek-Wilczkiewicz, A., Musiol, M., Serda, M., Czaplinska, B., Musiol, R. *Eur. J. Med. Chem.* **2016**, 112, 130-144.

61. Percec, V., Leowanawat, P., Sun, H.-J., Kulikov, O., Nusbaum, C. D., Tran, T. M., Bertin, A., Wilson, D. A., Peterca, M., Zhang, S., Kamat, N. P., Vargo, K., Moock, D., Johnston, E. D., Hammer, D. A., Pochan, D. J., Chen, Y., Chabre, Y. M., Shiao, T. C., Bergeron-Brlek, M., André, S., Roy, R., Gabius, H.-J., Heiney, P. A. *J. Am. Chem. Soc.* **2013**, 135, 9055-9077.

62. Ziegler, T., Hermann, C. *Tetrahedron Lett.* **2008**, 49, 2166-2169.

63. Clemente, M. J., Fitremann, J., Mauzac, M., Serrano, J. L., Oriol, L. *Langmuir* **2011**, 27, 15236-15247.

64. Bew, S. P., Legentil, L., Scholier, V., Sharma, S. V. *Chem. Commun.* **2007**, 389-391.

65. Rasmussen, L. K., Boren, B. C., Fokin, V. V. *Org. Lett.* **2007**, 9, 5337-5339.

66. Sasaki, T., Eguchi, S., Yamaguchi, M., Esaki, T. *J. Org. Chem.* **1981**, 46, 1800-1804.

67. Ko, K. S., Steffey, M. E., Brandvold, K. R., Soellner, M. B. *ACS Med. Chem. Lett.* **2013**, 4, 779-783.

68. Wang, Y.-C., Xie, Y.-Y., Qu, H.-E., Wang, H.-S., Pan, Y.-M., Huang, F.-P. *J. Org. Chem.* **2014**, 79, 4463-4469.

69. Chen, Y., Nie, G., Zhang, Q., Ma, S., Li, H., Hu, Q. *Org. Lett.* **2015**, 17, 1118-1121.

70. El Moncef, A., El Hadrami, E. M., Ben-Tama, A., de Arellano, C. R., Zaballos-Garcia, E., Stiriba, S.-E. *J. Mol. Struct.* **2009**, 929, 6-9.

71. Sau, S. C., Roy, S. R., Sen, T. K., Mullangi, D., Mandal, S. K. *Adv. Synth. Catal.* **2013**, 355, 2982-2991.

Chapter IV

Preparation of 4-Cyano-1,5-Disubstituted 1,2,3-Triazoles and Establishment of Chemoselective Sequential 1,2,3-Triazoles via NiAAC

4.1. Abstract

In the area of conjugate chemistry, internal alkynes including two different cargoes are attractive targets. But their poor regioselectivity when conjugated with azides are one of challenging factors. Propynenitriles, which own electron-withdrawing group, are considerable candidates to make exclusive 1,2,3-triazoles. After cross-coupling with azide, a nitrile group on triazole could be transformed and conjugated simply with other functional group. Here, the NiAAC methodology was applied to cyaonalkyne conjugation to achieve high yields and selectivity under mild conditions. The broad substrate scope also supports its tolerance and versatility. Additionally, preference order between cyanoalkyne and alkyne was figured out that propynenitriles are solely consumed, followed by the terminal or internal alkyne consumption. The tendency is applied in the establishment of sequential double copper- or nickel- catalyzed cycloadditions with high yields and selectivity. Methodologies presented in this chapter are potential building blocks for the development a programmed synthesis for complex molecules. The data described below are based on preliminary research.

4.2. Introduction

Azide and alkyne are versatile functional groups in applied science because of their chemical inertness, orthogonality, and small size. Cross-coupling of the corresponding two groups produce 1,2,3-triazoles, promising candidates in pharmaceutical studies. Research to prepare the five-membered heterocycle has led to various routes with or without transition metal catalysts. For example, copper[1] and silver[2] complexes catalyze the regioselective formation of 1,4-disubstituted 1,2,3-triazoles, and ruthenium[3] and nickel[4] catalysts facilitate preparation of the corresponding 1,5-disubstituted core. Compared to the astonishing development of terminal alkyne conjugation, internal alkynes have not been chosen as coupling partner because of relatively limited accessibility. Hetero-functionalized internal alkynes having specific dipole moments are primarily used to synthesize regioselective 1,4,5-trisubstituted triazoles. Azides could be paired with thioalkynes in the presence of iridium[5] or ruthenium[6] catalysts and with ynamides under appropriate conditions including iridium[7] or rhodium[8] catalysts.

4-Cyano 1,2,3-triaozles are potentially important scaffolds to load three different cargoes by coupling and modifying nitrile groups. But there is no typical method that can be applied to a broad substrate scope and mild conditions to access the corresponding triazoles (Scheme 4.1). Wang[9] and Reddy[10] groups independently reported that enamine or enolate prepared by mixing carbonyl cyanide and organocatalysts (e.g., diethyl amine, DBU) *in situ*, could make dipolar cycloaddition. Compared to the capability of various carbonyl reactant derivatives, available azides are limited to aryl and tosyl groups.[11] In 2018, Zhu group suggested enhanced synthesis of 1-cyanoalkynes, and ruthenium catalyzed azide−propynenitrile cycloaddition.[12] They utilized pentamethylcyclopentadienyl (Cp^*) ruthenium(II) catalyst and conditions, which are already published in 1,5-disubstituted 1,2,3-triazole synthesis.[13] Accessibility in preparing cyanoalkynes was enhanced, but method still suffered from long reaction time, usage of organic solvents, and elevated temperature.

Herein, I report a general synthetic method for the preparation of 4-cyano 1,2,3-triazoles using Cp_2Ni/Xantphos reagents. A broad substrate could be conjugated rapidly in water at room temperature. Based on the preference test, I could suggest several sequences using metal catalyzed cross-coupling to establish preparation of chemoselective complexes including different 1,2,3-triazole cores. Figures and tables below are preliminary data, subsequent repeat experiments could improve precision and quality of the result.

- Enamine/enolate-mediated coupling of azides

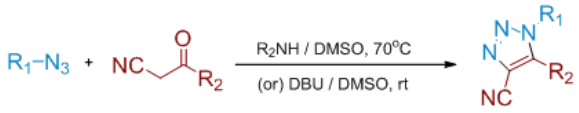

R_1= aryl, tosyl

Chem – Eur. J. **2011**, 17, 3584-3587 *Angew. Chem. Int. Ed.* **2014**, 53, 10420-10424

- Ruthenium catalyzed azide- cyanoalkyne cycloaddition

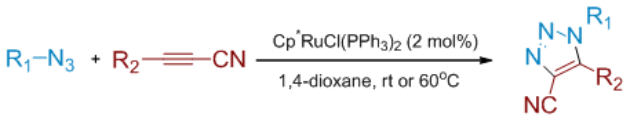

J. Org. Chem. **2018**, 83, 5092-5103

- This work

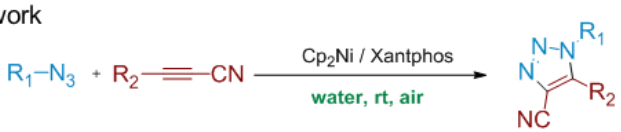

- Sequential & regioselective click reaction

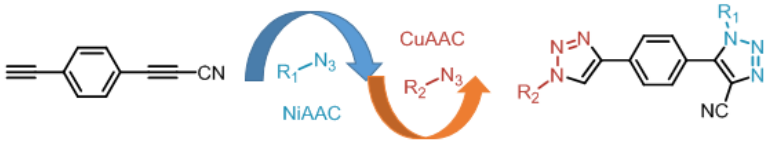

Scheme 4.1. Schematic representation of precedent and this works in synthesis of 4-cyano-1,5-disubstitutd 1,2,3-triazoles.

4.3. Results and discussion

Optimization process was conducted with 2,6-difluorobenzyl azide **1a** and 3-phenyl-2-propynenitrile **2a** (Table 4.1). With the consideration of previous paper regarding nickel catalyzed cycloaddition,[4] I decided initial standard conditions. Reaction screening showed 20 mol% of metal and ligand generated more **3aa** compared to 10 mol % case (entry 1 and 5). Reaction times are critical factors in optimization, resulting in quantitative total yield on entry 4. Reactions conducted in water showed generally lower yields compared to corresponding cases in toluene. Optimized reaction conditions are 10 mol % of nickelocene, Xantphos and equimolar amount of cesium carbonate at room temperature and 24 h in toluene or water. Selectivity ratios (~13:1) are slightly poor under various conditions, requiring column chromatography to exclude isomer **4aa**. The characteristic difference between 4-cyano triazoles and 5-cyano triazoles was measured by 1D NMR, 2D NMR and single-crystal X-ray diffraction measurement.

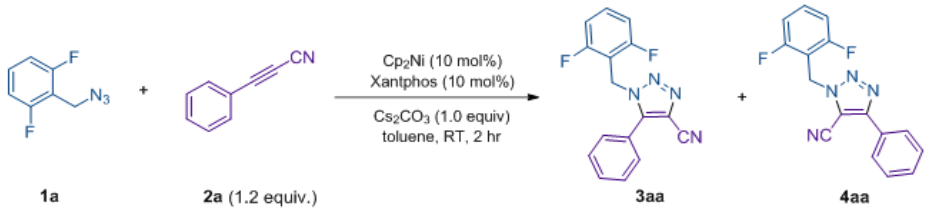

1a **2a** (1.2 equiv.) **3aa** **4aa**

entry	changes from standard condition	yield [%][b]	
		3aa	**4aa**
1	standard condition	75	6.0
2	Without Cs_2CO_3	69	4.8
3	16 hr	84	6.9
4	24 hr	95	6.3
5	20 mol% metal, ligand	83.5	6.7
6	20 mol% metal, ligand, water	80	4.9
7	24 hr, water	82	7.2
8	36 hr, water	82	7.2

[a] Reaction conditions: **1a** (0.38 mmol), **2a** (0.46 mmol, 1.2 equiv), Cp_2Ni (10 mol%), Xantphos (10 mol%), Cs_2CO_3 (1.0 equiv) in toluene (2.0 mL) at rt under air for 2 h. [b] Isolated yield. Cp, cyclopentadienyl.

Table 4.1. Optimization of reaction conditions.[a]

Then I investigated the substrate scope with various functional groups introduced azide and cyanoalkyne derivatives under optimized conditions. Additionally, yields obtained in toluene and water

are given to show solvent tolerance in the nickel catalyzed reaction. Incomplete substrate tables are attached at this stage (Scheme 4.2). Generally, entries require a day for full conversion of reactants, but benzyl azide **1b** is totally consumed within 2 h. Entries in aqueous media have weakness in yield because of poor solubility of reagents. Various azides (**1a**−**1h**) were screened to check the production of corresponding 4-cyano-1,5-disubstituted triazoles in the aspect of yield and selectivity. Different functional groups including fluoro-, trifluoromethyl-, hydroxy-, and nitro moieties were examined and various structures such as secondary, polycyclic, aliphatic, and heterocycle moieties are also potential candidates for supporting the generality of the method. In cyanoalkyne derivatives test, I could secure group tolerance, but selectivity ratios were different from poor 3:1 to excellent 18.2:1. Conjugation of biomolecules (e.g., carbohydrates, amino acids) would be feasible via Cp_2Ni/Xantphos catalytic system.

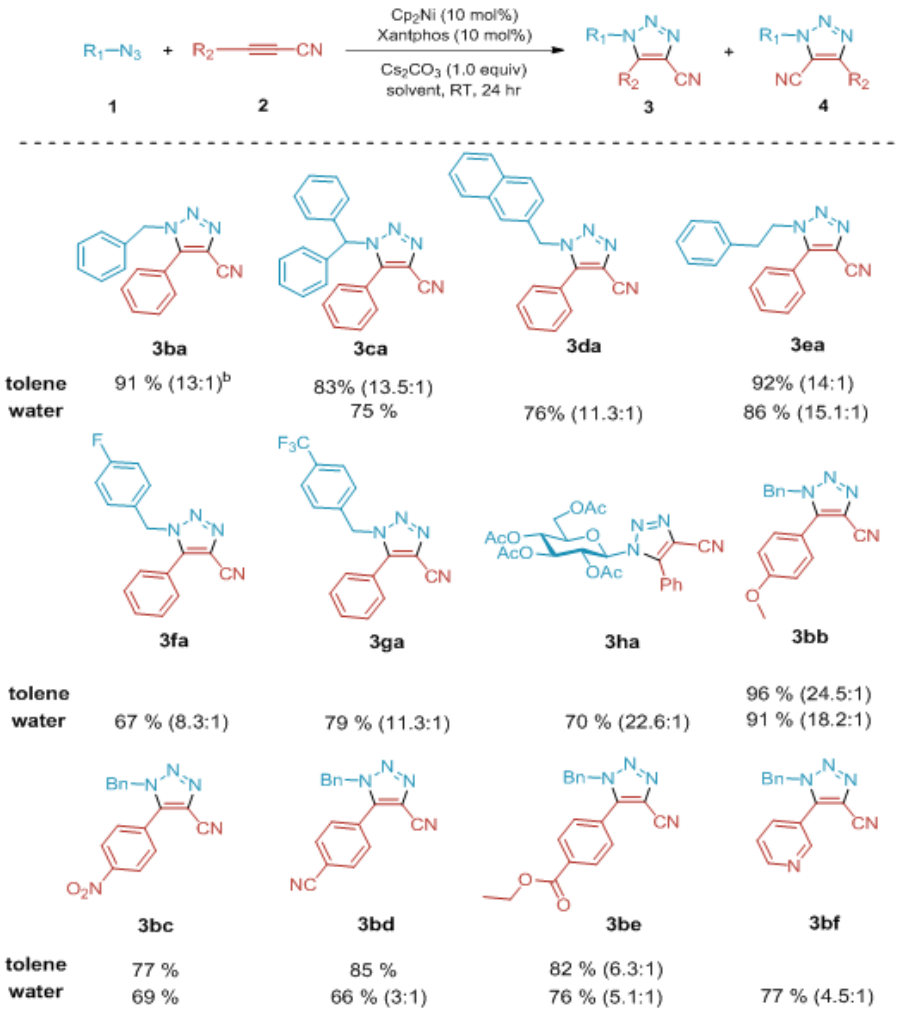

[a] Reaction conditions: **1a** (0.38 mmol), **2a** (0.46 mmol, 1.2 equiv), Cp_2Ni (10 mol%), Xantphos (10 mol%), Cs_2CO_3 (1.0 equiv) in toluene (2.0 mL) at rt under air for 2 h. [b] Isolated yield. Cp, cyclopentadienyl.

Scheme 4.2. Substrate scope of nickel catalyzed azide−cyanoalkyne cycloaddition[a]

The reactivity of cyanoalkynes in NiAAC was investigated by comparison with phenylacetylene (Scheme 4.3). Tests were conducted by mixing azide **1b**, cyanoalkyne **2a**, and terminal alkyne **2g** in equimolar amounts (1:1:1) under standard reaction conditions. An initial assumption is that triazole **3ba** and **5bg** could be synthesized as similar amounts because each alkyne conjugation to azide showed comparable reaction times. But interestingly, azide **1b** is fully consumed for the exclusive conjugation with **2a** to elicit **3ba** (87%) and **4ba** (8%). Preference results are even more favorable compared to the corresponding test in RuAAC, showing a 9:1 ratio of **3ba** and **5bg**.[12] The addition of extra **1b** proved that terminal alkyne **2g** was not damaged during the reaction, because it could be conjugated with azide in the absence of cyanoalkyne (Scheme 4.3, second line). There is a catalytic degradation in first click reaction, and additional nickelocene/Xantphos are essential for sequential cycloadditions (third line). Electron-withdrawing ability of cyanoalkynes or mechanistic difference when coordinated to metal complexes are potential reasons of preferences, requiring supplementary experimental evidence.

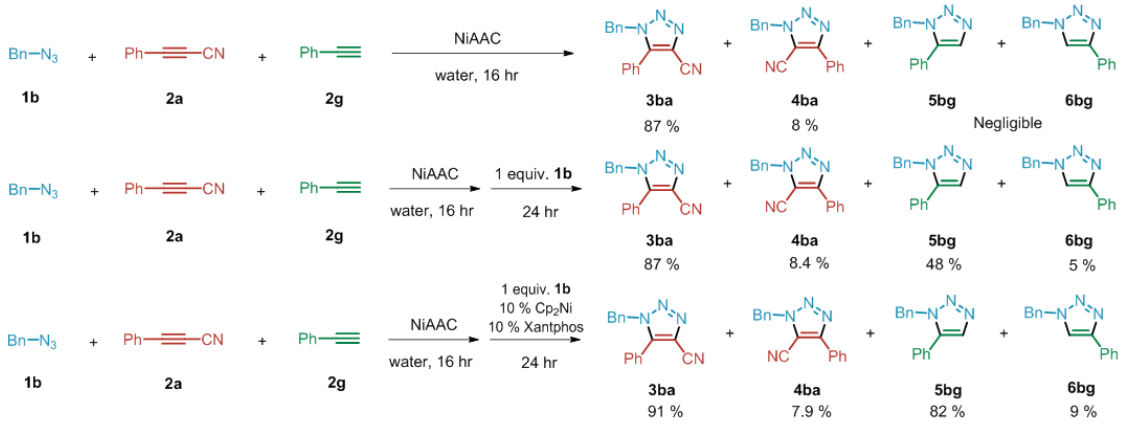

Scheme 4.3. Reactivity comparison test between cyanoalkyne and terminal alkyne.

Despite wide applications of CuAAC, sequential click reactions are poorly developed because of its strong reactivity. Some outstanding methodologies utilized different chemoselectivity of azides[14] (metal chelating effect to nitrogen, explained in Figure 1.11) or diverse alkyne pairs (alkyne versus cyclooctyne[15], or alkyne versus trimethylsilyl group protected alkyne[16]). The development of new sequential double click methods expands chemical tools to access complex molecules by one-pot and non-chromatographic purifications. Reactivity preferences described in scheme 4.3 give great importance to a molecular core **2h**, including terminal alkyne and cyanoalkyne (Scheme 4.4A). Copper-catalyzed cycloaddition elicits conjugation of terminal alkyne and azide, because CuAAC could not be reacted with internal alkyne moieties, on the other hand, nickel-catalyzed addition could produce cyanoalkyne−conjugated molecules exclusively. Remaining alkyne moiety would be coupled with extra

azide cargoes to furnish chemoselective sequential double click reactions. Scheme 4.4B represents methods utilizing molecule **2i**, having trimethylsilyl (TMS) group protected alkyne and cyanoalkyne. Because nickel complex could not catalyze the coupling of TMS protected internal alkynes, 4-cyano 1,2,3-triazoles were formed exclusively, subsequent deprotection by silver catalysts enabled sequential 1,3-dipolar cycloadditions. With the combination of different transition metal catalyzed cycloadditions, conceptually, various triazole isomers and more complex molecules could be prepared with multiple click reactions.

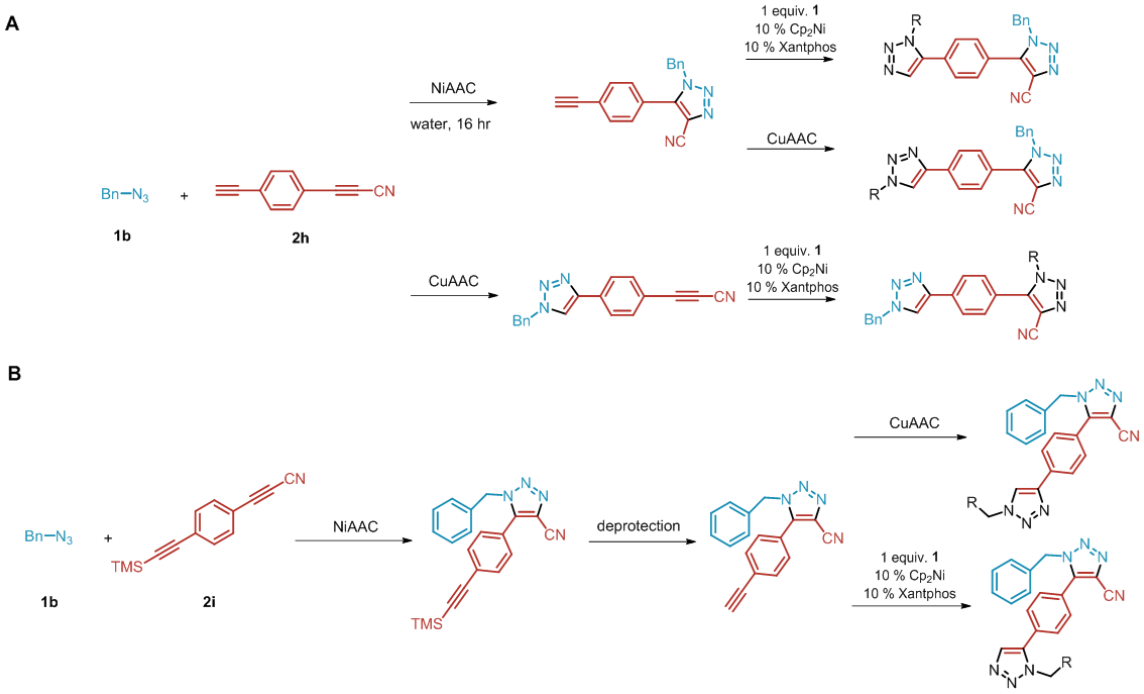

Scheme 4.4. Schematic representation of chemoselective sequential double click reactions.

4.4. Experimental

General information

Reactions were checked by thin-layer chromatography (TLC) using Merck silica gel $60F_{254}$ glass plate with the help of ultra-violet lamp (254 nm), or potassium permanganate solution. Flash column chromatography was carried out using Merck silica gel 60. All reagents were purchased from standard suppliers (Sigma-Aldrich, Alfa Aesar) and used without further purification. ^{1}H, ^{13}C, and ^{19}F NMR spectra were recorded on a Bruker Avance III HD (400 MHz for proton, 100 MHz for carbon). Chemical shifts are given on the δ-scale in ppm, and residual solvent peaks were used as internal standards.

Synthesis of organic azides

Generally, S_N2 type reaction is applied in preparation of organic azides. By simple mixing organic bromide (1.0 equiv) and sodium azide (1.5 equiv) in aprotic solvent DMSO or a mixture of 1:3 water/acetone solution, desired starting materials are made after stirring 24 hours at room temperature. Detailed experimental procedures are included in reference paper.[4] Sodium azide is extremely toxic and explosive. Avoiding metal spatula during azide experiments are recommended.

Synthesis of cyanoalkynes

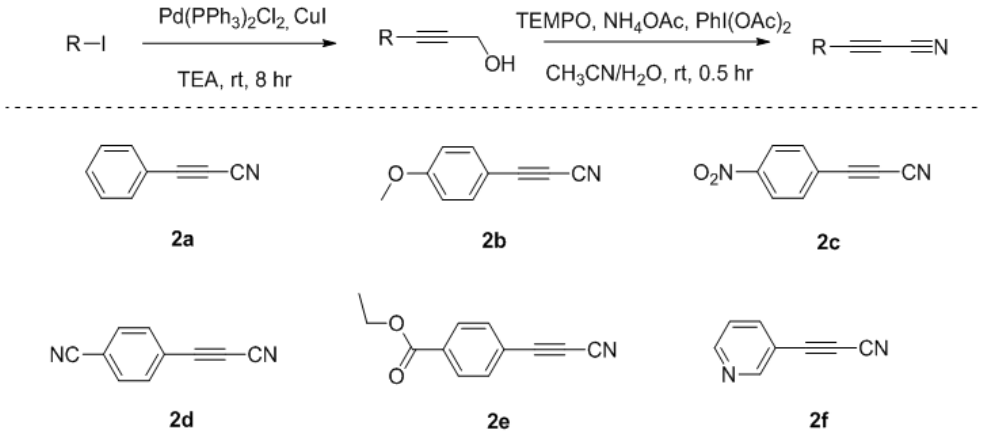

Scheme 4.5. Preparation of propynenitriles.

Cyanoalkynes are prepared through two-step reactions from iodo compounds (Scheme 4.5). At first, propargyl alcohol was introduced via Sonogashira reaction in the presence of palladium catalysts. To a suspension of $Pd(PPh_3)_2Cl_2$ (70 mg, 0.1 mmol) and CuI (38 mg, 0.2 mmol) in trimethylamine (40 mL), iodo-compounds (10 mmol) and propargyl alchohol (0.64 mL, 10.9 mmol) were added at room temperature, and stirred 8 hours under nitrogen atmosphere. Crude solutions were filtered through celite, following silica column chromatography to purify intermediate compounds. After column purification, intermediate propargyl alcohols could be transformed to corresponding nitriles through one-pot oxidative conversion.[17] To an acetonitrile/water (9:1) solvent 20 mL, (2,2,6,6-tetramethylpiperidin-1-yl)oxyl (TEMPO) (44 mg, 0.28 mmol), iodosobenzene diacetate (4.02 g, 12.4 mmol), and ammonium acetate (1.75 g, 22 mmol) were dissolved under nitrogen atmosphere. Intermediates (5.67 mmol) were added and stirred 30 minutes at room temperature. After water/diethyl ether separation, column chromatography was conducted to purify compound **2**.

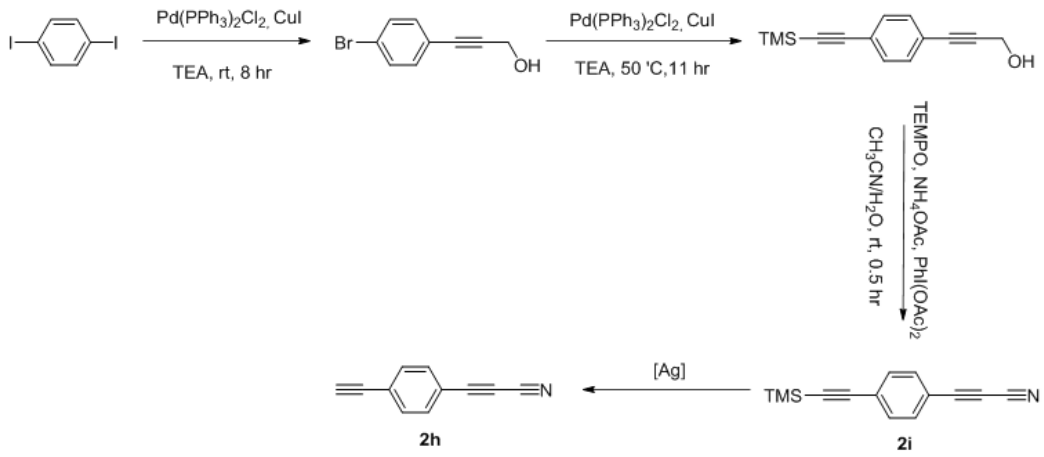

Scheme 4.6. Preparation of propynenitriles **2h** and **2i**.

Compound **2h** and **2i** are prepared from 1,4-diiodobenzene with similar methodology. One portion of iodo group was replaced with propargyl alcohol, then the other iodo group was converted to trimethylsilylacetylene. Compound 2h are easily prepared by eliminating trimethylsilyl group with silver metal complex such as silver nitrate or silver trifluoromethanesulfonate.

General Procedure for the nickel catalyzed cross-coupling

To a mixture of nickelocene (10 mol%) and Xantphos (10 mol%) in water or toluene (2.0 mL), cyanoalkyne **2** (1.2 equiv, 0.46 mmol), cesium carbonate (1.0 equiv, 0.38 mmol) and organic azide 1 (1.0 equiv, 0.38 mmol) were added and stirred at rt. After 24 hours, the suspension was diluted with DCM, washed with water, and dried over sodium sulfate. The desired product was purified by flash column chromatography and dried *in vacuo*.

Characterization data

At this stage, I've measured some preliminary data of ^{1}H NMR spectra. Other characterization data including ^{13}C NMR and HRMS would be conducted soon.

Compound **2i**: ^{1}H NMR (400 MHz, $CDCl_3$) δ 7.56 – 7.52 (m, 2H), 7.50 – 7.45 (m, 2H), 0.26 (s, 9H).

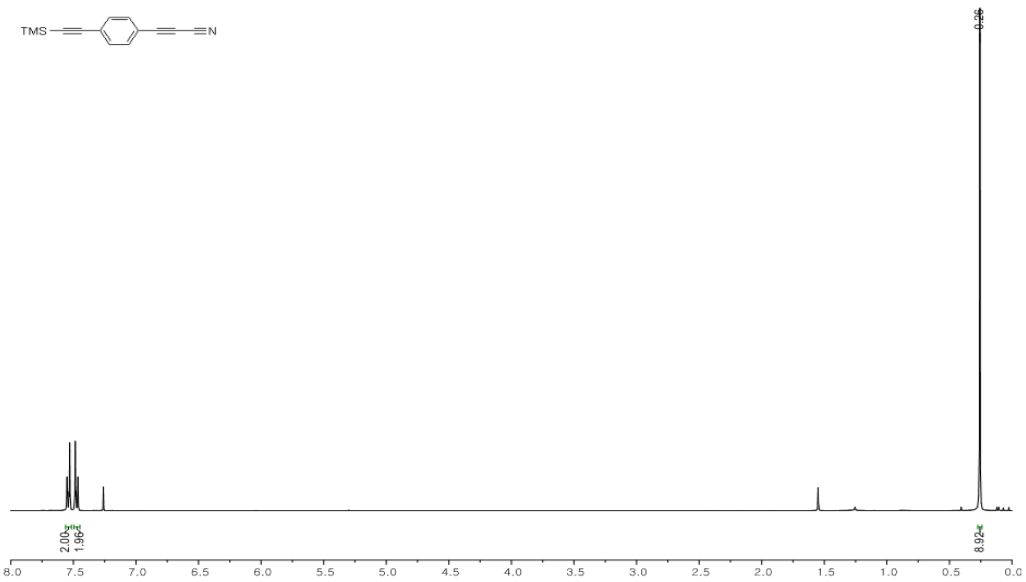

Figure 4.1. ^{1}H NMR (400 MHz, $CDCl_3$) of the compound **2i**.

Compound **2h:** ^{1}H NMR (400 MHz, $CDCl_3$) δ 7.59 – 7.54 (m, 2H), 7.54 – 7.49 (m, 2H), 3.30 (s, 1H).

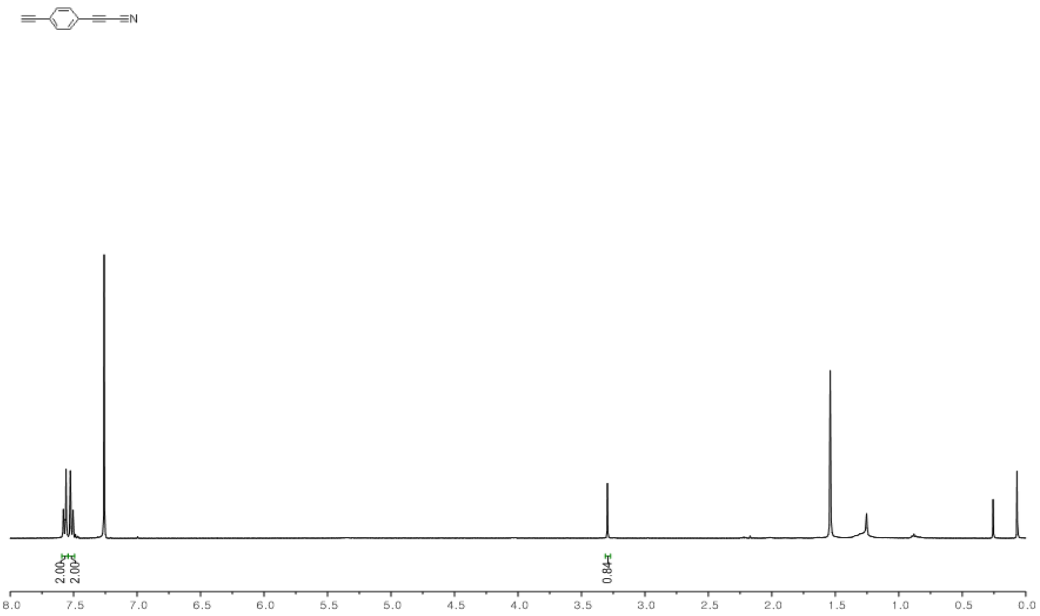

Figure 4.2. ^{1}H NMR (400 MHz, $CDCl_3$) of the compound **2h**.

Compound **3ba**: ^{1}H NMR (400 MHz, $CDCl_3$) δ 7.59 – 7.49 (m, 3H), 7.37 – 7.27 (m, 5H), 7.11 – 7.04 (m, 2H), 5.55 (s, 2H).

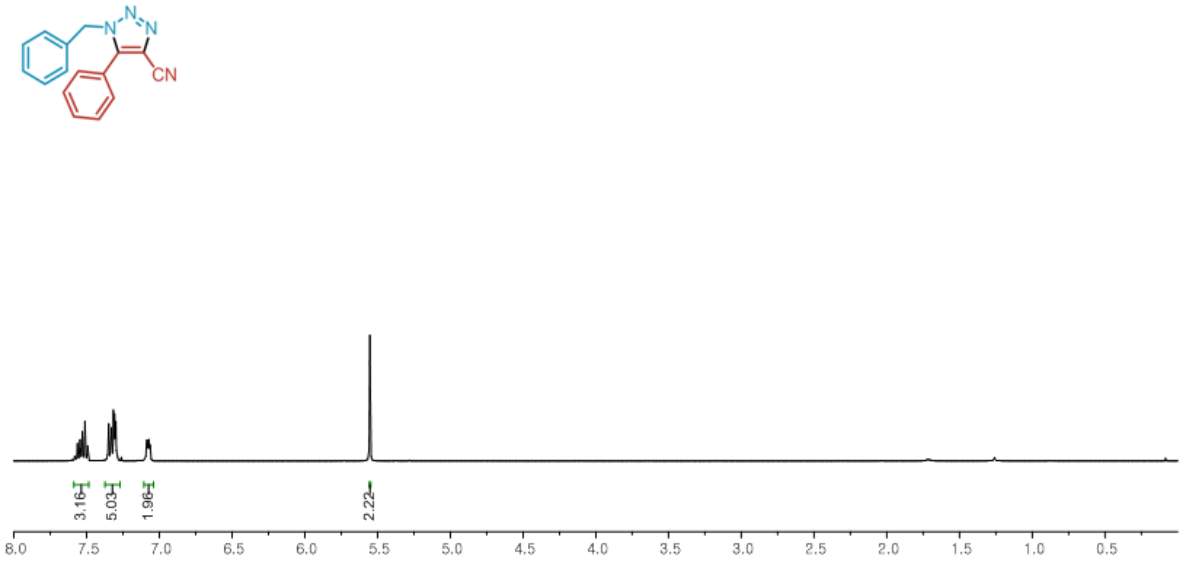

Figure 4.3. ^{1}H NMR (400 MHz, $CDCl_3$) of the compound **3ba**.

Compound **3ca**: ^{1}H NMR (400 MHz, $CDCl_3$) δ 7.63 – 7.53 (m, 3H), 7.42 – 7.34 (m, 8H), 7.25 – 7.17 (m, 4H), 6.70 (s, 1H).

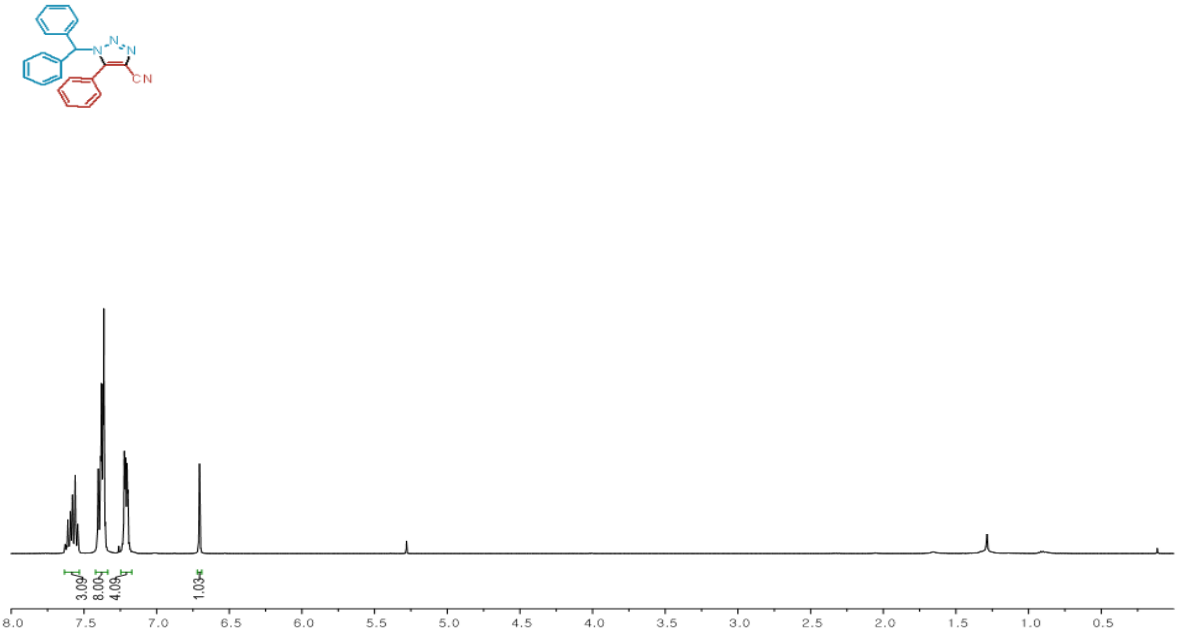

Figure 4.4. ^{1}H NMR (400 MHz, $CDCl_3$) of the compound **3ca**.

Compound **3fa:** ^{1}H NMR (400 MHz, $CDCl_3$) δ 7.60 – 7.49 (m, 3H), 7.37 – 7.31 (m, 2H), 7.09 – 7.02 (m, 2H), 7.02 – 6.92 (m, 2H), 5.52 (s, 2H).

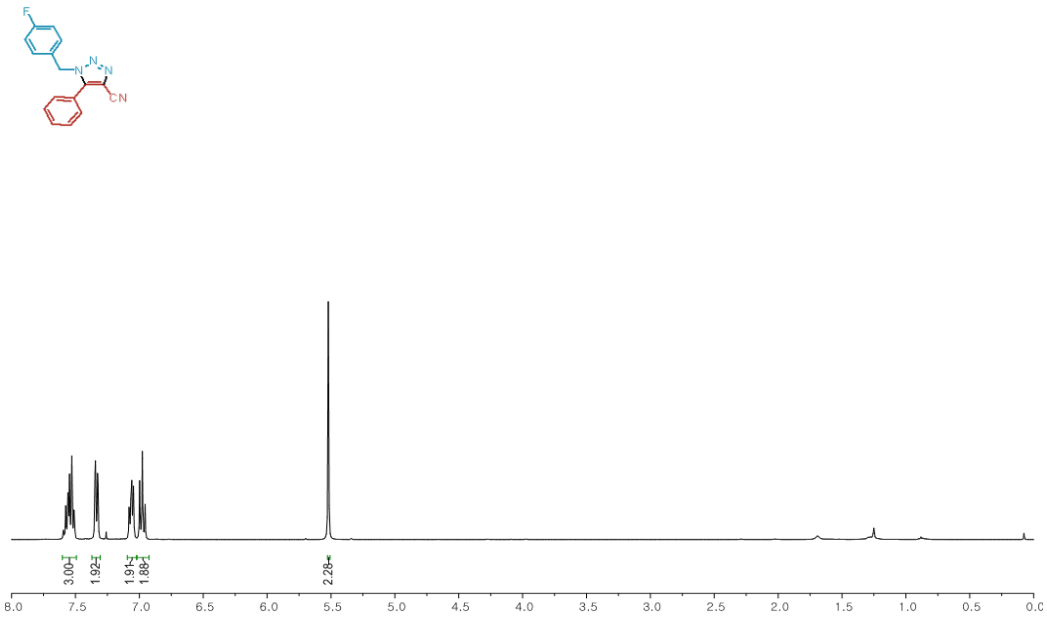

Figure 4.5. ^{1}H NMR (400 MHz, $CDCl_3$) of the compound **3fa**.

Compound **3ga:** ^{1}H NMR (400 MHz, $CDCl_3$) δ 7.53 – 7.42 (m, 2H), 7.26 (d, *J* = 6.8 Hz, 1H), 7.13 (d, *J* = 8.1 Hz, 1H), 5.54 (s, 1H).

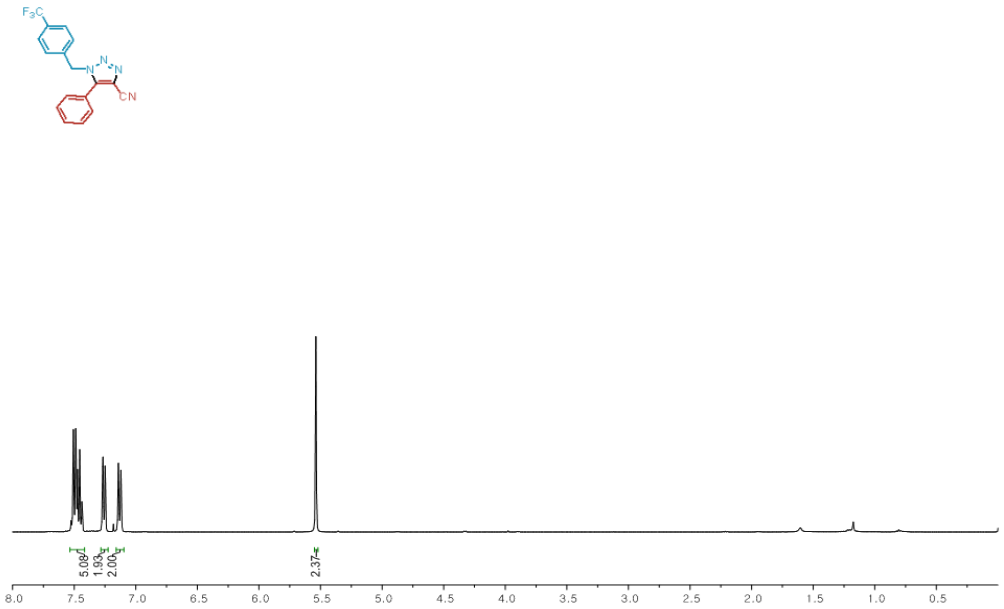

Figure 4.6. ^{1}H NMR (400 MHz, $CDCl_3$) of the compound **3ga**.

Compound **3ha**: ^{1}H NMR (400 MHz, $CDCl_3$) δ 7.66 – 7.54 (m, 5H), 5.87 (t, *J* = 9.4 Hz, 1H), 5.61 (d, *J* = 9.5 Hz, 1H), 5.28 (dd, *J* = 11.7, 7.2 Hz, 1H), 5.16 (t, *J* = 9.8 Hz, 1H), 4.20 (ddd, *J* = 14.8, 12.6, 4.0 Hz, 2H), 3.92 (ddd, *J* = 10.0, 5.6, 2.3 Hz, 1H), 2.09 (s, 3H), 2.01 (s, 3H), 1.97 (s, 3H), 1.82 (s, 3H).

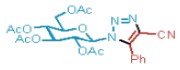

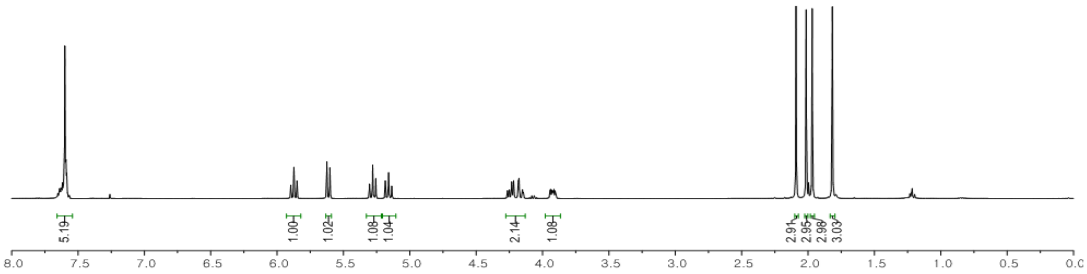

Figure 4.7. ^{1}H NMR (400 MHz, $CDCl_3$) of the compound **3ha**.

Compound **3bb:** ^{1}H NMR (400 MHz, $CDCl_3$) δ 7.25 – 7.13 (m, 5H), 7.05 – 6.97 (m, 2H), 6.96 – 6.88 (m, 2H), 5.45 (s, 2H), 3.77 (s, 3H).

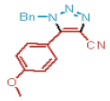

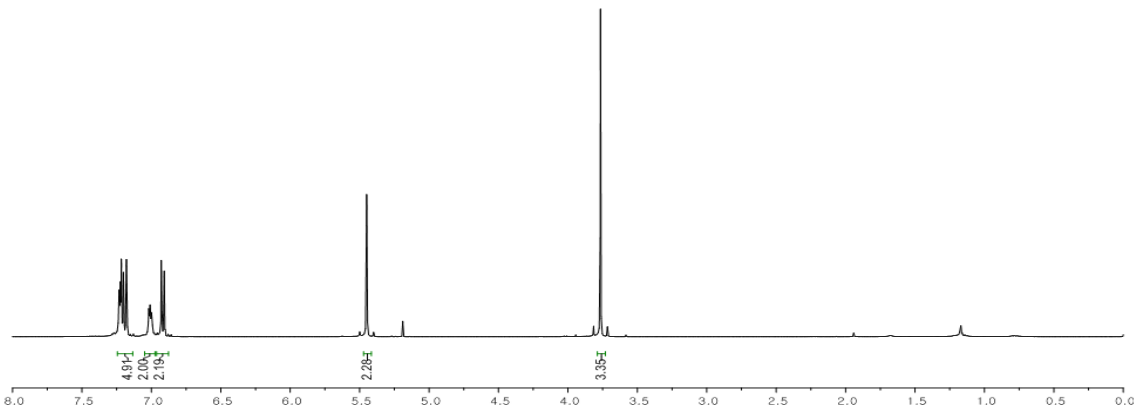

Figure 4.8. ^{1}H NMR (400 MHz, $CDCl_3$) of the compound **3bb**.

Compound **3bc:** ^{1}H NMR (400 MHz, $CDCl_3$) δ 8.38 – 8.31 (m, 2H), 7.56 – 7.49 (m, 2H), 7.38 – 7.27 (m, 3H), 7.11 – 7.02 (m, 2H), 5.60 (s, 2H).

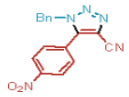

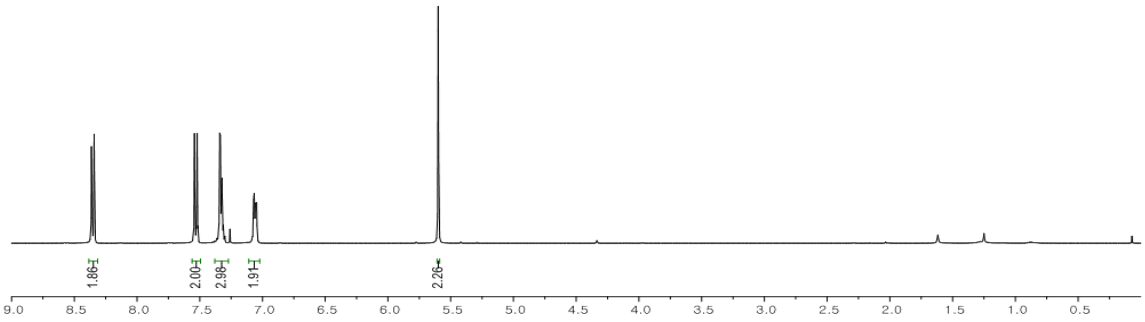

Figure 4.9. ^{1}H NMR (400 MHz, $CDCl_3$) of the compound **3bc**.

Compound **3bd**: ^{1}H NMR (400 MHz, $CDCl_3$) δ 7.80 (d, *J* = 8.5 Hz, 2H), 7.45 (d, *J* = 8.5 Hz, 2H), 7.32 (dd, *J* = 5.1, 1.9 Hz, 3H), 7.07 – 7.00 (m, 2H), 5.58 (s, 2H).

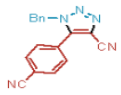

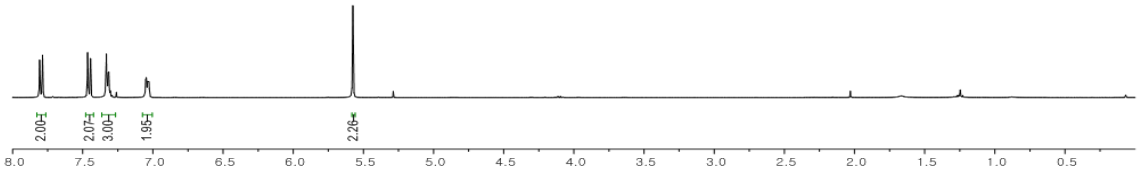

Figure 4.10. ^{1}H NMR (400 MHz, $CDCl_3$) of the compound **3bd**.

Compound **3be**: ^{1}H NMR (400 MHz, $CDCl_3$) δ 8.17 (d, *J* = 8.3 Hz, 2H), 7.42 (d, *J* = 8.6 Hz, 2H), 7.33 – 7.27 (m, 3H), 7.09 – 7.03 (m, 2H), 5.56 (s, 2H), 4.41 (q, *J* = 7.1 Hz, 2H), 1.41 (t, *J* = 7.1 Hz, 3H).

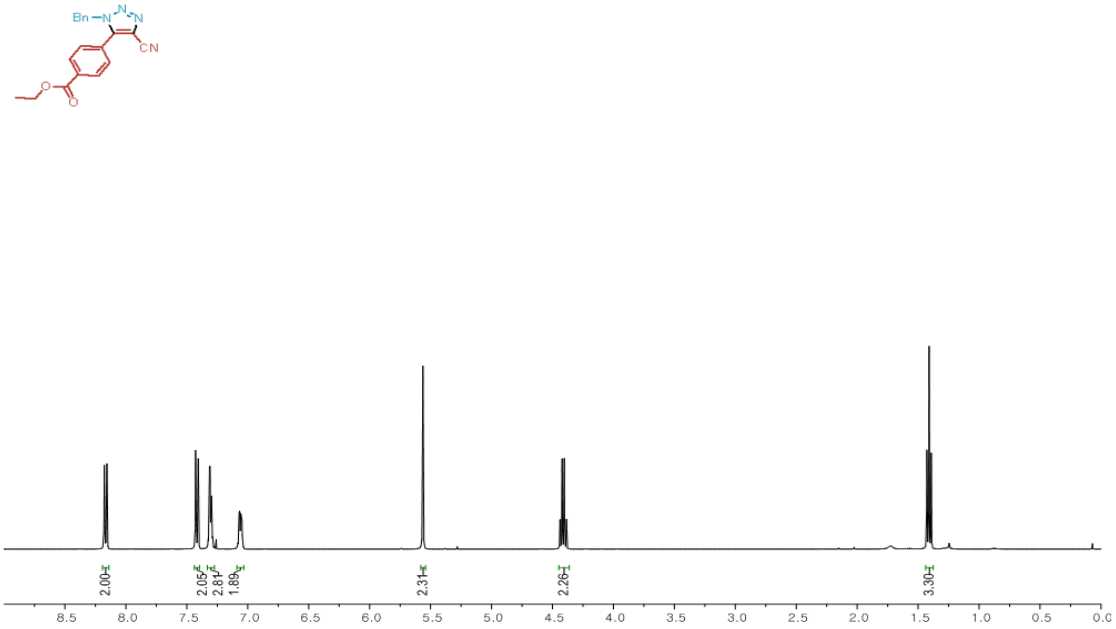

Figure 4.11. ^{1}H NMR (400 MHz, $CDCl_3$) of the compound **3be**.

Compound **3bf**: ^{1}H NMR (400 MHz, $CDCl_3$) δ 8.77 (d, *J* = 4.0 Hz, 1H), 8.57 (s, 1H), 7.64 (d, *J* = 7.8 Hz, 1H), 7.45 (dd, *J* = 7.4, 5.0 Hz, 1H), 7.29 (dd, *J* = 9.5, 6.0 Hz, 3H), 7.05 (dd, *J* = 6.3, 2.7 Hz, 2H), 5.57 (s, 2H).

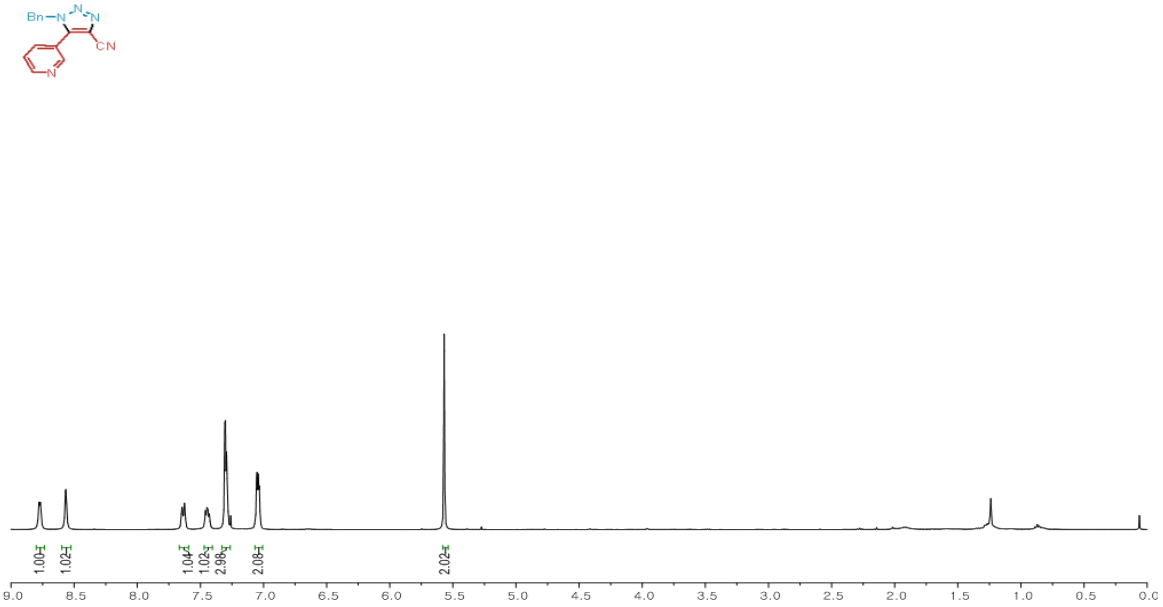

Figure 4.12. ^{1}H NMR (400 MHz, $CDCl_3$) of the compound **3bf**.

Compound **3bi**

^{1}H NMR (400 MHz, $CDCl_3$) δ 7.54 – 7.49 (m, 2H), 7.27 – 7.18 (m, 5H), 7.03 – 6.97 (m, 2H), 5.47 (s, 2H), 0.20 (s, 9H).

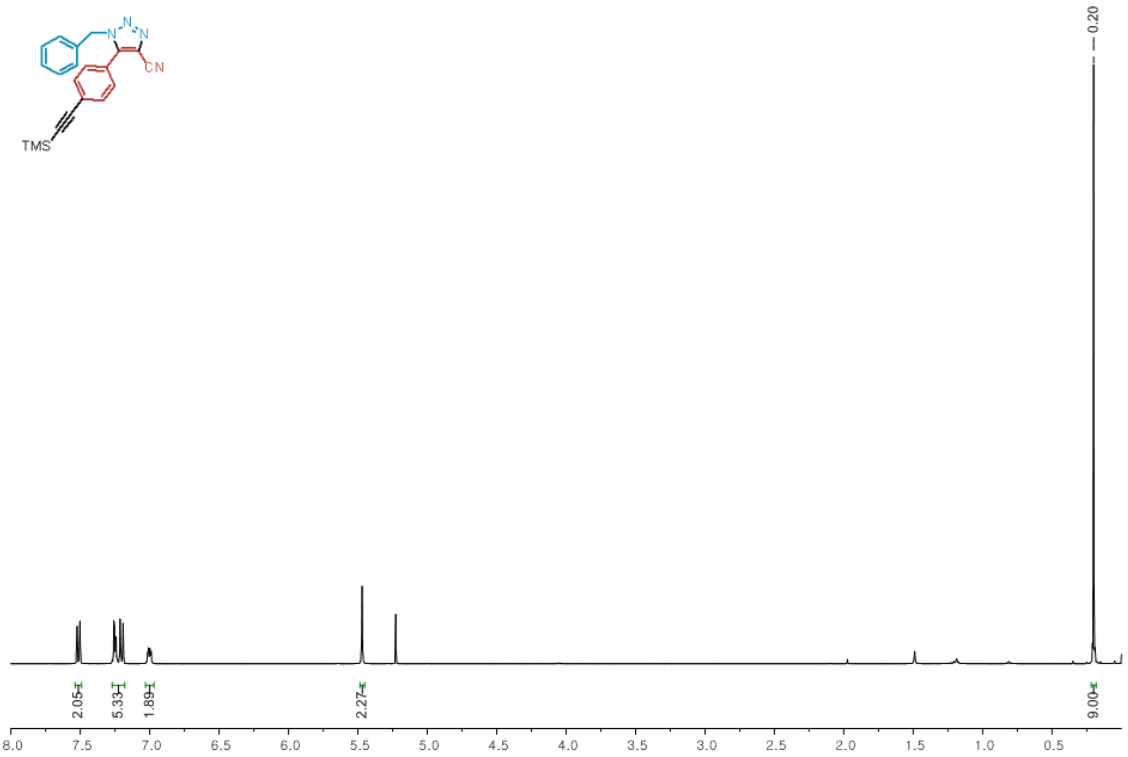

Figure 4.13. ^{1}H NMR (400 MHz, $CDCl_3$) of the compound **3bi**.

4.5. References

1. Rostovtsev, V. V., Green, L. G., Fokin, V. V., Sharpless, K. B. *Angew. Chem. Int. Ed.* **2002**, 41, 2596-2599.

2. McNulty, J., Keskar, K., Vemula, R. *Chem – Eur. J.* **2011**, 17, 14727-14730.

3. Zhang, L., Chen, X., Xue, P., Sun, H. H. Y., Williams, I. D., Sharpless, K. B., Fokin, V. V., Jia, G. *J. Am. Chem. Soc.* **2005**, 127, 15998-15999.

4. Kim, W. G., Kang, M. E., Lee, J. B., Jeon, M. H., Lee, S., Lee, J., Choi, B., Cal, P. M. S. D., Kang, S., Kee, J.-M., Bernardes, G. J. L., Rohde, J.-U., Choe, W., Hong, S. Y. *J. Am. Chem. Soc.* **2017**, 139, 12121-12124.

5. Ding, S., Jia, G., Sun, J. *Angew. Chem. Int. Ed.* **2014**, 53, 1877-1880.

6. Destito, P., Couceiro, J. R., Faustino, H., López, F., Mascareñas, J. L. *Angew. Chem. Int. Ed.* **2017**, 56, 10766-10770.

7. Song, W., Zheng, N. *Org. Lett.* **2017**, 19, 6200-6203.

8. Liao, Y., Lu, Q., Chen, G., Yu, Y., Li, C., Huang, X. *ACS Catal.* **2017**, 7, 7529-7534.

9. Danence Lee Jin, T., Gao, Y., Li, M., Huang, Y., Wang, J. *Chem – Eur. J.* **2011**, 17, 3584-3587.

10. Ramachary, D. B., Shashank, A. B., Karthik, S. *Angew. Chem. Int. Ed.* **2014**, 53, 10420-10424.

11. Ramachary, D. B., Gujral, J., Peraka, S., Reddy, G. S. *Eur. J. Org. Chem.* **2017**, 459-464.

12. Liu, P., Clark, R. J., Zhu, L. *J. Org. Chem.* **2018**, 83, 5092-5103.

13. Boren, B. C., Narayan, S., Rasmussen, L. K., Zhang, L., Zhao, H., Lin, Z., Jia, G., Fokin, V. V. *J. Am. Chem. Soc.* **2008**, 130, 8923-8930.

14. Yuan, Z., Kuang, G.-C., Clark, R. J., Zhu, L. *Org. Lett.* **2012**, 14, 2590-2593.

15. Beal, D. M., Albrow, V. E., Burslem, G., Hitchen, L., Fernandes, C., Lapthorn, C., Roberts, L. R., Selby, M. D., Jones, L. H. *Org. Biomol. Chem.* **2012**, 10, 548-554.

16. Aucagne, V., Leigh, D. A. *Org. Lett.* **2006**, 8, 4505-4507.

17. Vatèle, J.-M. *Synlett* **2014**, 25, 1275-1278.

Chapter V

Acknowledgement